

ISTANBUL TECHNICAL UNIVERSITY ★ GRADUATE SCHOOL OF SCIENCE
ENGINEERING AND TECHNOLOGY

QUASI-STATIC AND DYNAMIC ANALYSIS OF VISCOELASTIC PLATES



Ph.D. THESIS

Gülçin TEKİN ÖZKAN

Department of Civil Engineering

Structural Engineering Program

DECEMBER 2017

ISTANBUL TECHNICAL UNIVERSITY ★ GRADUATE SCHOOL OF SCIENCE
ENGINEERING AND TECHNOLOGY

QUASI-STATIC AND DYNAMIC ANALYSIS OF VISCOELASTIC PLATES



Ph.D. THESIS

Gülçin TEKİN ÖZKAN
(501112004)

Department of Civil Engineering

Structural Engineering Program

Thesis Advisor: Assoc. Prof. Dr. Fethi KADIOĞLU

DECEMBER 2017

İSTANBUL TEKNİK ÜNİVERSİTESİ ★ FEN BİLİMLERİ ENSTİTÜSÜ

VİSKOELASTİK PLAKLARIN KUAZİ-STATİK VE DİNAMİK ANALİZİ



DOKTORA TEZİ

**Gülçin TEKİN ÖZKAN
(501112004)**

İnşaat Mühendisliği Anabilim Dalı

Yapı Mühendisliği Programı

Tez Danışmanı: Doç. Dr. Fethi KADIOĞLU

ARALIK 2017

Gülçin Tekin Özkan, a Ph.D. student of İTÜ Graduate School of Science Engineering and Technology student ID 501112004, successfully defended the dissertation entitled “QUASI-STATIC AND DYNAMIC ANALYSIS OF VISCOELASTIC PLATES”, which she prepared after fulfilling the requirements specified in the associated legislations, before the jury whose signatures are below.

Thesis Advisor : **Assoc. Prof. Dr. Fethi KADIOĞLU**
Istanbul Technical University

Jury Members : **Prof. Dr. Abdullah AVEY**
Süleyman Demirel University

Asst. Prof. Dr. Hale ERGÜN
Istanbul Technical University

Prof. Dr. Tülay Aksu ÖZKUL
Istanbul Technical University

Assoc. Prof. Dr. Zafer KÜTÜĞ
Yıldız Technical University

Date of Submission : 06 November 2017

Date of Defense : 08 December 2017





To all of my family members,



FOREWORD

First of all, I am very thankful to all people who supported me to complete my Ph.D. thesis. I would like to express my sincere gratitude to my thesis advisor Assoc. Prof. Dr. Fethi KADIOĞLU for his invaluable guidance, encouragement and continuous support throughout the preparation of this thesis.

I also want to show my deepest appreciation to Prof. Dr. Ahmet Yalçın AKÖZ for encouraging my studies, for his valuable advices and his support while this thesis was taking shape.

This gratitude also extends to Prof. Dr. Abdullah AVEY and Asst. Prof. Dr. Hale ERGÜN for serving as thesis committee members.

I am specially thankful to my family for their patience and endless support over my whole education period.

My deepest appreciation goes to my husband for his constant encouragement throughout the research period and the course of this thesis.

I gratefully acknowledge the support of the Scientific and Technological Research Council of Turkey through project 213M332 and of the Research Foundation of Istanbul Technical University through project 37961.

November 2017

Gülçin TEKİN ÖZKAN



TABLE OF CONTENTS

	<u>Page</u>
FOREWORD	ix
TABLE OF CONTENTS	xi
ABBREVIATIONS	xiii
SYMBOLS	xv
LIST OF TABLES	xvii
LIST OF FIGURES	xix
SUMMARY	xxi
ÖZET	xxv
1. INTRODUCTION	1
1.1 Purpose of Thesis	4
1.2 Literature Review	6
1.3 Hypothesis	15
2. THEORY OF VISCOELASTICITY	17
2.1 Linearity	19
2.2 Linear Elastic Spring	19
2.2.1 Response to stress loading	20
2.2.2 Response to strain loading	20
2.3 Linear Viscous Dashpot	21
2.3.1 Response to stress loading	22
2.3.2 Response to strain loading	22
2.4 Rheological Models.....	23
2.4.1 Maxwell-Wiechert model	23
2.4.1.1 Response to stress loading	24
2.4.1.2 Response to strain loading	26
2.4.2 Kelvin-Voight model	27
2.4.2.1 Response to stress loading	28
2.4.2.2 Response to strain loading	30
2.5 Classification of Rheological Models	31
2.6 Standard Linear Solid.....	32
2.6.1 Three parameter standard solid model	33
2.6.2 Zener model	33
2.7 Operator Forms of Rheological Models	34
2.7.1 Differential operator form	34
2.7.2 Integral operator form	35
3. THEORY OF PLATES	39
3.1 Basic Assumptions	41
3.2 Fundamental Equations	42
3.2.1 Equilibrium equations	42
3.2.2 Kinematic equations (strain-displacement equations)	43
3.2.3 Compatibility equations	45
3.2.4 Constitutive equations.....	46
4. INTEGRAL TRANSFORMS	53

4.1 Heaviside Unit Step Function.....	54
4.2 Dirac Delta Function	56
4.3 The Laplace Transform	58
4.4 Basic Properties of the Laplace Transform	58
4.4.1 Linearity of Laplace transform.....	59
4.4.2 Shift property of Laplace transform	59
4.4.3 Derivative property of Laplace transform.....	59
4.4.4 Convolution property of Laplace transform.....	59
4.5 The Laplace-Carson Transform.....	60
4.6 Field Equations in Laplace-Carson Domain.....	60
5. VARIATIONAL PRINCIPLES.....	63
5.1 The Gâteaux Differential Method	65
5.1.1 Definition 1	65
5.1.2 Definition 2	66
5.2 Potential Operator.....	66
5.2.1 Theorem 1	66
5.2.2 Theorem 2	67
5.3 Functional.....	67
6. FINITE ELEMENT FORMULATION	73
6.1 Finite Element Method	73
6.2 Coordinate Transformation	79
6.3 Basic Steps to Obtain Element Matrix	82
6.4 Element Matrix in Laplace-Carson Domain.....	82
7. INVERSE TRANSFORM TECHNIQUES.....	87
7.1 Method of Maximum Degree of Precision (MDOP).....	88
7.2 Method of Dubner and Abate	89
7.3 Method of Durbin	90
7.4 Comparison of the Methods of Numerical Laplace Transform Inversion	91
7.4.1 Example 1.....	91
7.4.2 Example 2.....	94
7.4.3 Example 3.....	96
8. ILLUSTRATIVE EXAMPLES AND DISCUSSION	99
8.1 Example 1.....	102
8.2 Example 2.....	104
8.3 Example 3.....	107
8.4 Example 4.....	110
8.5 Example 5.....	111
8.6 Example 6.....	112
8.7 Example 7.....	113
8.8 Example 8.....	114
8.9 Example 9.....	115
8.10 Example 10.....	116
8.11 Example 11.....	117
8.12 Example 12.....	119
8.13 Example 13.....	120
8.14 Example 14.....	123
8.15 Example 15.....	123
9. CONCLUSIONS AND RECOMMENDATIONS	125
REFERENCES	129
CURRICULUM VITAE.....	137

ABBREVIATIONS

MDOP	: Maximum Degree of Precision
<i>ode(s)</i>	: Ordinary Differential Equation (s)
<i>pde(s)</i>	: Partial Differential Equation (s)
VPLT16	: Viscoelastic Plate Element





SYMBOLS

$aT, N, \Delta t$: Parameters control the flow of the numerical precision
D^*	: Operator Form of the Flexural Rigidity of the Plate
E^*	: Operator in the Hereditary Integral Form
E_i	: Linear Spring Constants, Young's Modulus
$F(s)$: Laplace Transform of a function $f(t)$
$\bar{F}(s)$: Laplace-Carson Transform of a function $f(t)$
h	: Thickness
$H(t)$: Heavise Unit Step Function
$I(u)$: Functional
$J(t)$: Creep Compliance
k_w	: Modulus of Foundation
L_x, L_y	: Length
$L\{ \}$: Laplace Operator
$L^{-1}\{ \}$: Inverse Laplace Operator
M_x, M_y	: Bending Moments
M_{xy}	: Twisting Moment
N_x, N_y	: In-plane Membrane Forces
N_{xy}	: In-plane Shear Force
P	: Point Load
$p_x, p_y, p_z = q$: Applied Distributed Loads in the x , y , and z directions
Q	: Operator
Q_x, Q_y	: Transverse Shear Forces
s	: Laplace Parameter
t	: Time
u, v, w	: Displacement Components in the x , y , and z directions
ω	: Vibration Frequency
x, y, z	: Cartesian Coordinate System
X, Y, Z	: Body Force Components in the x , y , and z directions
$Y(t)$: Relaxation Modulus
$[,]$: Inner Product
ρ	: Material Density
ψ	: Approximation or Interpolation or Shape Function
ν	: Poisson's Ratio
τ_r, τ_c	: Relaxation Time, Retardation or Creep Time
$\delta(t)$: Dirac Delta Function
η_i	: Linear Viscous Dashpot Constants, Viscosity Coefficient
σ	: Stress, Normal Stress Component
ε	: Strain, Normal Strain Component
τ_{ij}	: Tangent (Shear) Stress Component
γ_{ij}	: Shear Strain Component
φ	: Angle of Rotation of the Normal to the Middle Surface
κ	: Curvature of the Section



LIST OF TABLES

	<u>Page</u>
Table 7.1 : Performance of the MDOP method	94
Table 8.1 : Creep compliance functions of viscoelastic material models	102





LIST OF FIGURES

	<u>Page</u>
Figure 2.1 : Strain versus time plot for purely elastic deformation	17
Figure 2.2 : Strain versus time plot for purely plastic deformation	17
Figure 2.3 : Strain versus time plot for purely viscous deformation.....	18
Figure 2.4 : Strain versus time plot for viscoelastic deformation.	18
Figure 2.5 : Mechanical model of linear elastic spring.....	20
Figure 2.6 : Mechanical model of linear viscous dashpot.....	21
Figure 2.7 : Maxwell-Wiechert model.....	23
Figure 2.8 : Creep and recovery behavior of the Maxwell model	26
Figure 2.9 : Stress relaxation behavior of the Maxwell model	27
Figure 2.10 : Kelvin-Voight model.....	28
Figure 2.11 : Creep and recovery behavior of the Kelvin model.....	30
Figure 2.12 : Stress relaxation behavior of the Kelvin model	31
Figure 2.13 : Various combinations of Three-element and Four-element models (Findley et al, 1976).....	32
Figure 2.14 : Three parameter standard solid model	33
Figure 2.15 : Zener model.....	34
Figure 2.16 : Stress-time response of linear material generated from a superposition of step functions of strain versus time	36
Figure 2.17 : Linear superposition to derive hereditary integral.....	36
Figure 3.1 : Rectangular plate and associated coordinate system.....	41
Figure 3.2 : Stress components on plate element.....	42
Figure 3.3 : Angular deformation	45
Figure 3.4 : Section before and after deformation	47
Figure 3.5 : Force and moment resultants acting on a plate element.....	50
Figure 4.1 : Basic idea behind use of a transform for <i>odes</i>	54
Figure 4.2 : Heaviside unit step function	55
Figure 4.3 : Heaviside unit step function $H(t - t_0)$	55
Figure 4.4 : Impulse function $\delta_\epsilon(t - t_0)$	56
Figure 6.1 : (a) Finite element discretization of a one-dimensional domain (b) Linear finite element approximation over an element	75
Figure 6.2 : (a) Linear approximation (b) Quadratic approximation	77
Figure 6.3 : (a) Linear rectangular element (b) its interpolation functions.....	78
Figure 6.4 : Transformation of quadrilateral elements to the master element for numerical evaluation of integrals.....	80
Figure 6.5 : Interpolation functions for one-dimensional element in terms of the local coordinate ξ	81
Figure 6.6 : Interpolation functions for two-dimensional element in terms of the local coordinate system (ξ, η)	81
Figure 6.7 : Global and local coordinate system of rectangular master element	83
Figure 6.8 : Flowchart for Fortran program.....	86
Figure 7.1 : Effect of the changes in the value of the n parameter	92

Figure 7.2 : Effect of the changes in the value of the aT parameter in Dubner & Abate.....	95
Figure 7.3 : Effect of the changes in the value of the aT parameter in Durbin.....	96
Figure 7.4 : Effect of the changes in the value of the N parameter in Dubner & Abate.....	97
Figure 7.5 : Effect of the changes in the value of the N parameter in Durbin.....	98
Figure 8.1 : Geometrical properties of the simply supported plate subjected to a uniform pressure load $q = q(x, y)$	99
Figure 8.2 : Time histories of external loads.....	100
Figure 8.3 : Rheological models: mechanical analog for the Kelvin (a), Three-parameter-solid (b), Zener (c), Kelvin-chain (d) and Four-parameter-solid (e) model.....	101
Figure 8.4 : Comparison of theoretical and calculated deflection results under Type I loading (a) distributed load, (b) point load.....	103
Figure 8.5 : The displacement-time variation of the center point of an elastic plate.....	104
Figure 8.6 : Effect of the changes in the value of the aT parameter.....	106
Figure 8.7 : The displacement and bending moment-time variation results for the damping ratio $\eta/E = 1$	108
Figure 8.8 : Effect of different η/E ratios.....	111
Figure 8.9 : Comparison of theoretical and calculated deflection results of viscoelastic plates under point load.....	111
Figure 8.10 : Effect of the different η/E ratios under point load.....	112
Figure 8.11 : Variation of different E/E_1 ratio curves when the damping ratio equals to 1,5.....	112
Figure 8.12 : Comparison between different rheological models.....	113
Figure 8.13 : Time-dependent displacement response of a viscoelastic Kirchhoff plate with or without elastic foundation interaction.....	115
Figure 8.14 : Comparison between the two adopted viscoelasticity models.....	116
Figure 8.15 : Simply supported plate of variable thickness.....	116
Figure 8.16 : Variation of time-dependent displacements at the center of the viscoelastic plate with constant thickness (a) and with variable thickness (b) and (c).....	117
Figure 8.17 : Effect of different η/E and η_1/E_1 ratios.....	118
Figure 8.18 : The displacement-time variation results of viscoelastic plates under wave-type loading Type VI employing Durbin's method.....	119
Figure 8.19 : The displacement-time variation results of viscoelastic plates under wave-type loading Type VII employing Durbin's method.....	119
Figure 8.20 : Effect of viscosity coefficient on the vibration period and amplitude of displacement.....	121
Figure 8.21 : Effect of plate thickness on the vibration period and amplitude of displacement.....	122
Figure 8.22 : Dynamic behavior of Kelvin solid model.....	123
Figure 8.23 : Effect of foundation interaction on the vibration period and amplitude of displacement.....	124

QUASI-STATIC AND DYNAMIC ANALYSIS OF VISCOELASTIC PLATES

SUMMARY

The behavior of real bodies under external loads constitutes a significant part of solid mechanics. Rheology is the science, which studies the behavior of the material under the influence of applied stress. The mathematical form of the rheology is called the constitutive equations or stress-strain relations. This is, of course, an ideal case since all materials change shape, namely to undergo deformation when the self-weight of the materials is considered as a factor that causes stress. The amount of deformation changes depending on the amount of applied stress, environmental conditions (such as ambient temperature), rate and duration of loading and type of material. The behavior of materials can be divided into three main groups under different stress and temperature conditions: (1) Elastic behavior (2) Plastic behavior (3) Viscous behavior. Elastic behavior is time-independent. An elastic body undergoes an instantaneous strain, with stress application and the strain stays constant under the constant stress. The strain in the elastic body only depends upon the final value of stress and not upon its history. Plastic behavior is also time-independent. When a body that shows plastic behavior is stressed beyond the yield point, it experiences instantaneous deformation followed by plastic deformation. Plastic deformation, regardless of time and rate of loading, depends only on the maximum value of the stress in the past. In viscous behavior, stress is proportional to strain rate. When the body that exhibits viscous behavior is loaded, the deformation is not instantaneous but delayed and it increases with time. When the load is removed, there is a permanent deformation. There are also transition regions between the main groups of behavior. Numerous materials exhibit both viscous and elastic behavior under the applied stress. Viscoelastic behavior is commonly composed of combinations of elastic and viscous behavior.

There are some phenomena that occur in viscoelastic bodies such as instantaneous elasticity, creep, stress relaxation, instantaneous elastic recovery, delayed recovery and permanent or viscous deformation. The rate of loading and duration of applied load affect deformation of a viscoelastic material. The resulting strain will be the same regardless of the rate of loading for the elastic and plastic behavior; however, in a viscoelastic substance, the slow loading results in higher strain than the faster loading. The strain value at any time depends upon the whole stress history.

The values of strain should be limited in addition to the values of stress of structural systems in practice. For example, creep phenomenon occurs in metals at elevated temperatures and in concrete, wood and plastics at normal (room) temperatures. Special precautions that minimize the effects of creep should be taken especially in high-rise buildings. Moreover, machine components that operate at high temperatures, asphalt pavements deform under stress and these deformations are mostly irreversible. Another important phenomenon, which is actually in direct relation to the creep, is relaxation. The relaxation phenomenon should also be considered in some application areas. For instance, it is expected that the time dependent relaxation of stress in steel, which is used in prestressed reinforced concrete elements should be low.

This and other similar examples that represent the time dependence of the mechanical behavior of materials necessitate the need for considering time as a variable. A constitutive equation of viscoelastic behavior includes time as a variable in addition to the stress and strain variables.

It is very important to model the time-dependent behavior, in other words, viscoelastic behavior properly for the accurate analysis of structures made of viscoelastic materials. The most commonly used method by the science of rheology is to develop some rheological models and to make laws of deformation with the help of these models. With this purpose, starting with standard rheological models in literature (such as Kelvin, Maxwell, etc.) behavior of plates represented by different mechanical models is discussed within the scope of thesis for a more realistic approach.

Plates are important structural elements having more than one function. One of the main functions of plates is to transfer the applied loads to the supporting members of load-bearing system properly and the other one is to form a convenient basis for its purpose by providing continuity between members of load-bearing system. The fact that plates are one of the most commonly used structural elements in engineering makes the plate theories and applications as an interesting research topic.

In this thesis study, quasi-static and dynamic analysis of plates modeled with viscoelastic constitutive equations is studied under different types of time dependent loads considering the Kirchhoff plate theory that ignores the transverse shear stress.

Due to the difficulty of obtaining closed-form solutions for the problems which have complex geometries, loading conditions and constitutive relations, numerical solution techniques are employed. The finite element method is widely used because it is systematic and suitable for programming and it can be easily applied to solve complex problems in engineering disciplines.

In this study, which examines linear viscoelastic plate problems, a mixed finite element formulation is developed. By applying the Gâteaux differential approach, a new functional that includes the boundary conditions of the problem is proposed through the potential operator condition is satisfied. Hereditary integral form of the constitutive law is used in order to represent the viscoelastic behavior. The solutions obtained in the Laplace-Carson domain are transformed into the real-time domain using various numerical inverse Laplace transform methods. With this study, the performance of the numerical inverse transformation techniques such as Maximum Degree of Precision (MDOP), Dubner & Abate and Durbin are compared and, the detailed information is given about the content, parameter, precision, advantages/disadvantages and so on of transform methods. A special computer program is developed in Fortran programming language in order to perform analysis.

The unique aspects of this thesis study and the possible contributions of the proposed method to the literature can be summarized as follows: by using this new functional, moment and shear force values that are important for engineers can be obtained directly without any mathematical operation. In addition, geometric and dynamic boundary conditions can be obtained easily and a field variable can be included to the functional systematically. Moreover, shear locking problem can be eliminated.

The effectiveness of the mixed finite element formulation developed for the analysis of viscoelastic Kirchhoff plates is shown by several numerical examples. In addition, it is aimed to form the base for the analysis of viscoelastic plate problems by considering the original problems that have not been discussed in the literature yet.

The studies that use the formulation proposed within the scope of the thesis for the analysis of viscoelastic structural elements with arbitrary geometries still continue. Thus, the gap in the literature related to the analysis of viscoelastic structural elements with complex geometries will be able to fill and viscoelastic analysis, which is a more realistic approach, will be widely used for the investigation of engineering structures in the future.





VİSKOLEASTİK PLAKLARIN KUAZİ-STATİK VE DİNAMİK ANALİZİ

ÖZET

Reel cisimlerin dış yükler altındaki davranışı, katı cisim mekaniğinin önemli bir bölümünü teşkil eder. Reoloji maruz kalınan gerilmeye karşı malzemenin davranışını inceleyen bilim dalıdır. Reolojinin matematiksel ifadesi ise bünye denklemleri veya gerilme-şekil değiştirme bağıntıları olarak adlandırılır. Malzemelerin kendi ağırlıklarının da gerilme yaratan bir unsur olduğu düşünüldüğünde, her malzemenin şekil değiştirmesi yani deformasyona uğraması kaçınılmazdır. Şekil değişimi miktarı cismin maruz kaldığı gerilmenin şiddetine, çevre koşullarına, yükleme hızı ve süresine ve malzeme türüne göre değişir. Değişik gerilme ve sıcaklık koşulları altında cisimlerin davranışları üç ana gruba ayrılır: (1) Elastik davranış (2) Plastik davranış (3) Viskoz davranış. Elastik davranış zamandan bağımsızdır. Elastik cisimlerde şekil değiştirme gerilme ile aynı anda oluşur, gerilme sabit kalınca şekil değiştirme sabit kalır. Elastik cisimlerde şekil değiştirme gerilmenin son değerine bağlıdır, geçmişte aldığı değerlerin etkisi yoktur. Plastik davranışta zamandan bağımsızdır. Bu tür davranış gösteren cisme akma sınırının üstüne çıkan bir gerilme uygulandığında, ani şekil değiştirme ve onu izleyen plastik şekil değiştirme oluşur. Plastik şekil değiştirme zamandan ve yükleme hızından bağımsız olarak sadece gerilmenin geçmişte aldığı en büyük değerine bağlıdır. Viskoz davranışta gerilme ile şekil değiştirme hızı orantılıdır. Bu tür davranış gösteren cisme gerilme uygulandığında deformasyon aniden olmaz, gecikmeli şekil değişimi gösterir ve şekil değişimi zamana bağlı olarak artar. Yük kaldırıldığında, deformasyon kalıcıdır. Bu ana davranış grupları arasında geçiş bölgeleri de vardır. Pek çok malzeme gerilmeler altında hem elastik hem de viskoz davranış gösterir. Viskoelastik davranış genellikle viskoz davranışla elastik davranışın karışımlarından oluşur.

Viskoelastik davranış gösteren cisimlerde ani elastik uzama, sünme, gevşeme, ani elastik toparlanma, gecikmiş toparlanma ve kalıcı veya viskoz şekil değiştirme gibi olaylar gerçekleşir. Viskoleastik malzemede, yükleme hızının ve süresinin oluşacak şekil değiştirmeye etkisi vardır. Yükleme hızı ne olursa olsun elastik ve plastik davranışta aynı gerilme altında oluşan son şekil değiştirmeler aynı olacaktır ancak viskoleastik cisimde yavaş yükleme sonunda oluşan şekil değiştirme, hızlı yüklemenin sonunda oluşacak şekil değiştirmeden daha büyük olur. Herhangi bir andaki şekil değiştirme gerilmenin geçmişte aldığı bütün değerlere bağlıdır.

Uygulamada yapı sistemlerinde gerilmenin yanında şekil değiştirmenin de sınırlı olması gerekir. Örneğin metallerde yüksek sıcaklıklarda; beton, ahşap ve plastiklerde ise oda sıcaklığında sünme olayı gerçekleşir. Özellikle yüksek binalarda sünme etkisini azaltıcı önlemler almak gerekir. Ayrıca asfalt kaplamalar, yüksek sıcaklıkta çalışan makina parçaları gerilme altında deforme olurlar ve bu deformasyonlar çoğu kez tam olarak geri dönmezler. Gerçekte sünme olayından kaynaklanan bir diğer önemli olay ise gevşemedir. Gevşeme olayının da bazı uygulama alanlarında göz önüne alınması gerekir. Örneğin öngerilmeli betonarme elemanlarda kullanılan donatı çeliklerinde zamanla oluşacak gevşemenin düşük olması istenir.

Malzemelerin mekanik davranışlarının zamana bağlılığını temsil eden bu ve benzeri birçok örnek, zamanın da bir değişken olarak hesaba katılması gerekliliğini zorunlu kılmıştır. Viskoelastik davranışta bünye denklemlerinde gerilme ve şekil değiştirmenin yanında bir de zaman değişkeni vardır.

Zamana bağlı davranışın, diğer bir deyimle viskoelastik davranışın doğru bir şekilde modellenmesi, bu malzemeden yapılmış olan yapıların doğru analizi için son derece önemlidir. Reoloji biliminin en çok yararlandığı yöntem bir takım reolojik modeller geliştirmek ve bunların yardımı ile şekil değişimleriyle ilgili yasaları çıkarmaktır. Bu amaçla, tez kapsamında literatürdeki standart reolojik modellerden (Kelvin, Maxwell, vb.) başlanarak, daha gerçekçi yaklaşım için değişik mekanik modellerin temsil ettiği plak davranışları ele alınmıştır.

Plaklar, birden fazla işleve sahip önemli yapı elemanlarıdır. Plakların ana işlevlerinden biri, üzerine etkiyen yükleri oturduğu taşıyıcı sistem elemanlarına sağlıklı bir şekilde aktarmak, diğeri ise taşıyıcı sistem elemanları arasındaki sürekliliği sağlayarak işlevine uygun bir zemin oluşturmaktır. Mühendislikte plakların yaygın kullanım alanına sahip olan yapı elemanlarından biri olması, plak teorilerini ve uygulamalarını ilgi çekici araştırma konusu haline getirmiştir.

Bu tez çalışmasında, kalınlık doğrultusundaki kayma gerilmelerini göz ardı eden Kirchhoff plak teorisi esas alınarak, viskoelastik bünye denklemlerine sahip plakların zamanla değişen farklı yükleme türleri için kuazi-statik ve dinamik analizleri yapılmıştır.

Karmaşık geometrilere, yükleme koşullarına ve bünye denklemlerine sahip problemlerin kapalı çözümlerini elde etmede yaşanan zorluklardan dolayı, sayısal çözüm yöntemleri uygulanmaktadır. Sonlu elemanlar yöntemi, sistematik ve programlamaya elverişli olması ve mühendislik disiplinlerindeki karmaşık problemlerin çözümünde kolaylıkla uygulanabilmesinden dolayı yaygın olarak kullanılmaktadır.

Lineer viskoelastik plak problemlerinin incelendiği bu tez çalışmasında Laplace-Carson uzayında bir karışık sonlu eleman formülasyonu geliştirilmiştir. Gâteaux diferansiyel yaklaşımı uygulanarak, potansiyel operator koşulunun sağlatılması ile probleme ait sınır koşullarını da içeren yeni bir fonksiyonel önerilmiştir. Viskoelastik davranışı temsil etmek için Hereditary (bellekli) integral tipinde bünye bağıntıları kullanılmıştır. Laplace-Carson uzayında elde edilen çözümler, çeşitli sayısal ters Laplace dönüşüm yöntemleri kullanılarak gerçek zaman uzayına dönüştürülmüştür. Bu çalışma ile, En Büyük Duyarlılık Derecesi (MDOP), Dubner & Abate ve Durbin gibi sayısal ters dönüşüm tekniklerinin performansları kıyaslanmış ve dönüşüm yöntemlerinin içerikleri, parametreleri, hassasiyetleri, karşılıklı üstünlükleri vb. hakkında detaylı bilgi verilmiştir. Analizlerin gerçekleştirilebilmesi için Fortran programlama dili kullanılarak özel bir bilgisayar programı hazırlanmıştır.

Bu tez çalışmasının özgün değerleri ve önerilen yöntemin literatüre yapacağı katkılar şu şekilde özetlenebilir: önerilen yeni fonksiyonel kullanılarak, mühendislikte önemli olan moment ve kesme kuvveti değerleri doğrudan elde edilebilir. Buna ek olarak, probleme ait geometrik ve dinamik sınır koşulları kolaylıkla elde edilebilir ve herhangi bir alan değişkeni sistematik bir biçimde fonksiyonele aktarılabilir. Ayrıca, kayma kilitlenmesi gözlenmez.

Viskoelastik Kirchhoff plaklarının analizi için geliştirilen karışık sonlu eleman formülasyonunun etkinliği çeşitli sayısal uygulamalarla gösterilmiştir. Ayrıca

literatürde hiç ele alınmamış özgün problemlerin çözümü yapılarak viskoelastik plak problemlerinin analizi ile ilgili alt yapı oluşturulması hedeflenmiştir. Tez çalışması kapsamında sunulmuş bu yöntemin keyfi geometriye sahip viskoelastik yapı elemanlarının analizi için de kullanılması yönünde çalışmalar devam etmektedir. Böylece literatürde karmaşık geometrilere sahip viskoelastik yapı elemanlarının analizi ile ilgili boşluk doldurulabilecek ve daha gerçekçi olan viskoelastik analiz gelecekteki mühendislik yapılarının incelenmesinde çok daha yaygın olarak kullanılabilir.





1. INTRODUCTION

Plates are one of the most significant structural members which are used extensively in all fields of engineering such as bridge buildings, high-rise buildings, hydraulic structures, aircraft structures, etc. Because of the applications requiring high-load carrying capacity, lightweight, economic and technological effectiveness, it becomes very important to understand the behavior of plates.

If we look at the development of plate theory history, various plate theories are developed depends on the changes in structural materials. In the context of the plate theories, two different limit cases are usually considered one of which is the Kirchhoff's (classical thin) plate theory and the other one is the Reissner-Mindlin's plate theory. Reissner-Mindlin's first order shear deformation plate theory can be used for somewhat thicker plates when compared to Kirchhoff's plate theory and considers the influence of the transverse shear deformation on the deflection of the plate. Kirchhoff's plate theory forms the basis for calculating and designing of engineering structures and has widespread use in practice.

The classical (thin) plate theories assume that the material of the plate is linear elastic based on the fundamental assumption of the linear, elastic, small-deflection theory of bending. For linear elastic materials, the stress is proportional to the strain and when the external force is removed, internal forces generated by the deformation disappear. The deformation depends on many factors such as geometrical configuration of the body, the applied load, the exposure time, the mechanical properties of the material, etc.

Due to the internal forces dominate the response; characterizing the stress-strain relation of the material becomes a major concern in the practical design and analysis of engineering structures.

To simplify the analysis, it is generally assumed that the material behavior is elastic. However, in reality, most engineering materials exhibit noticeable time-effects. Therefore, real materials have viscous and elastic properties simultaneously due to

internal friction and time-dependent deformation so they are named as viscoelastic. In viscoelastic materials, viscosity, which is defined as the ratio of stress to strain rate, affects the time-dependent response. An instantaneous elastic response is observed upon loading then a slow and continuous change occurs in the response at a decreasing rate.

With regard to the actual material behavior, viscoelastic constitutive relations should be used instead of elastic constitutive relations for determination of the most realistic results. Hence, it is crucial to fully understand the mechanism and response of viscoelastic materials in order to analyze the behavior of structural components properly.

The constitutive equations of viscoelastic materials may be either linear or nonlinear. However, the assumptions of linear viscoelastic analysis will be considered in this thesis.

Theory of linear viscoelasticity focuses on the history of stress or strain. The behavior of viscoelastic materials modeled mathematically using mechanical analogs consisting of springs and dashpots. Spring and dashpot are the basic elements and used for modeling the elastic and viscous behaviors of viscoelastic materials, respectively.

In order to describe a wide range of linear viscoelastic materials, various combinations of spring and dashpot elements in series and/or parallel arrangement are used. To capture viscoelastic phenomena, the most commonly used models are the Maxwell model, the Kelvin-Voight model and complex combinations of these elementary models. The Maxwell model represents the material shows a typical property of a fluid whereas the Kelvin-Voight model represents the material shows a typical property of a solid. Neither the Kelvin-Voight solid model nor the Maxwell fluid model is sufficient for describing the response of linear viscoelastic solids and fluids certainly. Combinations of the classical models are used to illustrate the actual material's viscoelastic behavior that it undergoes strain slowly varying with time under constant stress (it creeps) and the stress in response to a constant strain diminishes gradually with time (it relaxes).

There are basically three approaches used in linear viscoelastic analysis. They are Laplace transformation, Fourier transformation and direct time integration method. Laplace transform and Fourier transform are used for solving differential equations

easily by turning differential equations into algebraic equations. Laplace and Fourier transformation approaches involve solving the problem in the transformed domain and reverting the results into the physical domain by applying inverse transformation. In the direct time integration approach, analysis involves the integration of the behavior over a series of time steps. Correspondence principle (the elastic-viscoelastic analogy) is another procedure in linear theory of viscoelasticity that is carried out by transforming the governing equations of viscoelastic problem into a set of corresponding elastic governing equations.

When these approaches are compared, Laplace transformation seems to be simpler and more efficient if an accurate numerical inverse transform method is available. There are many methods such as Schapery, Fourier, Durbin, Dubner & Abate and Maximum Degree of Precision (MDOP) in literature for numerical inversion.

Furthermore, Laplace-Carson transformation can also be used for the linear viscoelastic problems. Several studies exist in literature which calculated the linear viscoelastic response of the structure in the Laplace-Carson domain. In the present study, method of Laplace-Carson transform will be utilized for the analysis.

To analyze viscoelastic problems, most of the analytical methods use correspondence principle. However, an application of this method is restricted to very limited problems with simple geometry and loading conditions (Vallala et al, 2012). For the problems have complex geometries, loadings and constitutive relations, closed-form solution are often not possible and numerical solution techniques should be employed. Finite element method is one of the most powerful numerical solution techniques and has ability to handle all types of analysis in structural mechanics. The application of the Finite element method is the most common and has been presented by a number of authors. However, one well-known problem associated with the finite element analysis of the plate elements is shear-locking phenomenon. Whenever the plate thickness decreases, locking effect is clearly observed. To avoid shear locking, alternative finite element formulations (mixed type) are widely used.

Researchers suggested many principles to formulate mixed type finite element formulations. The Hellinger-Reissner and the Hu-Washizu principles are more popular ones and these variational principles are based on the minimization of the energy functional. Hellinger-Reissner principle involves stresses and displacements as

fundamental unknown variables. Hu-Washizu principle is a generalization of Hellinger-Reissner principle and involves stresses, strains and displacements as functional arguments. In derivation of a functional, the Gâteaux Differential method is more powerful and efficient variational tool when compared to conventional variational principles, Hellinger-Reissner and Hu-Washizu.

In this thesis, the quasi-static and dynamic behavior of viscoelastic Kirchhoff plates is studied numerically by using the mixed finite element method in transformed Laplace–Carson space. In the transformed Laplace–Carson space, a new functional has been constructed for viscoelastic Kirchhoff plates through a systematic procedure based on the Gâteaux differential. For numerical inversion, the Maximum Degree of Precision (MDOP), Dubner & Abate’s, and Durbin’s transform techniques are employed. The developed solution technique is applied to several quasi-static and dynamic example problems.

1.1 Purpose of Thesis

Most engineering materials exhibit viscoelastic properties with deformation depending on load and time. While the material undergoes deformation, energy dissipation occurs due to internal friction. Viscoelastic materials have a mix of two simple behaviors, viscous and elastic behaviors. Viscoelastic materials show pronounced influence of the rate of loading and display creep and relaxation. Such a material shows a slowly increasing deformation with time under sustained constant stress, that is, it creeps; and the stress diminishes gradually with time if deformed at constant strain, that is, it relaxes.

In certain cases, a viscoelastic evaluation is sufficiently complicated to challenge because modelling the behavior of progressive deformations (i.e., suffer from creep, relaxation and hysteresis problems) along the long-term structural response involves mathematical complexity.

Analysis of the structural elements like beams, plates or shells subjected to time varying loadings is one of the well-established areas of applied mechanics. Although many research activities have been devoted toward the development of theoretical and computational methods for the viscoelastic analysis of beams, very little has been done to analyze time-dependent (viscoelastic) behavior of plates. As a consequence of the

increasing applications of plates constructed with various shapes, it becomes increasingly important to be able to characterize the viscoelastic response of plates.

In this sense, the main objective of this thesis is to perform quasi-static and dynamic analysis of viscoelastic Kirchhoff plates. The other objectives and an outline of this thesis can be given as follows:

- to obtain the field equations for the viscoelastic Kirchhoff plates
- to utilize the method of the Laplace-Carson transform in order to remove the time derivatives from governing equations and boundary conditions
- to obtain the field equations in the Laplace-Carson space
- to construct a new functional for viscoelastic Kirchhoff plates through a systematic procedure based on the Gâteaux Differential method. In this functional, there exists four independent variables such as deflection w , internal forces (bending moments M_x and M_y , and twisting moment M_{xy}). In addition to this, dynamic and geometric boundary condition terms are included in the functional in a systematic way
- to develop mixed finite element formulations for viscoelastic Kirchhoff plates in the Laplace-Carson space
- to develop computer program in order to perform calculations in transformed space
- to analyze the problem and obtain the solutions in transformed space by applying the developed computer program
- to apply various numerical inverse transform techniques for transformation of the solutions obtained in the Laplace-Carson domain to the time domain
- to test the performance of the different inverse transform methods and to identify suitable methods for inverse transformation
- to compare the results of the present study with the results of the other studies available in the literature and to demonstrate the validity and effectiveness of the procedure for different time-dependent loads and viscoelastic material models
- to verify the results with different examples and to evaluate and discuss the obtained results

The possible contributions of this thesis to the scientific knowledge can be stated as follows:

- Mechanics of viscoelastic media is a challenging problem for researchers. Since performing viscoelastic analysis is believed to be too complicated, numerical studies in this area are relatively limited. This study presents a new mixed type finite element formulation based on the Gâteaux differential method for the quasi-static and dynamic analysis of linear viscoelastic Kirchhoff plates. The characteristics of the element are;
 - i. Simple, reliable, and efficient in computations
 - ii. Fairly accurate moment and shear force predictions
 - iii. Directly obtained boundary condition terms (geometric and dynamic)
 - iv. No shear-locking effect for very thin structures
- A numerical methodology discussed in this thesis can easily be applied for the analysis of viscoelastic structural members like laminated composite beams according to different beam theories, shells with complex geometry and constitutive relations, and plates with different theories in bending. Thus, new research infrastructures can be built for future studies.

1.2 Literature Review

Since the plate elements are being increasingly used in all fields of engineering, a considerable amount of research has been devoted to this subject. In order to describe the behavior of plates, various theories have been developed. The interested reader is referred to Timoshenko (1953), Truesdell (1968), Ventsel and Krauthammer (2001) and Szilard (2004) for more information about the historical background of the plate theories and their applications.

Of the numerous plate theories, two are widely accepted and used in engineering depending on whether transverse shear deformation is considered or not considered. These theories are Kirchhoff-Love (classical) plate theory (Kirchhoff, 1850) and Reissner-Mindlin (first-order shear) plate theory (Reissner, 1944, 1945 and Mindlin, 1951). Kirchhoff-Love plate theory is used for the analysis of thin plate of which its thickness to width ratio is less than 0,1 and for the analysis of plates with small deflections as the maximum deflection of the plate is less than two tenths of its thickness. Kirchhoff-Love plate theory neglects transverse shear deformation in the plate thickness whereas Reissner-Mindlin plate theory takes into account the influence of the transverse shear deformation on the deflection of the plate. The theory developed

by Mindlin also includes the effects of rotary inertia in addition to the effect of the transverse shear deformation. The reader is referred to relevant research papers Donnell et al. (1946), Salerno and Goldberg (1960) and Voyiadjis et al. (1985) for more information about the assumptions of these theories.

There are many works in the literature on the static and dynamic analysis of plates with various theories and geometries because determination of the plate deformations and stresses when it is subjected to loads is an important engineering problem. Initially, researchers usually focused on elastic problems, but when viscoelastic materials found wider utilization in practice, the need for studies on viscoelastic problems has increased. Assuming the material is elastic for simplification of the analysis proves to be inconsistent with reality due to the fact that most engineering materials exhibit noticeable time-effects and they are viscoelastic because of internal friction. Therefore, viscoelastic constitutive relations are more realistic than elastic constitutive relations to reflect the material behavior. The theoretical and mathematical background of viscoelasticity has long been established by Gurtin and Sternberg (1962), Pipkin (1972), Flügge (1975), Findley et al. (1976), Christensen (1982), Reddy (2008), Lakes (2009) and Gutierrez-Lemini (2014).

In structural analysis of time-dependent materials, linear viscoelasticity has been used for a long time. There are basically three approaches that can be used in linear viscoelastic analysis: Laplace transformation, Fourier transformation and direct time integration method. Flügge (1975) presented the application of the Laplace transform for the analysis of viscoelastic beams. Christensen (1982) used the Fourier transform for the transient response of viscoelastic beams. Rencis et al. (1990) used a time-stepping procedure based on Newmark's method for the quasi-static and dynamic viscoelastic responses of Euler-Bernoulli beams. Yi et al. (1992) developed a numerical algorithm to analyze the dynamic responses of anisotropic viscoelastic composite shell structures based on variational principles and direct time integration by the Newmark average acceleration method. Chen (1995) used the hybrid Laplace transform for the quasi-static and dynamic analysis of the linear viscoelastic Timoshenko beam and conventional beam having the Prony series form of relaxation modulus. Kocatürk and Şimşek (2006) used the direct time integration method of Newmark for the dynamic response of eccentrically prestressed viscoelastic Timoshenko beams under a moving harmonic load. Sorvari and Hämäläinen (2010)

analyzed and compared the behavior of the different time integrators of the integral model of linear viscoelasticity.

Correspondence principle is another procedure that is used for the analysis of viscoelastic problems. By employing correspondence principle, the problem of viscoelastic structures can be solved as elastic structures (Lee, 1955, Rizzo and Shippy, 1971, Tschoegl, 1989). Findley et al. (1976) used the correspondence principle and the superposition principle for the analysis of the viscoelastic beam problem. Wang et al. (1997) presented exact linking relationships between linear viscoelastic Euler-Bernoulli beam solutions and Timoshenko beam solutions under quasi-static loading by using the elastic-viscoelastic correspondence principle. Temel et al. (2004) studied the quasi-static and dynamic behavior of cylindrical helical rods made of linear viscoelastic materials in the Laplace domain by using the correspondence principle. Piovan and Cortínez (2008) studied the linear viscoelastic behavior of curved or straight shear flexible thin-walled beam members based on the correspondence principle. Zhu et al. (2011) presented a new approach for analyzing the time-dependent behavior of linear viscoelastic materials via the elastic-viscoelastic correspondence principle.

Most of the analytical methods use the correspondence principle to perform analysis of viscoelastic problems. However, closed-form solutions are often not possible for the problems that have complex geometry, loading conditions and constitutive relations. Hence, numerical solution techniques should be employed for practical analysis of viscoelastic problems. Finite element, Finite difference and Boundary element methods are the most commonly used numerical methods in solution of viscoelastic problems. Among the computational methods used for viscoelastic problems, the finite element method is the most common and versatile and it has been applied to static and dynamic problems in structural mechanics.

The application of the finite element method to viscoelastic problems has been presented by a number of authors. Adey and Brebbia (1973) presented a method capable of solving a large range of linear viscoelastic problems by using a Laplace transform approach. The finite element method was used for the analysis in the transform plane and least square collocation was used in order to obtain the inversion of the transformed displacements and stresses. Chen and Lin (1982) presented an incremental finite element method based on the Hamilton's variational principle for

dynamic analysis of viscoelastic structures with complicated geometries. White (1986) used constitutive law of hereditary integral type and applied the time interval form finite difference method to perform a finite element analysis in a quasi-static problem. Purushothaman et al. (1988) developed a finite element analysis for viscoelastic solids responding to periodic disturbances travelling at constant speed. In order to decompose the response into harmonic components, the discrete Fourier transformation was used and the viscoelastic material response was determined using the correspondence principle. Chen and Chan (2000) developed integral finite element method to estimate the dynamical characteristics of elastic-viscoelastic composite structures, namely sandwich beam, plate and shell structures with viscoelastic materials as core layers. Mesquita and Coda (2002) proposed an alternative methodology to treat quasi-static and dynamic viscoelastic problems by finite element method. In order to demonstrate the proposed formulation accuracy and stability, plates and shells applications were presented. An application of the boundary element method together with the numerical inversion of the Laplace transform to analyze the linear viscoelastic problems presented by Kusama and Mitsui (1982). To show the validity of the proposed method based on the elastic-viscoelastic correspondence principle, two numerical examples were presented.

In the past years, most researchers have focused mainly on a way of investigation of several responses of viscoelastic thin plates. Aboudi et al. (1990) investigated the dynamic stability of uniform homogenous viscoelastic thin plates subjected to harmonic in-plane loads based on the evaluation of the Lyapunov exponents. The viscoelastic behavior of the plate was given in terms of the Boltzmann superposition principle. Cheng and Zhang (1998) established the initial-boundary value problem for the static-dynamic analysis of viscoelastic thin plates by introducing a structural function. The corresponding variational principles were presented by means of the Boltzmann relaxation law of linear theory of viscoelasticity and convolution bilinear forms. Ilyasov and Aköz (2000) presented a method for the vibration and dynamic stability of viscoelastic triangular plates. The viscoelastic constitutive equations were written in the Boltzmann-Volterra form. Zhou and Wang (2007) investigated the transverse vibration and stability of the axially moving viscoelastic thin plate constituted by Kelvin-Voight model with constant thickness and with parabolically varying thickness. Based on the two dimensional viscoelastic differential constitutive

relation, dimensionless complex frequencies of an axially moving viscoelastic plate with different boundary conditions were calculated by the differential quadrature method. Hatami et al. (2008) developed an exact finite strip method for the free vibration analysis of axially moving viscoelastic thin plates. The exact stiffness matrix of a finite strip of plate was extracted in the frequency domain. By assembling the stiffness matrices of these finite strips, the global stiffness matrix of the whole plate was obtained. The eigenvalues of the global stiffness matrix have the form of complex numbers. Marynowski (2010) presented a calculation method on the basis of the elastic-viscoelastic equivalence for the free vibration analysis of axially moving viscoelastic thin plate. The viscoelastic properties of the plate material were determined in the complex frequency domain and numerical calculations of dynamic stability were conducted for a steel plate. Amoushahi and Azhari (2013) developed a semi analytical finite strip method to evaluate the deflection and buckling of viscoelastic thin plates subjected to different types of out-of-plane and in-plane loading. The mechanical properties of the viscoelastic materials were considered to be linear by expressing the relaxation modules in terms of Prony series. The displacement functions of the plate were assumed to be polynomials in the transverse direction and be continuous harmonic function series that satisfies the pre-set boundary conditions in the longitudinal direction.

In addition, numerous authors have investigated several responses of viscoelastic thick plates. In the paper by Wang and Tsai (1988), quasi-static and dynamic responses of the linear viscoelastic plate constituted by the Maxwell type and three-parameter solid-type models were analyzed on the basis of the Mindlin plate theory. For the analysis, a finite element model was developed by applying Hamilton's variational principle without any integral transformations. In this publication, the relaxation modulus was expressed by the Prony series, and the constitutive law of hereditary integral type with constant Poisson's ratio was assumed. In order to transform the integral equation to algebraic equations, a finite difference approach was used. To achieve a satisfactory convergence in the numerical solutions, a proper element type was investigated according to the convergent conditions such as the ratio of plate thickness to span, number of elements, boundary and loading conditions. Yi and Hilton (1994) developed a numerical procedure in the time domain using variational principles and a direct time integration method to analyze dynamic transient responses of viscoelastic composite

plates based on Mindlin theory. In order to evaluate the accuracy and convergence of the presented numerical algorithm, numerical solutions were compared with the analytical ones and dynamic transient responses of viscoelastic composite plates subjected to unit step loads were calculated. Jafari et al. (2011, 2014) proposed finite strip formulation for the buckling analysis of viscoelastic composite thin and moderately thick rectangular plates with variable thickness. The method of effective moduli and the higher-order shear deformation theory were used to solve the equations governing the stiffness and the geometry matrices of the composite plate. However, the developed methodology could not capture the deformation time history of the viscoelastic plates. The application of the higher-order global-local theory based on the double-superposition concept was employed by Shariyat (2011) for vibration and dynamic buckling analyses of composite/sandwich viscoelastic thick plates subjected to thermomechanical loads. Hermitian elements are employed to insure C^1 -continuous in-plane variations of displacement components. The transient behavior of orthotropic, viscoelastic thick plates was studied numerically by Temel and Şahan (2013). In this paper, using Kelvin model, the material constants were replaced with their complex counterparts in the Laplace domain according to the correspondence principle. For evaluation of the element matrices, numerical integrations of the stiffness and mass matrices and the load vector were computed by the Gauss-quadrature method. For moderately thick viscoelastic plates using first-order shear deformation theory, a fully discretized nonlinear finite strip method was reported by Amoushahi and Azhari (2014) for the static and instability analysis. For evaluation of the deflection, polynomial shape functions were used and the relaxation modulus was expressed by the Prony series. Later, the element-free Galerkin method to the quasi-static stability of moderately thick stepped skew viscoelastic composite plates subjected to in-plan forces was presented by Jaberzadeh and Azhari (2015). This study is based on the first-order shear deformation theory and the method of effective moduli. Nguyen et al. (2015) investigated the mechanical behaviors of viscoelastic laminates and sandwich plates based on the efficient higher-order plate theory. Time-dependent relaxation moduli was represented by Prony series and the equivalent linear elastic stress-strain relationship in the corresponding Laplace domain was used. The solutions in the Laplace domain were converted back into the real-time domain by employing the Fourier series algorithm. Han et al. (2016) developed an enhanced first order shear deformation theory through strain energy transformation for linear viscoelastic

analysis of laminated composite and sandwich plates with various cross-ply layup configurations in the Laplace domain. In order to overcome the complexity of dealing with linear viscoelastic materials, the convolution theorem of Laplace transformation was applied. The fast Fourier transform method was used to convert the stresses and displacements in the Laplace domain back into the real-time domain. Nguyen et al. (2016) analyzed the viscoelastic behavior of laminated and sandwich plates by developing a three-node triangular finite element based on the efficient higher-order plate theory. With the help of the Laplace transform, the integral form of the constitutive equation in the time domain was reduced to an algebraic equation in the Laplace domain. In order to obtain the responses in the real-time domain, the inverse Laplace transform technique developed by Crump was used. Yang et al. (2016) analyzed the vibration and damping characteristics of the sandwich conical shells and annular plates using a simple and efficient modified Fourier solution. A Rayleigh-Ritz technique based on the energy function was adopted to obtain natural frequencies and loss factors. The effects of layout orientations, number of layers, conical angles and thickness ratios on the vibration frequencies and loss factors of the sandwich shells and plates were discussed. Vibration and instability of axially moving viscoelastic microplate were investigated by Arani and Haghparast (2017) by using sinusoidal shear deformation theory. The viscoelastic structural properties of microplate were taken into consideration based on Kelvin's model. Using Hamilton's principle, equations of motion were obtained and solved by hybrid analytical-numerical solution at different boundary conditions. Influences of various parameters such as size effect, axially moving speed, viscoelastic structural damping coefficient, thickness and aspect ratio on the vibration characteristics of moving viscoelastic microplate were discussed in detail.

Compared with the amount of research studies devoted to stability analysis of viscoelastic thin and thick plates in the past years, the published works on quasi-static and/or dynamic analysis of viscoelastic thin plates appear to be scarce.

To the best of our knowledge, a simple and efficient calculation method to implement for the quasi-static and dynamic analysis of the viscoelastic Kirchhoff plate using the mixed-type finite element has not been described yet in the literature already published. This mixed finite element method based on the Gâteaux differential approach is regarded as one of the most powerful, reliable and efficient variational

principle, as it does not require any mathematical operation to obtain stress resultants and stress couples with excellent accuracy which are especially important for engineers. The proposed approach has also advantage that the boundary conditions of the problem can be easily obtained, and the whole field variables with boundary conditions on a regular basis can be included to the functional. In addition, shear-locking effect encountered in the development of plate elements based on shear plate theories can be eliminated. Specifically, decreasing the thickness of the plate element causes shear locking when employing the conventional finite element formulation. In the prevention of shear locking phenomena, the mixed finite element method can be used.

This method was originally introduced by Aköz and Özçelikörs (1985) for analysis of elastic plates and successfully applied by Aköz and his co-workers for analysis of viscoelastic structural elements. Kadioğlu (1999) constructed new functionals for viscoelastic helical rods, straight rods with a circular, non-circular or parabolic cross-section through a systematic procedure based on the Gâteaux differential. For the quasi-static and dynamic analysis, new mixed finite element formulations were derived in the Laplace-Carson domain. Special attention was devoted to the methods for numerical inversion of Laplace transforms. Different methods such as Schapery collocation, Maximum degree of precision, Dubner & Abate and Durbin for numerically transforming the solutions into the real time domain were tested and evaluated. Aköz and Kadioğlu (1999) developed two new functionals for viscoelastic Timoshenko beams on the Winkler foundation. For the quasi-static and dynamic analysis, two mixed finite element formulations were derived in the Laplace-Carson space. The viscoelastic responses in the time domain were obtained through various numerical inverse Laplace transforms. Kadioğlu and Aköz (1999) examined the dynamic response of viscoelastic circular beams. To represent viscoelastic behavior, two constitutive relations (one for bending and one for the shear force) in the hereditary integral form were assumed. In order to analyze viscoelastic circular beams, a mixed finite element VPB12 was developed with twelve independent variables. The performance of the element was investigated through the representative problems. In addition, Kadioğlu and Aköz (2000) investigated the quasi-static and dynamic behavior of linear viscoelastic parabolic beams. In viscoelastic modeling, three-parameter solid model was employed. A new mixed finite element formulation was

presented and various numerical examples were shown in order to demonstrate the proposed approach accuracy and efficiency. The quasi-static and dynamic behavior of viscoelastic circular beams on Winkler elastic foundation were studied by Kadioğlu and Aköz (2003). In this paper, utilizing the Kelvin and three-parameter Kelvin model, the stress-strain relations for viscoelastic materials were obtained in the hereditary integral form. For the analysis, a functional based on the Gâteaux differential approach was derived. Numerical results for the fixed ended semi-circular viscoelastic beam and circular viscoelastic beam on Winkler elastic foundation were presented to prove the efficiency of the proposed formulation.

Aköz et al. (2015) developed a new mixed finite element model to study the quasi-static and dynamic responses of linear viscoelastic Kirchhoff plates. The developed mixed finite element named VPLT16 was C^0 -continuous four-node linear isoparametric plate element with four degrees of freedom per node. Hereditary integral form of the constitutive law with constant Poisson's ratio was used. A new functional in the Laplace-Carson domain suitable for mixed finite element formulation in the same domain was developed by employing Gâteaux differential method. Various numerical Laplace inversion techniques were adopted to transform the obtained solution from the Laplace-Carson domain into the real-time domain. A set of numerical examples were presented to demonstrate the validity and accuracy of the proposed mixed finite element formulation. Moreover, the proposed formulation was successfully applied to the analysis of viscoelastic Kirchhoff plates constituted by different rheological models by Kadioğlu and Tekin (2015, 2016a, 2016b, 2017a and 2017c) and Tekin and Kadioğlu (2016b, 2016c, 2017c) and with variable thickness by Tekin et al. (2015), Tekin and Kadioğlu (2016a and 2017b) and Kadioğlu and Tekin (2017b).

Tekin and Kadioğlu (2017a) presented a new mixed-type finite element model to study the quasi-static and dynamic responses of first-order shear deformable (FSD) linear viscoelastic Mindlin-Reissner plates. The developed mixed finite element named VPLT32 was C^0 -continuous four-node linear isoparametric plate element with eight degrees of freedom per node. In the Laplace-Carson domain, a new functional was derived in terms of displacements, stresses and boundary conditions (geometric and dynamic) based on the Gâteaux differential method. In this study, three-parameter solid model and Zener rheological model were employed for modeling the behavior of

a viscoelastic thick plate material. In order to transform the solutions obtained in the Laplace-Carson domain to the real-time domain, Dubner and Abate numerical Laplace inversion technique was adopted. Several numerical examples were presented not only to demonstrate the validity and accuracy of the proposed mixed finite element formulation but also to examine the effects of load, geometry and material parameters on the viscoelastic response of FSD Mindlin-Reissner plates and to give a better insight into time-dependent behavior of engineering thick plate problems.

1.3 Hypothesis

The plate theory has still been a technically important subject, which has been studied more extensively. If we look at the historical background of the plate theory, Kirchhoff published an important thesis on the theory of thin plates. Most of the plates used in practical applications satisfy thin plate criterion. In this thesis, Kirchhoff plate theory is adopted under the hypotheses of linear viscoelasticity and small deflections.

Due to mathematical complexity in viscoelastic constitutive relations, closed-form solutions are often not possible and numerical solution techniques should be performed. Finite element method is the most powerful numerical procedure and has been applied to various problems in structural mechanics. However, as presented in literature, finite element method giving rise to locking phenomena such as shear locking occurs in plate elements when the thickness is very small. While dealing with the effects of locking, various methods have been suggested. To overcome shear-locking effect, a suitable mixed finite element formulation can be considered. In order to formulate mixed type finite elements, Gâteaux Differential method is efficient and reliable variational tool.

By using the Gâteaux Differential method, new energy functional in the transformed Laplace-Carson space for the quasi-static and dynamic analysis of the linear viscoelastic Kirchhoff plate is constructed. In order to remove the time derivatives from governing equations and boundary conditions, the method of the Laplace-Carson transform is adopted. For transforming obtained solutions to the real time domain, different numerical inverse transform methods; such as MDOP, Dubner and Abate and Durbin are used. The analysis is performed for different viscoelastic material models and types of time-dependent loadings to enhance accuracy and applicability of the results for subsequent studies.



2. THEORY OF VISCOELASTICITY

Viscoelasticity or Rheology is defined as the science of deformation by some scientists. Fundamental deformation of materials can be simplified by means of idealization theory and classified into three groups: elastic, plastic and viscous based on materials' stress-strain pattern.

Time-independent deformation which disappears on release of load is called elastic deformation. As illustrated in Figure 2.1, an immediate elastic deformation is obtained with loading. Then the deformation stays constant as long as the load is fixed and it disappears immediately by release of the load.

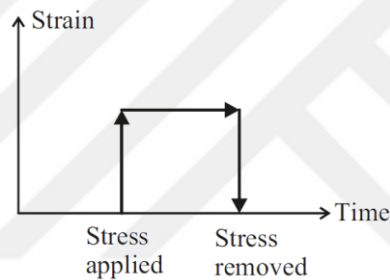


Figure 2.1 : Strain versus time plot for purely elastic deformation.

For an elastic material, stress is proportional to strain. When materials are subjected to increasing stress, the behavior is no longer elastic. The limiting stress above which the behavior is no longer elastic is called the elastic limit. Time-independent deformation which remains on release of load is called plastic deformation. As illustrated in Figure 2.2, the deformation continues to increase for a short while after the load is fully applied, and then remains constant as long as the load is fixed, but a permanent deformation remains on release of the load.

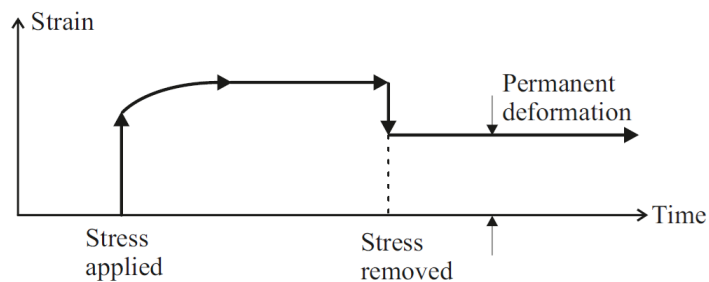


Figure 2.2 : Strain versus time plot for purely plastic deformation.

Time-dependent deformation steadily increases whilst the load is applied is called viscous deformation. Then, after the load is removed, the deformation shows no subsequent change and recovery does not occur as illustrated in Figure 2.3. Because flow requires shear, the strain and stress in Figure 2.3 correspond to the shear strain and shear stress, respectively.

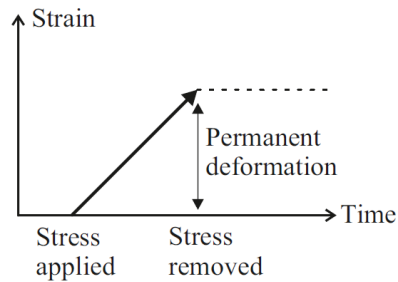


Figure 2.3 : Strain versus time plot for purely viscous deformation.

Some materials such as metals at elevated temperatures, concrete, plastics, natural and synthetic fibers and wood display mechanical response that combines the characteristics of both elastic solids and viscous fluids. These materials are called viscoelastic or time-dependent materials since time is a very important factor in their behavior. Time-dependent deformation of viscoelastic materials is illustrated in Figure 2.4.

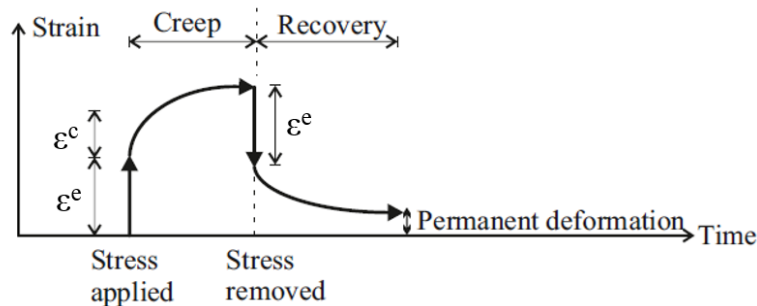


Figure 2.4 : Strain versus time plot for viscoelastic deformation.

As indicated in Figure 2.4, an elastic deformation is obtained with loading if loading is rapid enough, then a slow and continuous increase of deformation at a decreasing rate is observed. After the load is removed, a continuously decreasing strain follows an initial elastic recovery.

If the load is released, a reverse elastic strain followed by recovery of a portion of the creep strain will occur at a continuously decreasing rate. The disappearance of some of the strain more slowly than the purely elastic strain is also called delayed elasticity.

When testing and describing viscoelastic materials, it is preferable to apply a step strain or step stress in time. One of the most important phenomena in viscoelastic materials is termed creep that is defined as a slow continuous deformation of a material under constant stress (step stress). Other phenomenon is termed relaxation that is defined as the gradual decrease of stress under constant strain (step strain).

2.1 Linearity

If the linear superposition principle is valid and the stress at any time is proportional to the strain, the material is said to be linearly viscoelastic. The mathematical expressions of these two requirements are:

$$\begin{aligned}\varepsilon[c\sigma(t)] &= c\varepsilon[\sigma(t)] \\ \varepsilon[\sigma_1(t) + \sigma_2(t - t_1)] &= \varepsilon[\sigma_1(t)] + \varepsilon[\sigma_2(t - t_1)]\end{aligned}\tag{2.1}$$

where c is a constant, ε and σ are the resultant strain and applied stress, respectively. Illustration of these two requirements are given by Findley et al. (1976). According to Findley et al. (1976), most materials are nearly linear over certain ranges of the variables, stress, strain, time, temperature.

Viscoelasticity is the engineering discipline that is developed to provide a mathematical framework in order to describe the behavior of viscoelastic materials in detail. Linear (infinitesimal) viscoelasticity and especially the model of linear viscoelastic solid can be traced back to Boltzmann (1874) who considered an elastic material with memory and elaborated the model of linear viscoelastic solid. Quite often linear viscoelasticity is motivated through mechanical models composed of springs which are perfectly elastic and dashpots which are perfectly viscous.

2.2 Linear Elastic Spring

The mechanical behavior of a linear elastic spring depicted in Figure 2.5 is governed by Hooke's law (ideal solid): "stress is directly proportional to strain". This model is thus referred to as the Hooke model. The constitutive equation of the spring described by:

$$\sigma = E\varepsilon\tag{2.2}$$

where σ and ε are analogous to the spring force and displacement and E can be interpreted as a linear spring constant or a Young's modulus. In spring model, inertia effects are neglected and the constitutive equation is written in "stress-strain" form.

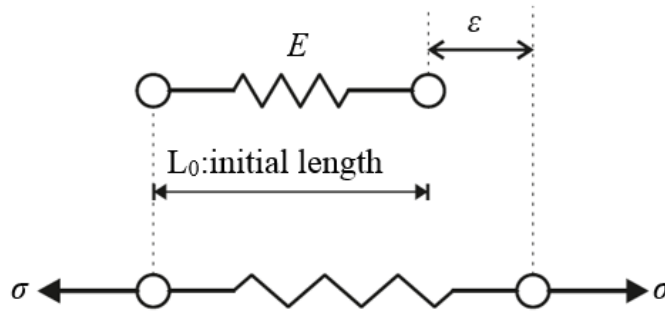


Figure 2.5 : Mechanical model of linear elastic spring.

2.2.1 Response to stress loading

For a specified stress loading that takes the form $\sigma(t) = f(t) H(t - t_0)$, the strain response of the spring is obtained as:

$$\varepsilon(t) = \frac{1}{E} f(t) H(t - t_0) \quad (2.3)$$

This shows that the strain response of an elastic spring is instantaneous and remains non-zero for as long as the applied stress is non-zero. This is the solid response characteristic. One of the most important test which is used very often to determine the viscoelastic response characteristics of a material is creep test. The creep compliance $J(t)$ of an elastic spring is defined as the strain response to a step stress, $\sigma(t) = \sigma_0 H(t - t_0)$, measured per unit of applied stress. The creep compliance has the form:

$$J(t - t_0) = \frac{\varepsilon(t)}{\sigma_0} = \frac{1}{E} H(t - t_0) \quad (2.4)$$

or simply

$$J(t) = \frac{1}{E} H(t) \quad (2.5)$$

2.2.2 Response to strain loading

For a specified strain loading that takes the form $\varepsilon(t) = f(t) H(t - t_0)$, the stress response of the spring is obtained as:

$$\sigma(t) = E f(t) H(t - t_0) \quad (2.6)$$

This shows that the stress response of an elastic spring is instantaneous and remains non-zero for as long as the applied strain is non-zero. This is the solid response characteristic. Another important test which is used very often to determine the viscoelastic response characteristics of a material is stress relaxation test. The relaxation modulus $Y(t)$ of an elastic spring is defined as the stress response to a step strain, $\varepsilon(t) = \varepsilon_0 H(t - t_0)$, measured per unit of applied strain. The relaxation modulus has the form:

$$Y(t - t_0) = \frac{\sigma(t)}{\varepsilon_0} = E H(t - t_0) \quad (2.7)$$

or simply

$$Y(t) = E H(t) \quad (2.8)$$

2.3 Linear Viscous Dashpot

The mechanical behavior of a linear viscous dashpot depicted in Figure 2.6 is governed by Newton's law (perfect liquid): "stress (force) is directly proportional to strain-rate (velocity)." This model is thus referred to as the Newton model. The constitutive equation of the dashpot described by

$$\sigma(t) = \eta \frac{d}{dt} \varepsilon(t) \quad (2.9)$$

Here, the coefficient η being the viscosity coefficient.

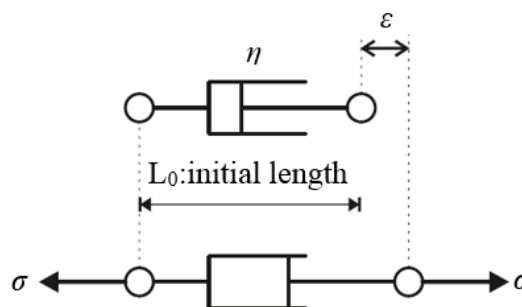


Figure 2.6 : Mechanical model of linear viscous dashpot.

2.3.1 Response to stress loading

For a specified stress loading that takes the form $\sigma(t) = f(t) H(t - t_0)$, the strain response of the linear viscous dashpot can be obtained by integrating the resulting expression between 0 and t as:

$$\varepsilon(t) = \varepsilon(0) + \frac{1}{\eta} \int_0^t f(s) H(s - t_0) ds \quad (2.10)$$

by using the initial condition $\varepsilon(0) = 0$, equation (2.10) becomes

$$\varepsilon(t) = \frac{1}{\eta} H(t - t_0) \int_{t_0}^t f(s) ds \quad (2.11)$$

The creep compliance $J(t)$ of a linear viscous dashpot is defined as the strain response to a step stress, $\sigma(t) = \sigma_0 H(t - t_0)$, measured per unit of applied stress. The creep compliance has the form:

$$J(t - t_0) = \frac{\varepsilon(t)}{\sigma_0} = \frac{(t - t_0)}{\eta} H(t - t_0) \quad (2.12)$$

or simply

$$J(t) = \frac{t}{\eta} H(t) \quad (2.13)$$

2.3.2 Response to strain loading

For a specified strain loading that takes the form $\varepsilon(t) = f(t) H(t - t_0)$, the stress response of the linear viscous dashpot is obtained by performing the differentiation using the properties of the unit step and delta functions as:

$$\begin{aligned} \sigma(t) &= \eta \frac{d}{dt} \varepsilon(t) = \eta \frac{d}{dt} [f(t) H(t - t_0)] \\ &= \eta \left[\frac{d}{dt} f(t) \right] H(t - t_0) + \eta f(t) \left[\frac{d}{dt} H(t - t_0) \right] \\ &= \eta \left[H(t - t_0) \frac{d}{dt} f(t) + f(t) \delta(t - t_0) \right] \end{aligned} \quad (2.14)$$

Due to the stress response contains a unit impulse function at $t = t_0$, it would take an infinite value at the instant when an instantaneous strain is imposed on a linear viscous dashpot.

The relaxation modulus $Y(t)$ of a linear viscous dashpot is defined as the stress response to a step strain, $\varepsilon(t) = \varepsilon_0 H(t - t_0)$, measured per unit of applied strain. By noting that $f(t) = \varepsilon_0$ and $\frac{d}{dt} f(t) = 0$, the relaxation modulus has the form:

$$Y(t - t_0) = \eta \delta(t - t_0) \quad (2.15)$$

or simply

$$Y(t) = \eta \delta(t) \quad (2.16)$$

2.4 Rheological Models

Rheological models are made up of more elaborate combinations of linear elastic springs and linear viscous dashpots. Two elementary rheological models developed from an assembly of a linear elastic spring and a linear viscous dashpot are the Maxwell or Maxwell-Wiechert model and the Kelvin or Kelvin-Voight model. The Maxwell model characterizes a viscoelastic fluid whereas the Kelvin-Voight model characterizes a viscoelastic solid.

2.4.1 Maxwell-Wiechert model

The Maxwell model is a two-element model consists of a linear spring and a linear viscous dashpot connected in series as depicted in Figure 2.7.

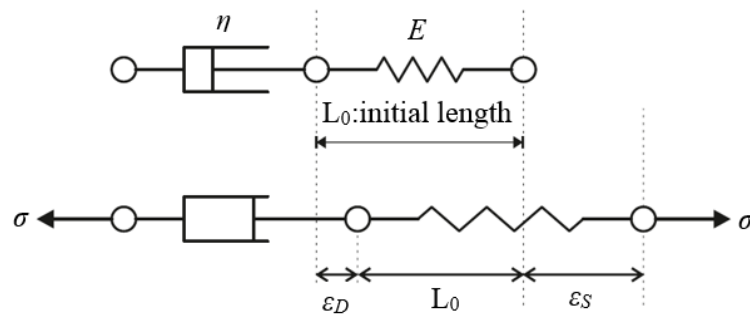


Figure 2.7 : Maxwell-Wiechert model.

The constitutive equation of the Maxwell model is developed using the following stress-strain relations of individual elements:

$$\text{For the spring: } \sigma_s = E \varepsilon_s \quad (2.17)$$

$$\text{For the dashpot: } \sigma_D = \eta \frac{d}{dt} \varepsilon_D = \eta \dot{\varepsilon}_D \quad (2.18)$$

When two elements are connected in series, each element carry the same amount of stress while the strains are different in each element as follows:

$$\sigma = \sigma_s = \sigma_D \quad (2.19)$$

$$\varepsilon = \varepsilon_s + \varepsilon_D \quad (2.20)$$

And the strain rate is:

$$\dot{\varepsilon} = \dot{\varepsilon}_s + \dot{\varepsilon}_D \quad (2.21)$$

Therefore, the constitutive equation of the model can be obtained by inserting (2.18) and the time derivative of (2.17) into equation (2.21) as follows:

$$\dot{\varepsilon} = \frac{\dot{\sigma}}{E} + \frac{\sigma}{\eta} \quad (2.22)$$

2.4.1.1 Response to stress loading

The strain-time relation under given stress condition can be obtained by solving an ordinary linear differential equation of first order. Applying a constant stress $\sigma = \sigma_0$ at time $t = 0$, a differential equation (2.22) has the solution

$$\varepsilon(t) = \frac{\sigma_0}{\eta} t + C_1 \quad , \quad t > 0 \quad (2.23)$$

with $\dot{\sigma} = 0$.

In order to determine C_1 , an initial condition is required. The sudden application of the constant stress σ_0 at time $t = 0$ means that $\dot{\sigma}(t)$ has a singularity at this point. To deal with it, equation (2.22) is integrated across this point:

$$\int_{-\tau}^{+\tau} \sigma dt + \frac{\eta}{E} [\sigma(+\tau) - \sigma(-\tau)] = \eta [\varepsilon(+\tau) - \varepsilon(-\tau)] \quad (2.24)$$

Let $\tau = 0$, then the first term goes to zero and equation (2.24) simplifies to

$$\frac{\eta}{E}[\sigma_0] = \eta[\varepsilon_0] \quad (2.25)$$

That is $\varepsilon_0 = \frac{\sigma_0}{E}$ and $\varepsilon_0 = \varepsilon(0^+)$ is the value of the ε immediately to the right of time $t = 0$. If equation (2.23) is re-written for $t = 0^+$, C_1 is obtained as:

$$\varepsilon(0^+) = \varepsilon_0 = C_1 = \frac{\sigma_0}{E} \quad (2.26)$$

As a result, equation (2.23) becomes:

$$\varepsilon(t) = \frac{\sigma_0}{\eta}t + \frac{\sigma_0}{E} \quad (2.27)$$

The creep compliance of the Maxwell model has the form:

$$J(t) = \frac{t}{\eta} + \frac{1}{E} \quad (2.28)$$

Equation (2.27) indicates that if the stress is removed at time t_1 , the elastic strain $\frac{\sigma_0}{E}$ in the spring returns to zero at the instant the stress is removed, while $\left(\frac{\sigma_0}{\eta}\right)t_1$ represents a permanent strain which does not disappear. Strain-time response of the Maxwell model under given stress condition is shown in Figure 2.8.

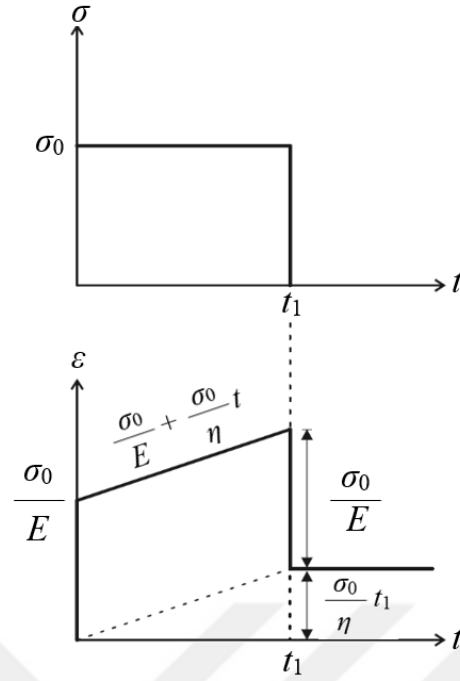


Figure 2.8 : Creep and recovery behavior of the Maxwell model.

2.4.1.2 Response to strain loading

In this case, the stress-time relation under given strain condition can be obtained by solving an ordinary linear differential equation of first order.

Applying a constant strain $\varepsilon = \varepsilon_0$ at time $t = t_0$, a differential equation (2.22) has the solution

$$\sigma(t) = C_2 e^{-\left(\frac{E}{\eta} t\right)}, \quad t > t_0 \quad (2.29)$$

with $\dot{\varepsilon} = 0$.

In order to determine C_2 , an initial condition $\sigma(t_0)$ or, more precisely, $\sigma(t_0^+)$ is required.

For $\sigma(t_0^-) = \sigma(t_0^+) = \sigma_0$, C_2 is obtained as:

$$C_2 = \sigma_0 e^{\left(\frac{E}{\eta} t_0\right)} \quad (2.30)$$

where $\sigma_0 = E\varepsilon_0$ and ε_0 is the initial strain at $t = t_0$. As a result, equation (2.29) becomes:

$$\sigma(t) = \sigma_0 e^{-\left(\frac{E}{\eta} (t-t_0)\right)} = \left[E e^{-\left(\frac{E}{\eta} (t-t_0)\right)} \right] \varepsilon_0 \quad (2.31)$$

From (2.31), the relaxation modulus of the Maxwell model has the form

$$Y(t - t_0) = E e^{-\frac{(t-t_0)E}{\eta}}, \quad t > t_0 \quad (2.32)$$

or simply

$$Y(t) = E e^{-\left(\frac{E}{\eta}t\right)}, \quad t > 0 \quad (2.33)$$

The relaxation modulus evaluated at $t = \tau_r$ or $t - t_0 = \tau_r$, where the time parameter $\tau_r = \frac{\eta}{E}$ is called a relaxation time, is $e^{-1} E \equiv 0,37 E$. In this case, the relaxation time of the Maxwell model represents the time it takes the stress to decay by about 63%. In other words, only 37% of the initial applied stress remains at $t = \tau_r$. Stress-time response of the Maxwell model under given strain condition is shown in Figure 2.9.

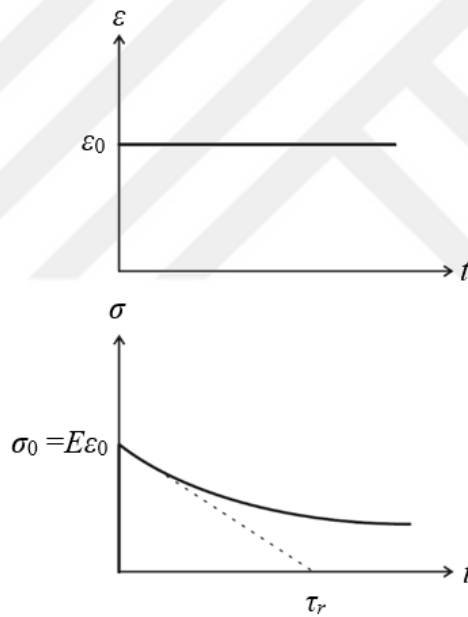


Figure 2.9 : Stress relaxation behavior of the Maxwell model.

2.4.2 Kelvin-Voight model

The Kelvin model is a two-element model consists of a linear spring and a linear viscous dashpot connected in parallel as depicted in Figure 2.10.

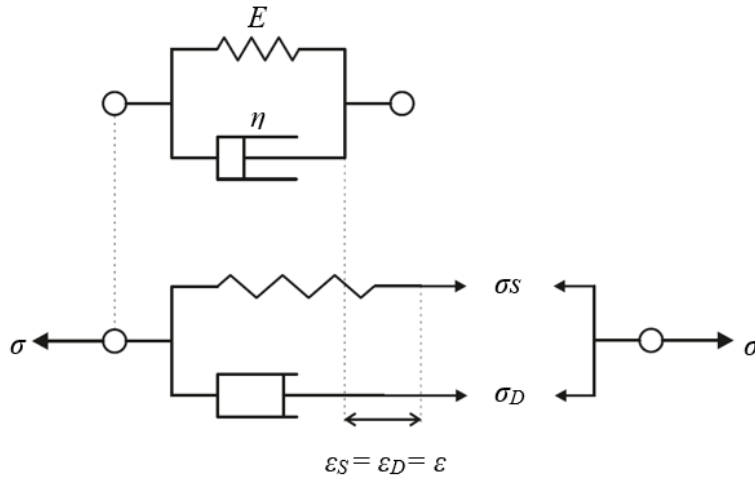


Figure 2.10 : Kelvin-Voight model.

The constitutive equation of the Kelvin model is developed using the following stress-strain relations of individual elements:

$$\text{For the spring: } \sigma_s = E \epsilon_s \quad (2.34)$$

$$\text{For the dashpot: } \sigma_D = \eta \frac{d}{dt} \epsilon_D = \eta \dot{\epsilon}_D \quad (2.35)$$

When two elements are connected in parallel, each element carry the same amount of strain while the stresses are different in each element as follows:

$$\sigma = \sigma_s + \sigma_D \quad (2.36)$$

$$\epsilon = \epsilon_s = \epsilon_D \quad (2.37)$$

Therefore, the constitutive equation of the model can be obtained by inserting equations (2.34) and (2.35) into (2.36) as follows:

$$\sigma = E\epsilon + \eta\dot{\epsilon} \quad (2.38)$$

2.4.2.1 Response to stress loading

The strain-time relation under a constant stress $\sigma = \sigma_0$ applied at time $t = t_0 = 0$ has the following form:

$$\varepsilon(t) = \frac{\sigma_0}{E} + C_3 e^{-\left(\frac{E}{\eta}t\right)} \quad (2.39)$$

In order to determine C_3 , an initial condition is required. Initial condition is $\sigma = \sigma_0$ and $\varepsilon = 0$ at $t = 0$. Introducing this into equation (2.39), C_3 is obtained as

$$C_3 = -\frac{\sigma_0}{E} \quad (2.40)$$

As a result, equation (2.39) becomes:

$$\varepsilon(t) = \frac{\sigma_0}{E} \left(1 - e^{-\left(\frac{E}{\eta}t\right)}\right) \quad (2.41)$$

This expression indicates that the strain increases with a decreasing rate and approaches asymptotically the value of $\frac{\sigma_0}{E}$ when t tends to infinity. The behavior described by equation (2.41) is appropriately called delayed elasticity.

The creep compliance of the Kelvin model has the form:

$$J(t) = \frac{1}{E} \left(1 - e^{-\left(\frac{E}{\eta}t\right)}\right) = \frac{1}{E} \left(1 - e^{-\frac{t}{\tau_c}}\right) \quad (2.42)$$

The parameter $\tau_c = \frac{\eta}{E}$, introduced here, is called a retardation or creep time which has the dimensional units of time. At $t = \tau_c$,. In this case, only 37% of the asymptotic strain remains to be accomplished after $t = \tau_c$, $\varepsilon(t) = \frac{\sigma_0}{E} \left(1 - \frac{1}{e}\right) = 0.63 \frac{\sigma_0}{E}$. Strain-time response of the Kelvin-Voight model under given stress condition is shown in Figure 2.11.

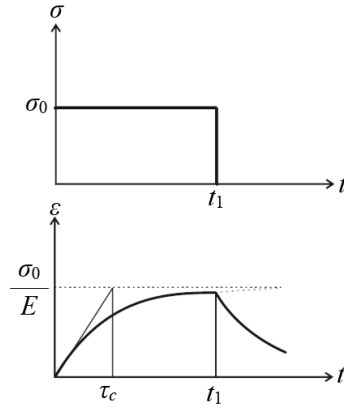


Figure 2.11 : Creep and recovery behavior of the Kelvin model.

2.4.2.2 Response to strain loading

In this case, the stress-time relation under given strain condition is the point of interest. Equation (2.38) is not a differential equation in stress. To assess the response of the model to the step change in strain, the Heaviside $H(t)$ and Dirac delta $\delta(t)$ functions are used. By using the expressions $\varepsilon(t) = \varepsilon_0 H(t - t_0)$ and $\dot{\varepsilon}(t) = \varepsilon_0 \delta(t - t_0)$, (2.38) yields:

$$\sigma = E \varepsilon_0 H(t - t_0) + \eta \varepsilon_0 \delta(t - t_0) \quad (2.43)$$

where the first term describes the change in stress in the spring and the second term describes the infinite stress pulse on application of the strain.

The relaxation modulus of the Kelvin-Voight model has the form:

$$Y(t - t_0) = EH(t - t_0) + \eta \delta(t - t_0) \quad (2.44)$$

or simply

$$Y(t) = EH(t) + \eta \delta(t) \quad (2.45)$$

As such, the stress-time response of the Kelvin-Voight model under given strain condition $\varepsilon(t) = \varepsilon_0 H(t - t_0) - \varepsilon_0 H(t - t_1)$, shown in Figure 2.12, is obtained as

$$\sigma(t) = \varepsilon_0 \left\{ [EH(t - t_0) + \eta \delta(t - t_0)] - [EH(t - t_1) + \eta \delta(t - t_1)] \right\} \quad (2.46)$$

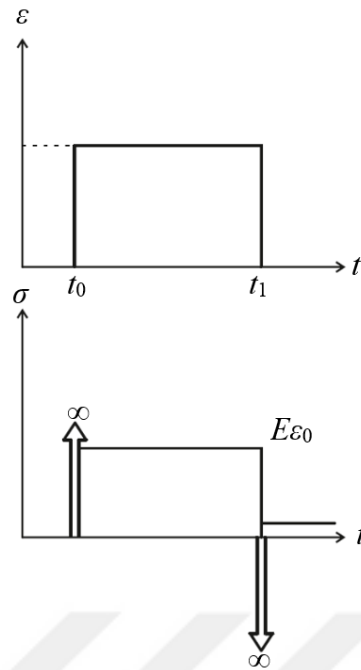


Figure 2.12 : Stress relaxation behavior of the Kelvin model.

2.5 Classification of Rheological Models

The Maxwell and the Kelvin-Voight models are widely used in theoretical studies because of their simplicity. However, neither the Maxwell nor Kelvin-Voight models provide good representations of real viscoelastic behavior. Creep functions predicted by the Maxwell model and relaxation functions predicted by the Kelvin model are unrealistic for the viscoelastic materials. For linearly elastic materials, a stress-strain curve is a straight line whereas linearly viscoelastic materials give rise to a curved stress-strain plot. The Maxwell model has creep curve which is fitted by a straight line. More clearly, this model shows no time-dependent recovery and does not show the decreasing strain rate under constant stress which is a characteristic of primary creep (Findley et al, 1976). The Kelvin-Voight model does not exhibit the instantaneous response (instantaneous elasticity), which is associated with a solid, because the strain in two elements (a spring and a dashpot) is required to be equal and the dashpot is not allowed to have an instantaneous strain.

Composite models which are formed by judicious combinations of linear elastic spring and viscous dashpot elements can predict both creep and relaxation functions well. So that, these models are capable of reproducing more realistic viscoelastic behavior. There are several possible combinations of three-element and four-element models.

These models are classified into four groups by Findley et al. (1976) as shown in Figure 2.13. Group I exhibits a solid-like character with retarded elasticity (instantaneous elastic deformation and delayed elastic deformation). Model (a) and Model (c) in Group I are called "the standard linear (viscoelastic) solid". Group II exhibits a liquid-like character, viscous flow, plus delayed elasticity. Group III exhibits an instantaneous elastic response followed by viscous flow and delayed elasticity. Group IV shows delayed elasticity with two retardation times. Clearly, the choices are very many however this thesis study restricts attention to models which exhibit solid-like character.

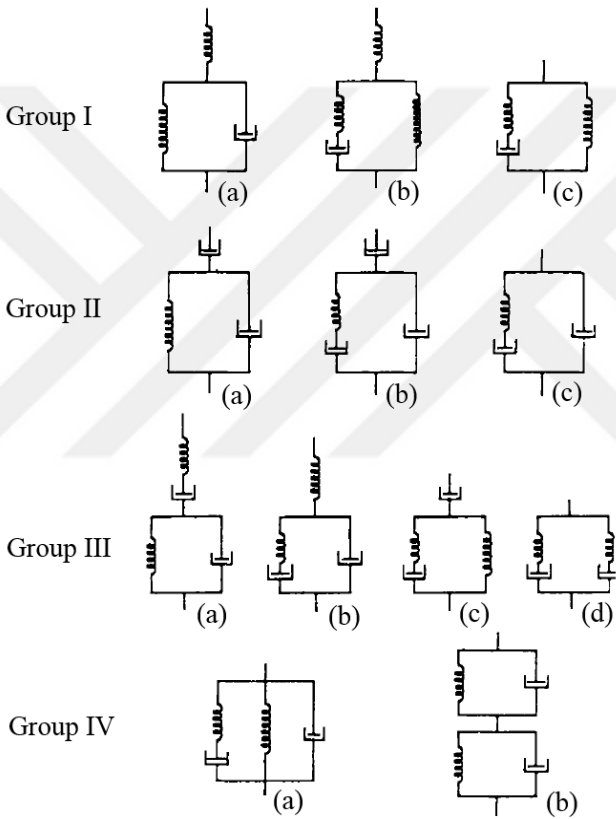


Figure 2.13 : Various combinations of Three-element and Four-element models (Findley et al, 1976).

2.6 Standard Linear Solid

Standard linear solid model has two equivalent versions. One of them consists of a Kelvin-Voight unit in series with a linear spring element. The other one is composed of a Maxwell unit in parallel with a linear spring element. These three-element models include the essential characteristics of the behavior of viscoelastic solids. These characteristics can be demonstrated by evaluating their responses to the creep and

stress relaxation tests. Their responses to stress and strain loadings can be determined in a similar way as to the Maxwell and Kelvin-Voight models. In so doing, it should be noted that the form of response to strain loading is of the same form as its response to stress loading and vice versa.

2.6.1 Three parameter standard solid model

For the three parameter standard solid model obtained by adding a spring element in series to the Kelvin-Voight element in Figure 2.14, the constitutive equation is derived using the following relations:

$$\sigma_K = E_K \varepsilon_K + \eta_K \dot{\varepsilon}_K \quad , \quad \sigma_S = E_0 \varepsilon_S \quad , \quad \sigma = \sigma_K = \sigma_S \quad (2.47)$$

In this arrangement, the Kelvin-Voight unit and the series spring element experience the same stress and equal to the imposed stress σ , while the total strain ε is the sum of the strain in each arm (the Kelvin-Voight arm and the series spring):

$$\varepsilon = \varepsilon_K + \varepsilon_S \quad (2.48)$$

Therefore, the constitutive equation of the three parameter standard solid model is given by:

$$(E_0 + E_K)\sigma + \eta_K \frac{d}{dt}\sigma = (E_0 E_K)\varepsilon + (E_0 \eta_K) \frac{d}{dt}\varepsilon \quad (2.49)$$

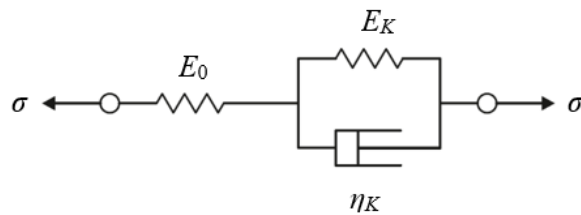


Figure 2.14 : Three parameter standard solid model.

2.6.2 Zener model

For the Zener model obtained by adding a spring element in parallel to the Maxwell element in Figure 2.15, the constitutive equation is derived using the following relations:

$$\dot{\varepsilon}_1 = \frac{\sigma_M}{\eta_M}, \quad \varepsilon_2 = \frac{\sigma_M}{E_M}, \quad \sigma_S = E_0 \varepsilon_S, \quad \varepsilon = \varepsilon_M = \varepsilon_S, \quad \varepsilon_M = \varepsilon_1 + \varepsilon_2 \quad (2.50)$$

In this arrangement, the Maxwell unit and the parallel spring element experience the same strain ε , while the total stress σ is the sum of the stress in each arm (the Maxwell arm and the parallel spring):

$$\sigma = \sigma_M + \sigma_S \quad (2.51)$$

Therefore, the constitutive equation of the Zener model is given by:

$$\left(\frac{1}{\eta_M} \right) \sigma + \left(\frac{1}{E_M} \right) \frac{d}{dt} \sigma = \left(\frac{E_0}{\eta_M} \right) \varepsilon + \left(1 + \frac{E_0}{E_M} \right) \frac{d}{dt} \varepsilon \quad (2.52)$$

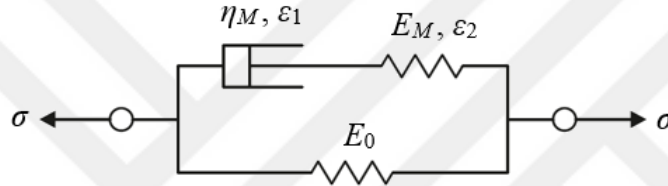


Figure 2.15 : Zener model.

2.7 Operator Forms of Rheological Models

In order to represent the stress-strain-time relations of viscoelastic materials, two alternative forms are generally used:

- Differential Operator Form
- Integral Operator Form

2.7.1 Differential operator form

Since the mathematical processes required for the analysis are reasonably simple, the differential operator form has been widely used. A differential operator form of the constitutive equation of a general rheological model (mechanical model constructed through spring-and-dashpot arrangement) is:

$$p_0 \sigma + p_1 \dot{\sigma} + p_2 \ddot{\sigma} + \dots + p_m \frac{d^m}{dt^m} \sigma = q_0 \varepsilon + q_1 \dot{\varepsilon} + q_2 \ddot{\varepsilon} + \dots + q_n \frac{d^n}{dt^n} \varepsilon \quad (2.53)$$

Here dots denote the derivative of the variable with respect to time and p_0, p_1, p_2, \dots and q_0, q_1, q_2, \dots are material constants which are known in terms of the spring constants E_i

and dashpot constants η_i of the model. Equation (2.53) can be written in a more compact form as follows:

$$\tilde{P}\sigma = \tilde{Q}\varepsilon \quad (2.54)$$

where \tilde{P} and \tilde{Q} are m order and n order linear differential operators with respect to time, respectively.

$$\tilde{P} = \sum_{k=0}^m p_k \frac{d^k}{dt^k} \quad , \quad \tilde{Q} = \sum_{j=0}^n q_j \frac{d^j}{dt^j} \quad (2.55)$$

Moreover, the stress-strain and strain-stress equations of a general rheological model can be written in symbolic form as follows:

$$\sigma = \frac{\tilde{Q}}{\tilde{P}} \varepsilon \quad , \quad \varepsilon = \frac{\tilde{P}}{\tilde{Q}} \sigma \quad (2.56)$$

2.7.2 Integral operator form

An advantage that the integral operator form has over the differential operator form is that the integral operator form can be able to describe the time dependence more generally.

"Integrals are summing operations, and this view of viscoelasticity takes the response of the material at time t to be the sum of the responses to excitations imposed at all previous time" (Roylance, 2001, p. 17). This principle is a statement of linearity. Mathematically if a linearly viscoelastic material is subjected to a strain of magnitude ε_0 , suddenly applied and held constant thereafter, the stress response of the material to the applied step strain can be given as follows:

$$\sigma(t) = Y(t) \varepsilon_0 H(t) \quad (2.57)$$

Now assume that the same material is subjected to a step down strain of magnitude ε_0 , but applying the step down loading t_1 units of time. The stress response of the material to the applied step down strain can be given as follows:

$$\sigma(t) = -Y(t - t_1) \varepsilon_0 H(t - t_1) \quad (2.58)$$

If the material is linear, the total stress response due to both subjected strain loading can be obtained by superposition of these two individual effects (using the Boltzmann's superposition principle) as:

$$\sigma(t) = \varepsilon_0 [Y(t)H(t) - Y(t-t_1)H(t-t_1)] \tag{2.59}$$

The total stress response $\sigma(t)$ of the material is illustrated in Figure 2.16.

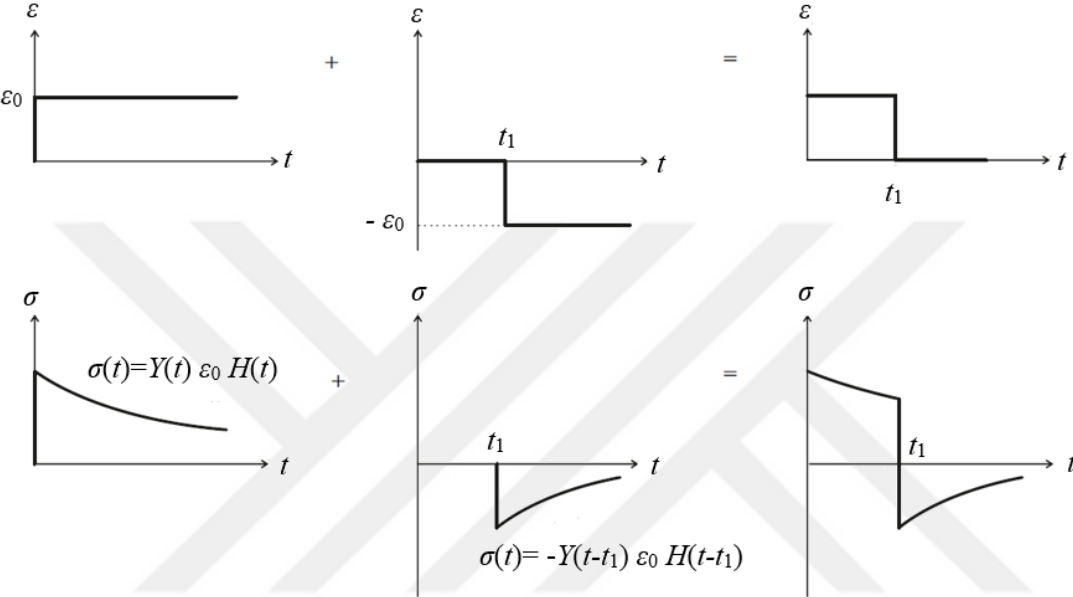


Figure 2.16 : Stress-time response of linear material generated from a superposition of step functions of strain versus time.

It is an easy matter to extend these results for prediction of response to arbitrary history of strain $\varepsilon(t)$ as a function of time t .

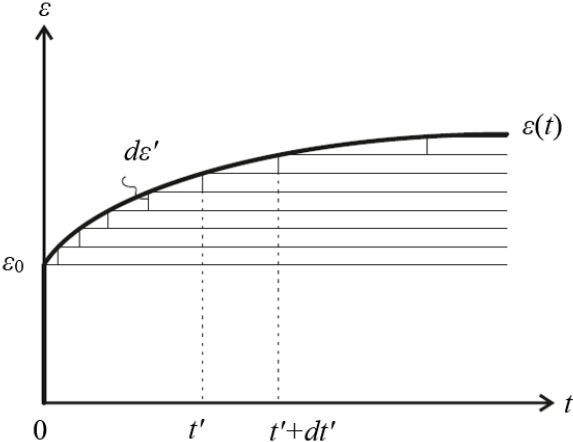


Figure 2.17 : Linear superposition to derive hereditary integral.

As shown in Figure 2.17, this arbitrary strain history can be divided into the basic part $\varepsilon_0 H(t)$ and a sequence of infinitesimal strain increments $d\varepsilon(t') H(t-t')$. The corresponding stress at time t can be written using the Boltzmann's superposition principle as:

$$\sigma(t) = \varepsilon_0 Y(t) + \int_0^t Y(t-t') d\varepsilon(t') = \varepsilon_0 Y(t) + \int_0^t Y(t-t') \frac{d}{dt'} \varepsilon(t') dt' \quad (2.60)$$

Equation (2.60) indicates that the stress at any given time depends on all that has happened before on the entire strain history $\varepsilon(t')$ for $t' < t$. Equation (2.60) is called a hereditary integral. An alternate form for (2.60) can be obtained through integration by parts as:

$$\sigma(t) = \varepsilon_0 Y(t) + [Y(t-t') \varepsilon(t')]_0^t - \int_0^t \frac{d}{dt'} Y(t-t') \varepsilon(t') dt' \quad (2.61)$$

where

$$\frac{d}{dt'} Y(t-t') = -\frac{d}{d(t-t')} Y(t-t') \quad (2.62)$$

and thus equation (2.61) reduces to the following second version of the hereditary integral:

$$\sigma(t) = Y(0) \varepsilon(t) + \int_0^t \frac{d}{d(t-t')} Y(t-t') \varepsilon(t') dt' \quad (2.63)$$

Including the initial part due to ε_0 into the integral and even moving its lower limit to $-\infty$, produces the following form of the hereditary integral:

$$\sigma(t) = \int_{-\infty}^t Y(t-t') \frac{d}{dt'} \varepsilon(t') dt' \quad (2.64)$$

Arguments similar to those presented for the relaxation modulus $Y(t)$ can be used to derive the hereditary integrals for the creep compliance $J(t)$. If an arbitrary history of stress $\sigma(t)$ is approximated by the sum of a series of infinitesimal stress increments in addition to its basic part $\sigma_0 H(t)$, corresponding strain can be given by:

$$\varepsilon(t) = \sigma_0 J(t) + \int_0^t J(t-t') \frac{d}{dt'} \sigma(t') dt' \quad (2.65)$$

$$\varepsilon(t) = J(0)\sigma(t) + \int_0^t \frac{d}{d(t-t')} J(t-t')\sigma(t') dt' \quad (2.66)$$

$$\varepsilon(t) = \int_{-\infty}^t J(t-t') \frac{d}{dt'} \sigma(t') dt' \quad (2.67)$$



3. THEORY OF PLATES

A plate is defined as a plane, load-carrying element of which one dimension, referred to as thickness h , is very small compared with the other dimensions (width and length). The static and dynamic loads carried by plates are predominantly perpendicular to the plate surfaces. The plate as a flat body develops bending moments in two directions, torsional (twisting) moments and transverse shear forces to resist the loads.

Plates may be classified according to their ratio of thickness to characteristic length (h / L). This classification is conditional (depends on the type of loading, boundary conditions, accuracy of analysis, etc.). An example of a well-accepted classification is the one published by Ventsel and Krauthammer (2001).

1. Thick Plates $\left(\frac{h}{L} \geq \frac{1}{8} \dots \frac{1}{10} \right)$ have all the components of stresses, strains, and displacements and the general equations of three-dimensional elasticity are used for the analysis of such bodies.
2. Membranes $\left(\frac{h}{L} \leq \frac{1}{80} \dots \frac{1}{100} \right)$ have no flexural rigidity and carrying loads by axial tensile forces and central shear forces¹.
3. Thin Plates $\left(\frac{1}{8} \dots \frac{1}{10} \geq \frac{h}{L} \geq \frac{1}{80} \dots \frac{1}{100} \right)$ with flexural rigidity. This group can be subdivided into the following two categories depending on the value of the ratio $\frac{w}{h}$, where w is defined as the maximum deflection of the plate.
 - a. Stiff Plates $\left(\frac{w}{h} \leq 0,2 \right)$ are flexurally rigid thin plates, carrying loads two dimensionally, mostly by internal bending and torsional moments

¹ Central shear force acts in the plane of the plate.

and by transverse shear forces². The middle plane³ (or simply midplane) deformations and the membrane forces are negligible. In engineering practice, *plate* is understood to mean a stiff plate unless otherwise specified.

- b. Flexible Plates $\left(\frac{w}{h} \geq 0,3\right)$ represent a combination of stiff plates and membranes, carrying loads by the combined action of internal (bending and torsional) moments, shear forces and membrane (axial) forces.

The theory of plates involves traditionally the analysis of stress and strain in the plate subjected to loads. Along with the change in structural materials at the end of the 19th century, various plate theories were developed. Of the numerous plate theories, two different limit cases are widely accepted and used in engineering applications: the Kirchhoff theory of plates (classical plate theory) and the Mindlin-Reissner theory of plates (shear-deformable plate theory).

Kirchhoff (1850) introduced the well-known hypothesis of classical plate theory for thin plates, that is:

1. Points of the plate lying initially on a normal to the middle plane of the plate remain on the normal to the middle surface of the plate after deformation. This means that transverse shear deformations are negligible.
2. The stress in the direction which is normal to the plate middle plane can be disregarded.
3. There is no deformation in the middle plane of the plate.

Since characterizing the stress-strain relation of the material becomes a major concern in the practical design and analysis of engineering structures, plate theories can also be grouped according to their stress-strain relationships. Linear-elastic plate theories are based on the assumption of a linear relationship between stress and strain according to the well-known Hooke's law, whereas non-linear elasticity, plasticity and

² Transverse shear forces acts perpendicularly to the plane of the plate.

³ Middle plane (or simply midplane) is a plane parallel to the plate's surfaces which divides the thickness h into equal halves. Being subjected to transverse loads, an initially flat plate deforms and the midplane passes into some curvilinear surface, which is referred to as the middle surface.

viscoelasticity consider more complex stress-strain relationships. With regard to the actual material behavior, viscoelastic constitutive relations should be used instead of the elastic constitutive relations for determination of the most realistic results.

This chapter is concerned with basic assumptions of the linear, viscoelastic, small-deflection theory of bending for thin plates and fundamental equations

- i. Equilibrium equations
- ii. Kinematic equations (strain-displacement equations)
- iii. Compatibility equations
- iv. Constitutive equations (stress-strain relations)

required for the calculation of the linear, time-dependent response of thin plates.

3.1 Basic Assumptions

A load-free plate with top and bottom surfaces lie at $z = \pm \frac{h}{2}$ and an associated Cartesian coordinate system (x, y, z) located at its middle plane are shown in Figure 3.1. The plate's middle plane coincides with the xy plane and the z coordinate is perpendicular to it. The basic assumptions used in the derivation of the fundamental equations of a viscoelastic plate body may be stated as follows:

- i. The material of the plate is homogenous, isotropic and linear viscoelastic
- ii. The plate is initially flat
- iii. The validity of Kirchhoff's classical theory of thin plates is assumed
- iv. The middle surface of the plate remains unstrained after bending
- v. Since the displacement of the middle plane is small compared with the thickness of the plate, the slope of the deflected surface is therefore very small and the square of the slope is a negligible quantity in comparison with unity

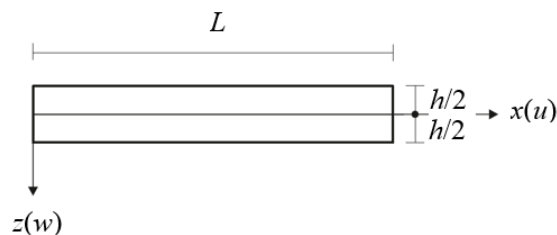


Figure 3.1 : Rectangular plate and associated coordinate system.

3.2 Fundamental Equations

3.2.1 Equilibrium equations

In order to completely define the state of stress at a point anywhere in the interior of the plate body, an infinitesimal parallelepiped with faces parallel to the Cartesian coordinate planes and side lengths dx , dy and dz in the x , y , and z directions, respectively is considered (Figure 3.2). For the parallelepiped to be in equilibrium, the static equilibrium conditions, namely, the sum of all the forces in each of the directions and sum of the moments of the forces about the three reference axes should both be zero must be satisfied.

Stresses acting on the faces of this parallelepiped describe the intensity of the internal forces at a point on a particular face. These stresses can be broken down into two components, a normal stress component and tangent (shear) stress component. For normal stress, the single subscript that indicates the direction of an outer normal to the face on which the stress component acts is used. For the shear stress, the first subscript indicates the direction of the plane normal on which the shear stress is acting while the second subscript indicates the direction in which it is acting.

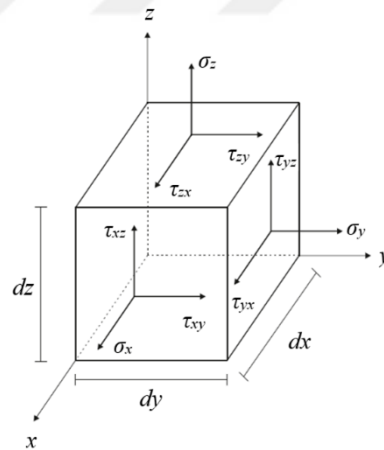


Figure 3.2 : Stress components on plate element.

By considering the following six static equilibrium conditions:

$$\text{Force Equilibrium: } \sum F_x = 0 \quad , \quad \sum F_y = 0 \quad , \quad \sum F_z = 0 \quad (3.1)$$

$$\text{Moment Equilibrium: } \sum M_x = 0 \quad , \quad \sum M_y = 0 \quad , \quad \sum M_z = 0 \quad (3.2)$$

and designate the components of the body force in the x , y and z directions by X , Y , and Z , the following differential equations of equilibrium is obtained by considering the force equilibrium conditions in the x , y , and z directions, respectively.

$$\begin{aligned}\frac{\partial \sigma_x}{\partial x} + \frac{\partial \tau_{yx}}{\partial y} + \frac{\partial \tau_{zx}}{\partial z} + X &= 0 \\ \frac{\partial \tau_{xy}}{\partial x} + \frac{\partial \sigma_y}{\partial y} + \frac{\partial \tau_{zy}}{\partial z} + Y &= 0 \\ \frac{\partial \tau_{xz}}{\partial x} + \frac{\partial \tau_{yz}}{\partial y} + \frac{\partial \sigma_z}{\partial z} + Z &= 0\end{aligned}\quad (3.3)$$

By considering the moment equilibrium conditions about the x , y , and z axes, respectively, the following relations imply equality of shear stresses on perpendicular planes (reciprocity law of shear stresses) are obtained:

$$\begin{aligned}\tau_{yz} &= \tau_{zy} \\ \tau_{zx} &= \tau_{xz} \\ \tau_{xy} &= \tau_{yx}\end{aligned}\quad (3.4)$$

These relations show that the state of stress at a point can be completely defined by six independent stress components instead of nine stress components. Since the three equilibrium equations (3.3) are not sufficient for determination of the six stress components, the problem is internally statically indeterminate. In order to obtain additional equations, the deformation of the body as well as the stress-strain relations of the material of the body need to be considered.

3.2.2 Kinematic equations (strain-displacement equations)

These equations express the strain components in terms of displacements which in turn describe the deformation of a body. Deformation of the body occurs as a result of relative displacement between two points in the body. The general displacement of the point may be composed of

- i. Rigid body displacement
- ii. Deformation

In the rigid body displacement, the shape and size of the body remain unchanged whereas the deformation causes the body to change its size and shape. The concept of strain is derived from that of deformation. There are two aspects of deformation,

namely translation and rotation. Translation gives a measure of elongation or contraction and it is called the normal strain. Rotation gives a measure of relative rotation of orthogonal lines and it is referred to as shear strain. Normal strain is denoted by ε with a subscript corresponds to the direction along which the strain is measured. Whereas the shear strain is denoted by γ with double subscripts indicate the coordinate plane in which the shear strain occurs. The strain-displacement relations assuming that the deformation of the body is small can be obtained purely from geometrical consideration by comparing the deformed state with the initial state of the rectangle as shown in Figure 3.3. In the view of that the components of the displacement in the x , y , and z directions are u , v and w , respectively, the strain-displacement relations can be obtained as:

$$\begin{aligned}\varepsilon_x &= \frac{\partial u}{\partial x} \\ \varepsilon_y &= \frac{\partial v}{\partial y} \\ \varepsilon_z &= \frac{\partial w}{\partial z}\end{aligned}\tag{3.5}$$

and

$$\begin{aligned}\gamma_{xy} &= \frac{\partial u}{\partial y} + \frac{\partial v}{\partial x} \\ \gamma_{yz} &= \frac{\partial v}{\partial z} + \frac{\partial w}{\partial y} \\ \gamma_{zx} &= \frac{\partial w}{\partial x} + \frac{\partial u}{\partial z}\end{aligned}\tag{3.6}$$

by neglecting the square and the products of derivative of displacements. In equations (3.5) and (3.6), ε_x , ε_y and ε_z are called the normal or linear strains and γ_{xy} , γ_{yz} , γ_{zx} are called the shear strains in xy , yz , zx planes, respectively.

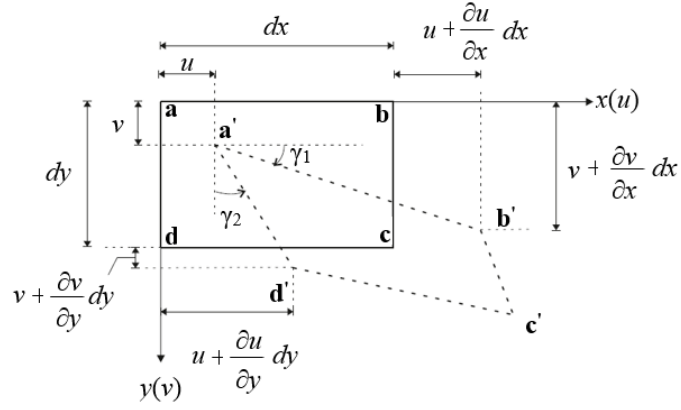


Figure 3.3 : Angular deformation.

3.2.3 Compatibility equations

By means of the six equations given by (3.5) and (3.6), the six strain components can be uniquely determined if the three displacement components are given. On the other hand, if the six strain components are given and three displacement components are asked, the displacement components cannot be uniquely determined unless the given strain components satisfy some specific relations. These relations are called the compatibility equations and if the displacement components u , v and w are to be single valued and continuous functions of the Cartesian coordinates x , y and z , then the corresponding strain components obtained from the kinematic equations (3.5) and (3.6) satisfy the following compatibility equations:

$$\begin{aligned} \frac{\partial^2 \varepsilon_x}{\partial y^2} + \frac{\partial^2 \varepsilon_y}{\partial x^2} &= \frac{\partial^2 \gamma_{xy}}{\partial x \partial y} \\ \frac{\partial^2 \varepsilon_y}{\partial z^2} + \frac{\partial^2 \varepsilon_z}{\partial y^2} &= \frac{\partial^2 \gamma_{yz}}{\partial y \partial z} \\ \frac{\partial^2 \varepsilon_z}{\partial x^2} + \frac{\partial^2 \varepsilon_x}{\partial z^2} &= \frac{\partial^2 \gamma_{zx}}{\partial z \partial x} \end{aligned} \quad (3.7)$$

and

$$\begin{aligned} 2 \frac{\partial^2 \varepsilon_x}{\partial y \partial z} &= \frac{\partial}{\partial x} \left(-\frac{\partial \gamma_{yz}}{\partial x} + \frac{\partial \gamma_{zx}}{\partial y} + \frac{\partial \gamma_{xy}}{\partial z} \right) \\ 2 \frac{\partial^2 \varepsilon_y}{\partial z \partial x} &= \frac{\partial}{\partial y} \left(\frac{\partial \gamma_{yz}}{\partial x} - \frac{\partial \gamma_{zx}}{\partial y} + \frac{\partial \gamma_{xy}}{\partial z} \right) \\ 2 \frac{\partial^2 \varepsilon_z}{\partial x \partial y} &= \frac{\partial}{\partial z} \left(\frac{\partial \gamma_{yz}}{\partial x} + \frac{\partial \gamma_{zx}}{\partial y} - \frac{\partial \gamma_{xy}}{\partial z} \right) \end{aligned} \quad (3.8)$$

Since the material properties were not used in derivation of the equilibrium conditions and the kinematic relations, these relationships are valid for any type of material. The constitutive equations describe the relation between stresses and strains and vary from material to material. The relationships established in this chapter are restricted to viscoelastic materials.

3.2.4 Constitutive equations

In Section 2.7, two alternative forms used to define the constitutive equations of linear viscoelastic materials were described. In this study, the stress-strain relations of viscoelastic materials will be described by integral operator form, the hereditary integrals. No matter how integral representation over differential operator forms sometimes leads to difficult mathematics in stress analysis it has the advantage of greater flexibility when it comes to rendering the measured properties of an actual (viscoelastic) material (Flügge, 1975).

The constitutive equation of linear viscoelastic materials can be written in hereditary integral form as follows:

$$\begin{aligned}\sigma(t) &= Y(0)\varepsilon(t) + \int_0^t \frac{d}{d(t-t')} Y(t-t') \varepsilon(t') dt' \\ \varepsilon(t) &= J(0)\sigma(t) + \int_0^t \frac{d}{d(t-t')} J(t-t') \sigma(t') dt'\end{aligned}\tag{3.9}$$

where t denotes time, t' is a dummy variable for integration and $\sigma(t)$ and $\varepsilon(t)$ are the time-dependent stress and strain, respectively. $J(t)$ is a time-dependent compliance and $Y(t)$ is a time-dependent relaxation modulus.

By invoking the foregoing assumptions, the field equations of the viscoelastic classical or Kirchhoff plates will be derived.

To express the strain-curvature relations, a section of the plate by a plane parallel to Oxz , $y = \text{const.}$, before and after deformation is considered as shown in Figure 3.4.

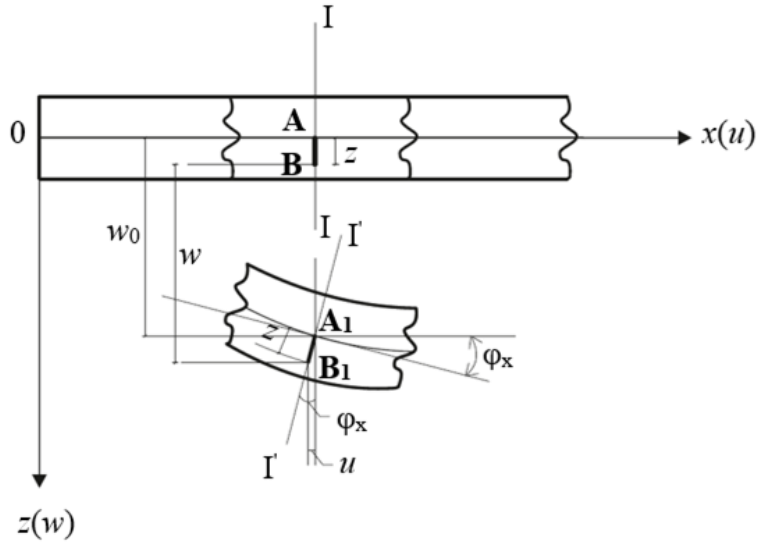


Figure 3.4 : Section before and after deformation.

Using the Kirchhoff's first assumption given in Section 3 and integrating the equations (3.5) and (3.6) for ε_z , γ_{yz} and γ_{xz} , the following equations are obtained:

$$\begin{aligned}
 w &= w_0 \\
 v &= v_0 - z \frac{\partial w}{\partial y} \\
 u &= u_0 - z \frac{\partial w}{\partial x}
 \end{aligned}
 \tag{3.10}$$

where u , v and w are the displacements of points at a distance z from the middle surface. In addition u_0 , v_0 , w_0 denote the displacements of a material point at $(x, y, 0)$ in (x, y, z) coordinate directions.

Let's consider a segment **AB** in the positive z direction (as in Figure 3.4). After the deformation, point **A** displaced a distance w parallel to the original z direction and reached to its final position **A1**. Based upon the Kirchhoff's first assumption given in Section 3, the deformed position of point **B**, which initially lies at a distance z from the point **A** (undeformed middle plane), must lie on the normal to the middle surface. The final position of **B** is denoted by **B1**. Using the Kirchhoff's second and third assumptions given in Section 3, the distance z between the above mentioned points remains unchanged during deformation and is also equal to z . The displacement components u and v can be expressed in the form:

$$\begin{aligned} u &= -z\varphi_x \\ v &= -z\varphi_y \end{aligned} \quad (3.11)$$

Here, $\varphi_x = \frac{\partial w}{\partial x}$ and $\varphi_y = \frac{\partial w}{\partial y}$ correspond to the angles of rotation of the normal (line I-I) to the middle surface in the $0xz$ and $0yz$ plane, respectively. Substitution of (3.10) into the first two (3.5) and into the first (3.6) yields:

$$\begin{aligned} \varepsilon_x &= -z \frac{\partial^2 w}{\partial x^2} \\ \varepsilon_y &= -z \frac{\partial^2 w}{\partial y^2} \\ \gamma_{xy} &= -2z \frac{\partial^2 w}{\partial x \partial y} \end{aligned} \quad (3.12)$$

Here, ε_x , ε_y , γ_{xy} refers to the in-plane strain components at a point of the plate located at a distance z from the middle surface. In (3.12), the second derivatives of the deflection, which corresponds to the normal component of the displacement vector w , define the curvature of the section.

The curvatures of the section κ_x and κ_y along the x and y axes, respectively are defined by the following relations:

$$\begin{aligned} \kappa_x &= -\frac{\partial^2 w}{\partial x^2} \\ \kappa_y &= -\frac{\partial^2 w}{\partial y^2} \end{aligned} \quad (3.13)$$

These curvatures characterize the phenomenon of bending of the middle surface in planes parallel to the $0xz$ and $0yz$ coordinate planes, respectively. They are referred to as "bending curvature". The derivative $\frac{\partial^2 w}{\partial x \partial y}$ in (3.12) defines the warping of the middle surface at a point with coordinates x and y is referred to as "twisting curvature with respect to the x and y axes" (Ventsel and Krauthammer, 2001) and it is defined by:

$$\kappa_{xy} = \kappa_{yx} = -\frac{\partial^2 w}{\partial x \partial y} \quad (3.14)$$

In particular, the main interest in the theory of plates is to introduce the total statically equivalent forces and moments, known as stress resultants and stress couples. The

stress resultants are in-plane and transverse shear forces and the stress couples are bending and twisting moments. In order to obtain the stress resultant quantities and stress couple quantities, the integral relations of stresses through the plate's thickness must be defined mathematically as:

$$\begin{Bmatrix} N_x \\ N_y \\ N_{xy} = N_{yx} \end{Bmatrix} = \int_{-h/2}^{+h/2} \begin{Bmatrix} \sigma_x \\ \sigma_y \\ \tau_{xy} \end{Bmatrix} dz \quad (3.15)$$

$$\begin{Bmatrix} M_x \\ M_y \\ M_{xy} = M_{yx} \end{Bmatrix} = \int_{-h/2}^{+h/2} \begin{Bmatrix} \sigma_x \\ \sigma_y \\ \tau_{xy} \end{Bmatrix} z dz \quad (3.16)$$

$$\begin{Bmatrix} Q_x \\ Q_y \end{Bmatrix} = \int_{-h/2}^{+h/2} \begin{Bmatrix} \tau_{xz} \\ \tau_{yz} \end{Bmatrix} dz \quad (3.17)$$

where N_x and N_y are in-plane membrane forces due to stretching of the plate middle plane, N_{xy} is an in-plane shear force, M_x and M_y are bending moments about the y and x axes, respectively, M_{xy} and M_{yx} are twisting moments, and Q_x and Q_y are transverse shear forces. The stress resultants given by (3.15) and (3.17) have the units of forces per unit length of the plate middle plane and the stress couples given by (3.16) have the units of moments per unit length of the plate middle plane. Positive sign convention for the stress resultants and stress couples is illustrated in Figure 3.5 by considering equilibrium of an element, with side lengths dx and dy , of the plate subjected to the external loading. In most plate applications, the external loading includes distributed load and/or concentrated load normal to the plate (z direction), or in-plane tensile, bending or shear loads applied to the edge of the plate.

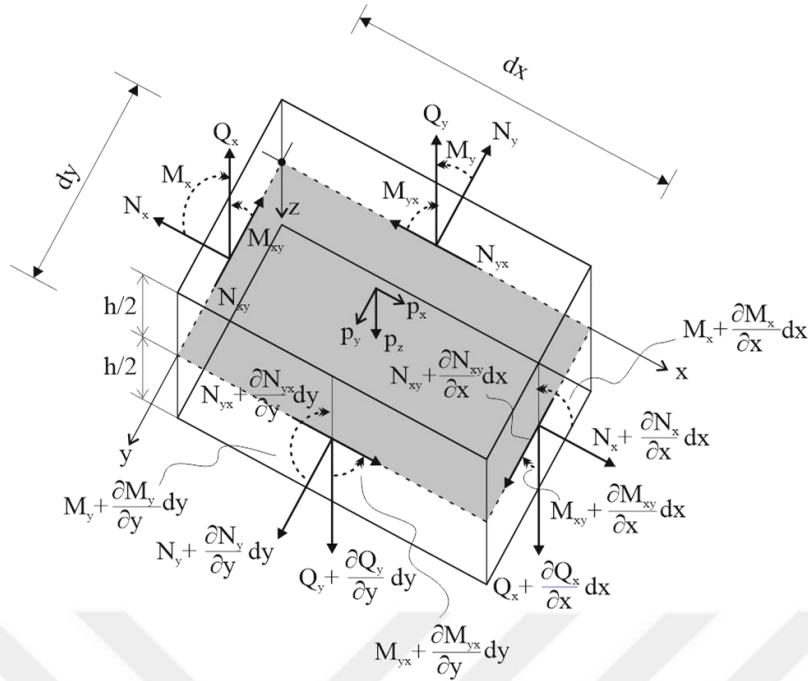


Figure 3.5 : Force and moment resultants acting on a plate element.

As illustrated in Figure 3.5, it is assumed that the plate middle plane is subjected to applied distributed loads p_x , p_y , and p_z with units of force per unit area. In reality, these loads are applied to the top or bottom surface of the plate but they are transferred to the middle plane since the force and moment resultants are assumed to be applied to the middle plane of the plate element. In addition, the stress resultants and couples are shown by a single vector for the sake of simplicity by noting that as the element is very small, they may be considered to be distributed uniformly over the middle plane of the plate element. Because of the reciprocity law of shear stresses $\tau_{xy} = \tau_{yx}$, the in-plane shear forces and twisting moments on perpendicular faces of an infinitesimal plate element are identical, i.e., $N_{xy} = N_{yx}$ and $M_{xy} = M_{yx}$. In addition, the variation of an intensity of the force and moment stress resultants between the edges of the plate element by a value of partial differential is shown in Figure 3.5.

For the system of force and moments shown in Figure 3.5, the following five equilibrium equations (two in-plane and one transverse force equilibrium equations in the x , y and z axes, respectively and two moment equilibrium equations about the x and y axes, respectively) can be obtained as follows:

$$\frac{\partial N_x}{\partial x} + \frac{\partial N_{yx}}{\partial y} + p_x = 0 \quad (3.18)$$

$$\frac{\partial N_{xy}}{\partial x} + \frac{\partial N_y}{\partial y} + p_y = 0 \quad (3.19)$$

$$\frac{\partial Q_x}{\partial x} + \frac{\partial Q_y}{\partial y} + p_z = 0 \quad (3.20)$$

$$\frac{\partial M_x}{\partial x} + \frac{\partial M_{yx}}{\partial y} - Q_x = 0 \quad (3.21)$$

$$\frac{\partial M_{xy}}{\partial x} + \frac{\partial M_y}{\partial y} - Q_y = 0 \quad (3.22)$$

Referring to these equations, the problem can be decomposed into two sets of problems which are uncoupled with each other, as in-plane problems and out-of-plane problems. The out-of-plane problem is regarded as a bending problem and the in-plane problem is also called as a stretching problem of a plate. The present study is focused solely on a bending problem (out-of-plane problem) which is governed by equations (3.20), (3.21) and (3.22). These three equations involve five unknowns M_x , M_y , $M_{xy} = M_{yx}$, Q_x and Q_y . In order to derive the governing equation of the classical plate bending theory, differentiate the two moment equilibrium equations, (3.21) and (3.22), with respect to x and y , respectively and substitute these two equations into the transverse force equilibrium equation (3.20). p_z is denominated from now on as q . Finally, the following equation is obtained:

$$\frac{\partial^2 M_x}{\partial x^2} + 2 \frac{\partial^2 M_{xy}}{\partial x \partial y} + \frac{\partial^2 M_y}{\partial y^2} = -q \quad (3.23)$$

To relate the stress-strain, two operators E_1^* and E_2^* are introduced as follows:

$$\begin{aligned}\sigma_x &= E_1^* \varepsilon_x + E_2^* \varepsilon_y \\ \sigma_y &= E_2^* \varepsilon_x + E_1^* \varepsilon_y\end{aligned}\quad (3.24)$$

These operators operate on any function f as below:

$$\begin{aligned}E_1^* f &= E_1(0) f(t) + \int_0^t \frac{d}{d(t-t')} E_1(t-t') f(t') dt' \\ E_2^* f &= E_2(0) f(t) + \int_0^t \frac{d}{d(t-t')} E_2(t-t') f(t') dt'\end{aligned}\quad (3.25)$$

Using Mohr circle, it can be easily shown that shear stress and shear strain relation can be expressed using the same operators as follows:

$$\tau_{xy} = \frac{1}{2}(E_1^* - E_2^*) \gamma_{xy}\quad (3.26)$$

By substituting the strain-displacement relations (kinematic relations) into the stress-strain relations (constitutive equations) and integrating over the plate thickness, the stress couples can be derived in terms of the displacement as follows:

$$\begin{aligned}M_x &= -\frac{h^3}{12} \left[E_1^* \frac{\partial^2 w}{\partial x^2} + E_2^* \frac{\partial^2 w}{\partial y^2} \right] \\ M_y &= -\frac{h^3}{12} \left[E_1^* \frac{\partial^2 w}{\partial y^2} + E_2^* \frac{\partial^2 w}{\partial x^2} \right] \\ M_{xy} &= -\frac{h^3}{12} [E_1^* - E_2^*] \frac{\partial^2 w}{\partial x \partial y}\end{aligned}\quad (3.27)$$

Expressions for the bending and twisting moments may now be rewritten considering the new operator as follows:

$$\begin{aligned}M_x &= -D^* \left[\frac{\partial^2 w}{\partial x^2} + \nu \frac{\partial^2 w}{\partial y^2} \right] \\ M_y &= -D^* \left[\frac{\partial^2 w}{\partial y^2} + \nu \frac{\partial^2 w}{\partial x^2} \right] \\ M_{xy} &= -(1-\nu) D^* \frac{\partial^2 w}{\partial x \partial y}\end{aligned}\quad (3.28)$$

Here, D^* is the operator form of the flexural rigidity of the plate and it is derived assuming that the Poisson ratio, which is denoted by ν , is constant as:

$$D^* = E_1^* \frac{h^3}{12}\quad (3.29)$$

4. INTEGRAL TRANSFORMS

Differential equations are at the heart of physics, chemistry, biology and other areas of natural sciences, as well as areas such as engineering and economics. A differential equation is any mathematical equation relating the values of the function to the values of its derivatives, either ordinary derivatives or partial derivatives. In applications, the functions usually represent physical quantities, the derivatives represent their rates of change, and the equation defines a relationship between the two. When considering differential equations, it is important to distinguish between the dependent variable and the independent variable. In an ordinary differential equation (*ode*), there can be more than one dependent variable, but there can only be one independent variable e.g., $f(t)$ where f is the dependent variable and t is the independent variable. However, in a partial differential equation (*pde*), there is more than one independent variable e.g., $f(x, y, z, t)$ where the four independent variables are x, y, z and t , while f is the dependent variable. An *ode* contains ordinary derivatives in it. Likewise, a *pde* contains partial derivatives. Typically, *pdes* are much harder to solve than *odes*. For the solution of certain breeds of differential equations, two extremely powerful methods: the Fourier and the Laplace transforms have become essential working tools of nearly every engineer and applied scientist. Beside their practical use, they are also of fundamental importance in applied mechanics, providing a transform the given problem into one that is easier to solve. In the case of an *ode* with constant coefficients, the transformed problem becomes an algebraic problem. When a *pde* is transformed, it becomes an *ode* or lower order *pde*. The solution of the transformed problem in either case will be a function of the transform variable and any remaining independent variables. Inverting this solution produces the solution of the original problem. In order for these transform techniques to work, the *ode* or *pde* that the transform is being applied to must be linear. The basic idea behind a transform can be represented diagrammatically for *odes* as follows:

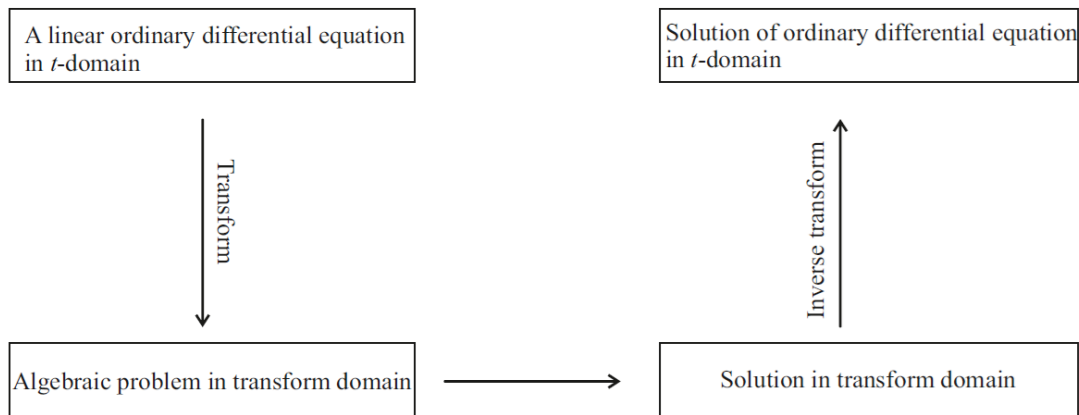


Figure 4.1 : Basic idea behind use of a transform for *odes*.

The Fourier transform is intimately related with the Laplace transform. The use of Fourier and Laplace transforms in applications is quite extensive. In this thesis, the major emphasis will be on briefly discussing how Laplace transform method is used for solving problems associated with linear *pdes*.

We will start by introducing the Heaviside unit step function and the Dirac delta function as these functions will be used in future sections for the modeling of physical problem and in the representation of certain solution.

4.1 Heaviside Unit Step Function

Heaviside unit step function is a widely used fundamental function in the study of physical and engineering problems. The Heaviside unit step function is a discontinuous function that is defined as:

$$H(t) = \begin{cases} 1 & \text{for } t > 0 \\ 0 & \text{for } t < 0 \end{cases} \quad (4.1)$$

That is, the value of the function $H(t)$ at $t = 0$ is not defined. The value of the function is always unity when the argument of the function is greater than zero, and its value is zero when the argument of the function is always less than zero. A graph of the Heaviside unit step function is illustrated in Figure 4.2.

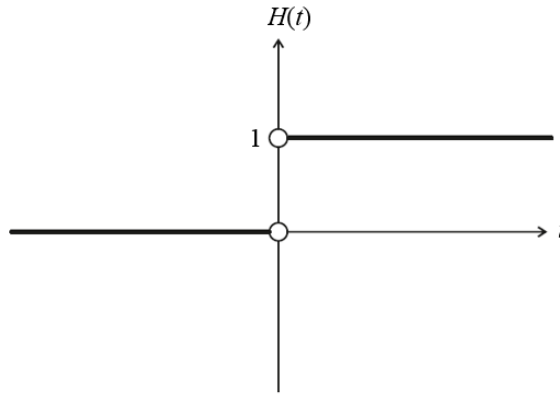


Figure 4.2 : Heaviside unit step function.

Heaviside unit step function can be used to crop and shift functions. For instance, the function $H(t - t_0)$ is just $H(t)$ shifted, or dragged so that it turns on at $t = t_0$ as in Figure 4.3.

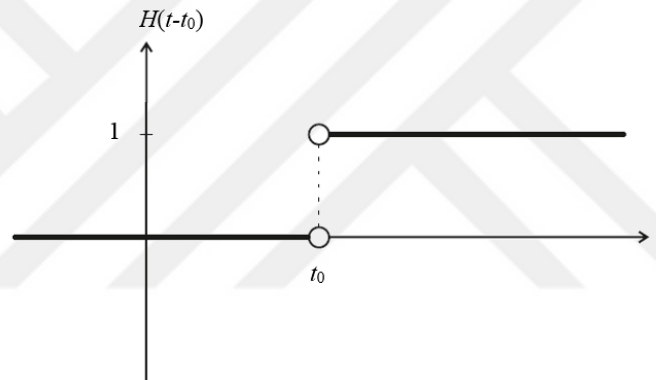


Figure 4.3 : Heaviside unit step function $H(t - t_0)$.

Moreover multiplying an arbitrary function $f(t)$ by the Heaviside unit step function $H(t - t_0)$ crops $f(t)$ so that it turns on at $t = t_0$:

$$H(t - t_0)f(t) = \begin{cases} f(t) & \text{for } t > t_0 \\ 0 & \text{for } t < t_0 \end{cases} \quad (4.2)$$

The Heaviside unit step function can be used to define the impulse function. Although impulse function is not really a true function in the mathematical sense, it has a wide range of applications in many physical problems. The impulse function of height $\frac{1}{\varepsilon}$ between t_0 and $t_0 + \varepsilon$, and zero elsewhere can be defined as follows:

$$\delta_\varepsilon(t - t_0) = \frac{1}{\varepsilon} [H(t - t_0) - H(t - (t_0 + \varepsilon))] \quad (4.3)$$

A graph of impulse function $\delta_\varepsilon(t - t_0)$ is constructed by subtracting two Heaviside unit step functions as illustrated in Figure 4.4.

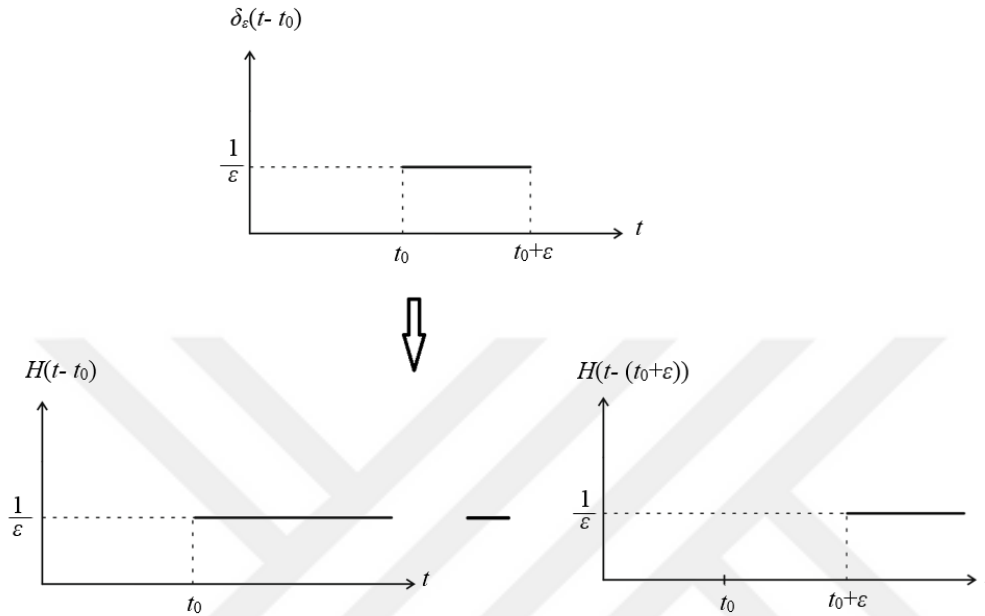


Figure 4.4 : Impulse function $\delta_\varepsilon(t - t_0)$.

It should be noted that the area under the impulse curve is always unity. An impulse function is also known as a “delta function”. There are different types of delta functions as Dirac delta function and Kronecker delta function. Although, these functions appear as an impulse in general, they have slightly different properties.

4.2 Dirac Delta Function

The Dirac delta function known as unit-impulse function was introduced by Dirac (1958) and developed by Schwartz (1950, 1951). It is defined as a generalized function or distribution.

The (time-delayed) Dirac delta function $\delta(t - t_0)$ have the value zero everywhere except at the point t_0 , where it has the value of infinity.

$$\delta(t - t_0) = \lim_{\varepsilon \rightarrow 0} \delta_\varepsilon(t - t_0) \quad (4.4)$$

At the point t_0 , this function subtends on area of unity.

$$\int_{-\infty}^{+\infty} \delta(t - t_0) dt = 1 \quad (4.5)$$

A very useful property for the Dirac delta function is the shifting property that is given by the integral of the time-delayed Dirac delta as follows:

$$\int_{-\infty}^{+\infty} f(t) \delta(t - t_0) dt = f(t_0) \quad (4.6)$$

Another property gives a close relationship between the Heaviside unit step function and Dirac delta function as follows:

$$\begin{aligned} \frac{d}{dt} H(t - t_0) &= \delta(t - t_0) \\ \Downarrow \\ H(t - t_0) &= \int_{-\infty}^t \delta(t - t_0) dt \end{aligned} \quad (4.7)$$

The Kronecker delta δ_{ij} is a function of two variables i and j . The function is equal to one if the variables are equal. Otherwise, the Kronecker delta is equal to zero:

$$\delta_{ij} = \begin{cases} 1 & \text{for } i = j \\ 0 & \text{for } i \neq j \end{cases} \quad (4.8)$$

This function satisfies the shifting property:

$$\sum_{i=-\infty}^{\infty} a_i \delta_{ik} = a_k \quad (4.9)$$

The Kronecker delta is a discrete function whereas the Dirac delta is a continuous function. An integral of Dirac delta function is exactly equal to one. The Kronecker delta function is similarly infinitesimally thin, but its amplitude is equal to one, not its area. For more information about the relationship between them, the reader is referred to Signals and Systems/Engineering Functions (2017).

4.3 The Laplace Transform

Suppose that $f(t)$ is a piecewise continuous function of t specified for $t > 0$. The Laplace transform of $f(t)$, denoted by $F(s) = L\{f(t)\}$, is defined by the integral transform:

$$L\{f(t)\} = F(s) = \int_0^{\infty} f(t) e^{-st} dt \quad (4.10)$$

Laplace transform is a linear operator of a function $f(t)$ with a real argument $t (t \geq 0)$ that transforms it to a function $F(s)$ with a complex argument s .

When a function is called piecewise continuous (or sectionally continuous) in an interval, an interval can be broken into a finite number of subintervals in each of which the function is continuous and has a finite limit at the endpoints of each subinterval.

The Laplace transform may not exist if $f(t)$ becomes singular in an interval $0 \leq t \leq \infty$. However, we assume continuity for $f(t)$ for the large majority of engineering problems. The Laplace transform operates on $[0, \infty]$ unlike the Fourier transform that operates on $[-\infty, \infty]$. Therefore, the Laplace transform is useful for initial value problems since it incorporates in a natural way the initial conditions.

The operator $L\{ \}$ has an inverse operator $L^{-1}\{ \}$. Then the inverse Laplace transform is given by the following integral form where integration takes place in the complex s -plane.

$$f(t) = L^{-1}\{F(s)\} = \frac{1}{2\pi i} \int_{a-i\infty}^{a+i\infty} F(s) e^{st} ds \quad (4.11)$$

where $i = \sqrt{-1}$ and a is a real number.

4.4 Basic Properties of the Laplace Transform

Laplace transforms satisfy a number of general properties. Here, some of the simplest and quite useful properties of the Laplace transform will be presented without their proofs. For more comprehensive list of the Laplace transform properties with proofs, see, Andrews and Philips (2003) and Dyke (2014).

4.4.1 Linearity of Laplace transform

The Laplace transform is a linear transform. Linearity is one of the simplest and most frequently invoked property of the Laplace transform. That is, let's say we have two functions $x(t)$ and $y(t)$ with Laplace transforms given by $X(s)$ and $Y(s)$, respectively. Then, the Laplace transform of any linear combination of $x(t)$ and $y(t)$ can be easily given by:

$$L\{ax(t) + by(t)\} = aL\{x(t)\} + bL\{y(t)\} = aX(s) + bY(s) \quad (4.12)$$

where a and b are arbitrary constants.

4.4.2 Shift property of Laplace transform

Another simple property of the Laplace transform is the time-shift (a delay in time). That is, let's say shifting the original function $x(t)$ in time by a constant amount t_0 causes the Laplace transform $X(s)$ to be multiplied by a complex exponential.

$$L\{x(t - t_0)\} = e^{-st_0} X(s) \quad (4.13)$$

4.4.3 Derivative property of Laplace transform

The Laplace transform of $x'(t)$, the first derivative of $x(t)$, is given by:

$$L\left\{\frac{d}{dt}x(t)\right\} = sX(s) - x(0) \quad (4.14)$$

For higher order derivatives, the Laplace transform of the function $x(t)$:

$$L\left\{\frac{d^n}{dt^n}x(t)\right\} = s^n X(s) - s^{n-1}x(0) - s^{n-2}x'(0) \quad (4.15)$$

4.4.4 Convolution property of Laplace transform

The convolution of two given functions $f(t)$ and $g(t)$ is written $f * g$ and is defined by the integral taken over an infinite range:

$$f * g = \int_{-\infty}^{+\infty} f(t') g(t - t') dt' \quad (4.16)$$

The delay time $\tau = t - t'$ may be put in either function as:

$$f * g = \int_{-\infty}^{+\infty} f(t - \tau) g(\tau) d\tau \quad (4.17)$$

For functions $f(t)$ and $g(t)$ is zero for negative arguments, the integration limits can be truncated as:

$$f * g = \int_0^t f(t - \tau) g(\tau) d\tau \quad \text{for } f, g : [0, \infty) \quad (4.18)$$

A convolution integral expresses the amount of overlap of one function as it is shifted over another function.

The Laplace transform of the convolution of $x(t)$ and $y(t)$ with corresponding Laplace transforms $X(s)$ and $Y(s)$ is given by:

$$L\{x(t) * y(t)\} = X(s)Y(s) \quad (4.19)$$

4.5 The Laplace-Carson Transform

For the purposes of viscoelasticity, it is sufficient to consider functions $f(t)$ of variable t , of real or complex values, piecewise indefinitely differentiable and identical to zero for $t \leq 0$. The Laplace-Carson transform of a function $f(t)$, $t \geq 0$ is an integral transform defined as:

$$\bar{F}(s) = s \int_0^{\infty} f(t) e^{-st} dt = s F(s) \quad (4.20)$$

In order to denote the Laplace-Carson transform of a time-varying function $f(t)$, the notation $\bar{F}(s)$ is used. When equation (4.20) is considered, it is obvious that the Laplace-Carson transform of any function corresponds to the s -multiplied Laplace transform of that function.

4.6 Field Equations in Laplace-Carson Domain

In order to remove the time derivatives from governing equations and boundary conditions, the method of Laplace-Carson transform is employed.

By taking Laplace-Carson transform of equations (3.23) and (3.28), the following field equations are obtained in the Laplace-Carson domain:

$$\begin{aligned}
-\frac{\partial^2 \bar{M}_x}{\partial x^2} - 2\frac{\partial^2 \bar{M}_{xy}}{\partial x \partial y} - \frac{\partial^2 \bar{M}_y}{\partial y^2} &= \bar{q} \\
-\bar{M}_x - \bar{D}^* \left[\frac{\partial^2 \bar{w}}{\partial x^2} + \nu \frac{\partial^2 \bar{w}}{\partial y^2} \right] &= 0 \\
-\bar{M}_y - \bar{D}^* \left[\frac{\partial^2 \bar{w}}{\partial y^2} + \nu \frac{\partial^2 \bar{w}}{\partial x^2} \right] &= 0 \\
-\bar{M}_{xy} - (1-\nu) \bar{D}^* \frac{\partial^2 \bar{w}}{\partial x \partial y} &= 0
\end{aligned} \tag{4.21}$$

For a plate, boundary conditions written in symbolic form are:

$$\begin{aligned}
\bar{T} - \hat{T} &= 0 \\
-\bar{M} + \hat{M} &= 0 \\
\bar{w}' - \hat{w}' &= 0 \\
-\bar{w} + \hat{w} &= 0
\end{aligned} \tag{4.22}$$

Here, terms with “^” are the known boundary conditions. The final forms of the boundary conditions will be obtained after carrying out the following variational process.



5. VARIATIONAL PRINCIPLES

Variational principles are scientific principles used within the calculus of variations wherein the stationary property of a function of functions, namely a functional, is studied. In solid and structural mechanics problems, the functional includes all the fundamental properties of the problem such as the governing equations, boundary and/or initial conditions and constraint conditions and represents the total energy of the system.

The application of the variational principles, such as the principle of minimum potential energy, the principle of minimum complementary energy and the minimum of some combinations of potential and complementary energies provides a powerful tool in mathematical formulation of the finite element approach.

Many different variational principles have been developed based on the rapid development of the finite element method. Basically, the following finite element models may be considered in solid mechanics:

- i. Kinematic finite element models (unknowns are kinematically admissible displacement fields and the best known instance of such models are those arising from the application of the principle of minimum potential energy, entirely expressed in terms of displacements)
- ii. Equilibrium finite element models (unknowns are stresses and the classical example is provided by the finite elements constructed for the application of the principle of minimum complementary energy)
- iii. Mixed type finite element models (unknowns are usually displacements and stresses which are used simultaneously and variables of different nature are approximated by independent finite element interpolations)

In finite element method, “approximate displacement fields yield approximate equilibrium configurations. Although this may lead to sufficiently accurate displacement fields, the accuracy of the approximate displacement field rapidly deteriorates when differentiations are required to compute other results, such as

stresses” (Santos et al, 2010, p. 810). However, in the mixed finite element method, different types of variables can be handled independently in approximation procedures. Depending on the applied variational principles, the formulations of the mixed type finite element models are changed.

The basis of variational formulation is the principle of virtual work, sometimes it is called the principle of virtual displacements, which states that the virtual work done by the external and internal forces is zero if and only if the body is in equilibrium. This principle is equivalent to the equations of equilibrium of the system and is independent of the stress-strain relations of the material of the body. However, the constitutive relations should be taken into account for the formulations of variational principles. The principle of minimum potential energy is the most frequently applied variational principle in the finite element method. The potential energy in the system is defined by the strains. In order to satisfy the equilibrium position of the system, the total work should be minimum. The minimum is obtained when the variation of the total potential energy is equal to zero. In the case of linear systems, the potential and the complementary energy should be of the same value, except that the complementary energy in the system is expressed in terms of the stresses. These variational principles are applied for the purpose of deriving approximate solutions to practical problems for which there is no exact solution. Different combinations of the potential and the complementary energies are sometimes applied in practice. These combinations give different types of functionals, as Hellinger-Reissner, Hu-Washizu, Gâteaux. These variational principles are known as mixed variational principles.

The use of mixed variational principles in mechanics began with the work of Reissner (1948, 1953) who presented a variational principle for elasticity problems which allowed the simultaneous variation of stresses and displacements. Reissner (1948, 1953) extended an earlier idea of Hellinger (1914) by showing how to correctly include boundary conditions. Therefore, this mixed variational principle is referred to as the Hellinger-Reissner variational principle. This principle eliminates the strain as a primary dependent variable; consequently, only the displacement and the stress remain as arguments in the functional for which variations are constructed. A generalization of this principle is known as the Hu-Washizu variational principle, presented by Hu (1955) and Washizu (1955), in which stresses, displacements, and strains are arguments in the functional. By using the Lagrange multipliers, equilibrium conditions

and kinematic conditions can be included into the functional which is derived by the Hellinger-Reissner principle and Hu-Washizu principle, respectively. The Hu-Washizu principle is based on the potential energy function and the Hellinger-Reissner principle is based on the complementary energy function.

In literature, new energy functional that gains an advantage over the classical potential energy and complementary energy functions is derived by Gâteaux differential method. The Gâteaux differential method is a powerful variational tool when compared by the well-known variational principles of Hellinger-Reissner and Hu-Washizu. In Gâteaux differential method, all field equations and boundary condition terms can be included into the functional by mathematical manipulations. A detailed discussion about the Gâteaux differential method and its advantages over the Hellinger-Reissner and Hu-Washizu principles are given in the following section.

5.1 The Gâteaux Differential Method

The Gâteaux differential generalizes the concept of directional derivative. In this thesis, efficient and systematic procedure based on the Gâteaux differential has been developed in order to construct a new energy functional for the quasi-static and dynamic analysis of viscoelastic plates, as mixed-type finite element analysis. The Gâteaux differential procedure has several advantages over the well-known mixed-type formulations introduced based on the Hellinger-Reissner and Hu-Washizu principles. A detailed comparison of the Gâteaux differential approach with the Hellinger-Reissner and Hu-Washizu principles has been presented in the literature (Saleeb and Chang, 1987; Omurtag et al, 1997; Omurtag and Kadioğlu, 1998; Aköz and Özütok, 2000). Here, we just summarize some of the most representative ones:

- Technique can easily be applied to any field equation.
- Displacement, internal force (moment and shear force) and frequency values can be obtained directly without any mathematical operation.
- Geometric and dynamic boundary conditions can be obtained easily.
- Shear locking problem can be eliminated.

5.1.1 Definition 1

Let U and V denote normed linear spaces and Q is an operator from U into V . The Gâteaux differential of the operator Q at u in the direction η is defined as the limit:

$$dQ(u; \eta) = \lim_{\tau \rightarrow 0} \frac{1}{\tau} [Q(u + \tau\eta) - Q(u)] \quad (5.1)$$

where η is a fixed nonzero element of U , τ is a real number, u and $u + \tau\eta$ are arbitrary elements of U .

5.1.2 Definition 2

Let $I: U \rightarrow \mathbb{R}$ is a functional on a space U which has a Gâteaux differential $dI(u_0; \eta)$ at a point $u_0 \in U$ which is linear and continuous in η . The operator Q defined as follows is called the gradient of the functional I at u_0 ,

$$Q(u_0) = \text{grad } I(u_0) \equiv \lim_{\tau \rightarrow 0} \frac{\partial I(u_0 + \tau\eta)}{\partial \tau}, \quad \eta \in U \quad (5.2)$$

A point $u_0 \in U$ is called a critical point of the functional $I(u)$ if

$$\text{grad } I(u_0) = 0 \quad (5.3)$$

where 0 is the zero element. If $Q(u) = \text{grad } I(u)$, the problem of finding solutions to the equation:

$$Q(u) = 0 \quad (5.4)$$

is, therefore, equivalent to finding critical points of the functional I . Equation (5.4) is then called the Euler equation for the functional $I(u)$.

5.2 Potential Operator

An operator $Q(u)$ is said to be a potential, if and only if there exists a Gâteaux differentiable functional $I(u)$ such that $Q(u) = \text{grad } I(u)$.

5.2.1 Theorem 1

Let Q is a continuous operator which has a linear Gâteaux differential $dQ(u; \eta)$; the necessary and sufficient condition that Q be potential operator is that:

$$\langle dQ(u; \eta), \xi \rangle = \langle dQ(u; \xi), \eta \rangle \quad (5.5)$$

5.2.2 Theorem 2

Let $Q : U \rightarrow V$ is a continuous and potential operator, then there exists a functional $I(u)$ whose gradient is the operator Q , which is given by:

$$I(u) = \int_0^1 \langle Q(u_0 + r(u - u_0)), u - u_0 \rangle dr + I_0 \quad (5.6)$$

where $I_0 = I(u_0)$ and r is a real parameter. More information about these theorems can be found from the work of Oden and Reddy (1976).

5.3 Functional

All field equations in the Laplace-Carson domain including boundary conditions for viscoelastic Kirchhoff plates (see equations (4.21) and (4.22)) can be written in operator form as:

$$\bar{Q} = \bar{P}\bar{u} - \bar{f} \quad (5.7)$$

where \bar{P} represents the coefficient matrix, \bar{u} represents unknown vector $\bar{u} = \{\bar{w}, \bar{M}_x, \bar{M}_y, \bar{M}_{xy}\}$ and \bar{f} represents the load vector in the Laplace-Carson space.

This operator can be written explicitly in matrix form as:

$$\begin{bmatrix} 0 & \bar{P}_{12} & \bar{P}_{13} & \bar{P}_{14} & 0 & 0 & 0 & 0 \\ \bar{P}_{21} & \bar{P}_{22} & \bar{P}_{23} & 0 & 0 & 0 & 0 & 0 \\ \bar{P}_{31} & \bar{P}_{32} & \bar{P}_{33} & 0 & 0 & 0 & 0 & 0 \\ \bar{P}_{41} & 0 & 0 & \bar{P}_{44} & 0 & 0 & 0 & 0 \\ 0 & 0 & 0 & 0 & 0 & 0 & 0 & 1 \\ 0 & 0 & 0 & 0 & 0 & 0 & -1 & 0 \\ 0 & 0 & 0 & 0 & 0 & 1 & 0 & 0 \\ 0 & 0 & 0 & 0 & -1 & 0 & 0 & 0 \end{bmatrix} \begin{Bmatrix} \bar{u}_1 \\ \bar{u}_2 \\ \bar{u}_3 \\ \bar{u}_4 \\ \bar{w} \\ \bar{w}' \\ \bar{M} \\ \bar{T} \end{Bmatrix} = \begin{Bmatrix} \bar{f}_1 \\ \bar{f}_2 \\ \bar{f}_3 \\ \bar{f}_4 \\ \hat{T} \\ -\hat{M} \\ \hat{w}' \\ -\hat{w} \end{Bmatrix} \quad (5.8)$$

where

$$\begin{aligned}\bar{P}_{12} = \bar{P}_{21} &= -\bar{D}^* \left(\frac{\partial^2}{\partial x^2} + v \frac{\partial^2}{\partial y^2} \right) ; & \bar{P}_{22} = \bar{P}_{33} &= -\bar{D}^* \\ \bar{P}_{13} = \bar{P}_{31} &= -\bar{D}^* \left(\frac{\partial^2}{\partial y^2} + v \frac{\partial^2}{\partial x^2} \right) ; & \bar{P}_{23} = \bar{P}_{32} &= -v\bar{D}^* \\ \bar{P}_{14} = \bar{P}_{41} &= -\bar{D}^*(1-v) \frac{\partial^2}{\partial x \partial y} ; & \bar{P}_{44} &= -\frac{1}{2}\bar{D}^*(1-v)\end{aligned}\quad (5.9)$$

$$\bar{f}_1 = \bar{q} \quad ; \quad \bar{f}_2 = \bar{f}_3 = \bar{f}_4 = 0 \quad ; \quad \bar{u}_1 = w$$

$$\bar{u}_2 = \frac{\bar{M}_x - v\bar{M}_y}{\bar{D}^*(1-v^2)} \quad ; \quad \bar{u}_3 = \frac{\bar{M}_y - v\bar{M}_x}{\bar{D}^*(1-v^2)} \quad ; \quad \bar{u}_4 = \frac{2\bar{M}_{xy}}{\bar{D}^*(1-v)}$$

If the Gâteaux derivative of the operator \bar{Q} in the Laplace-Carson domain is defined as:

$$d\bar{Q}(\bar{u}, \bar{u}') = \left. \frac{\partial \bar{Q}(\bar{u} + \tau \bar{u}')}{\partial \tau} \right|_{\tau=0} \quad (5.10)$$

and the potentiality requirement

$$\langle d\bar{Q}(\bar{u}, \bar{u}'), \bar{u}^* \rangle = \langle d\bar{Q}(\bar{u}, \bar{u}^*), \bar{u}' \rangle \quad (5.11)$$

is satisfied, the functional can be obtained. Here, $d\bar{Q}(\bar{u}, \bar{u}')$ and $d\bar{Q}(\bar{u}, \bar{u}^*)$ are the Gâteaux derivatives of the operator \bar{Q} in the \bar{u}' and \bar{u}^* directions and $\langle d\bar{Q}(\bar{u}, \bar{u}'), \bar{u}^* \rangle$ represents the inner product of two vectors. The explicit forms of these expressions are:

$$\begin{aligned}
\langle d\bar{Q}(\bar{u}, \bar{u}'), \bar{u}^* \rangle &= -[\bar{M}'_{x,xx}, \bar{w}^*] - [\bar{M}'_{y,yy}, \bar{w}^*] - 2[\bar{M}'_{xy,xy}, \bar{w}^*] \\
&- \frac{\bar{D}^*}{\bar{D}^*(1-v^2)} [\bar{w}'_{,xx}, \bar{M}_x^*] + \frac{\bar{D}^*v}{\bar{D}^*(1-v^2)} [\bar{w}'_{,xx}, \bar{M}_y^*] \\
&- \frac{\bar{D}^*v}{\bar{D}^*(1-v^2)} [\bar{w}'_{,yy}, \bar{M}_x^*] + \frac{\bar{D}^*v^2}{\bar{D}^*(1-v^2)} [\bar{w}'_{,yy}, \bar{M}_y^*] \\
&- \frac{1}{\bar{D}^*(1-v^2)} [\bar{M}'_x, \bar{M}_x^*] + \frac{v}{\bar{D}^*(1-v^2)} [\bar{M}'_x, \bar{M}_y^*] \\
&- \frac{\bar{D}^*}{\bar{D}^*(1-v^2)} [\bar{w}'_{,yy}, \bar{M}_y^*] + \frac{\bar{D}^*v}{\bar{D}^*(1-v^2)} [\bar{w}'_{,yy}, \bar{M}_x^*] \\
&- \frac{\bar{D}^*v}{\bar{D}^*(1-v^2)} [\bar{w}'_{,xx}, \bar{M}_y^*] + \frac{\bar{D}^*v^2}{\bar{D}^*(1-v^2)} [\bar{w}'_{,xx}, \bar{M}_x^*] \\
&- \frac{1}{\bar{D}^*(1-v^2)} [\bar{M}'_y, \bar{M}_y^*] + \frac{v}{\bar{D}^*(1-v^2)} [\bar{M}'_y, \bar{M}_x^*] \\
&- 2[\bar{w}'_{,xy}, \bar{M}_{xy}^*] - \frac{2}{\bar{D}^*(1-v)} [\bar{M}'_{xy}, \bar{M}_{xy}^*] \\
&+ [\bar{T}', \bar{w}^*]_{\sigma} - [\bar{M}', (\bar{w}')^*]_{\sigma} \\
&+ [(\bar{w}')', \bar{M}^*]_{\epsilon} - [\bar{w}', \bar{T}^*]_{\epsilon}
\end{aligned} \tag{5.12}$$

$$\begin{aligned}
\langle d\bar{Q}(\bar{u}, \bar{u}^*), \bar{u}' \rangle &= -[\bar{M}^*_{x,xx}, \bar{w}'] - [\bar{M}^*_{y,yy}, \bar{w}'] - 2[\bar{M}^*_{xy,xy}, \bar{w}'] \\
&- \frac{\bar{D}^*}{\bar{D}^*(1-v^2)} [\bar{w}^*_{,xx}, \bar{M}_x'] + \frac{\bar{D}^*v}{\bar{D}^*(1-v^2)} [\bar{w}^*_{,xx}, \bar{M}_y'] \\
&- \frac{\bar{D}^*v}{\bar{D}^*(1-v^2)} [\bar{w}^*_{,yy}, \bar{M}_x'] + \frac{\bar{D}^*v^2}{\bar{D}^*(1-v^2)} [\bar{w}^*_{,yy}, \bar{M}_y'] \\
&- \frac{1}{\bar{D}^*(1-v^2)} [\bar{M}^*_x, \bar{M}_x'] + \frac{v}{\bar{D}^*(1-v^2)} [\bar{M}^*_x, \bar{M}_y'] \\
&- \frac{\bar{D}^*}{\bar{D}^*(1-v^2)} [\bar{w}^*_{,yy}, \bar{M}_y'] + \frac{\bar{D}^*v}{\bar{D}^*(1-v^2)} [\bar{w}^*_{,yy}, \bar{M}_x'] \\
&- \frac{\bar{D}^*v}{\bar{D}^*(1-v^2)} [\bar{w}^*_{,xx}, \bar{M}_y'] + \frac{\bar{D}^*v^2}{\bar{D}^*(1-v^2)} [\bar{w}^*_{,xx}, \bar{M}_x'] \\
&- \frac{1}{\bar{D}^*(1-v^2)} [\bar{M}^*_y, \bar{M}_y'] + \frac{v}{\bar{D}^*(1-v^2)} [\bar{M}^*_y, \bar{M}_x'] \\
&- 2[\bar{w}^*_{,xy}, \bar{M}_{xy}'] - \frac{2}{\bar{D}^*(1-v)} [\bar{M}^*_{xy}, \bar{M}_{xy}'] \\
&+ [\bar{T}^*, \bar{w}']_{\sigma} - [\bar{M}^*, (\bar{w}')^*]_{\sigma} \\
&+ [(\bar{w}')^*, \bar{M}']_{\epsilon} - [\bar{w}^*, \bar{T}']_{\epsilon}
\end{aligned} \tag{5.13}$$

After the application of a related mathematical procedure, it is seen that the potentiality requirement is satisfied. If so, the operator \bar{Q} is potential then the functional

corresponding to the field equations can be written in explicit form by using equation (5.6) as:

$$\mathbf{I}(\bar{\mathbf{u}}) = \int_0^1 \left\{ \begin{aligned} & -r\bar{M}_{x,xx}\bar{w} - r\bar{M}_{y,yy}\bar{w} - 2r\bar{M}_{xy,xy}\bar{w} - \bar{q}\bar{w} \\ & - \frac{\bar{D}^* r}{\bar{D}^*(1-v^2)} (\bar{w}_{,xx}\bar{M}_x - v\bar{w}_{,xx}\bar{M}_y - v^2\bar{w}_{,yy}\bar{M}_y + v\bar{w}_{,yy}\bar{M}_x) \\ & - \frac{r}{\bar{D}^*(1-v^2)} \bar{M}_x\bar{M}_x + \frac{vr}{\bar{D}^*(1-v^2)} \bar{M}_x\bar{M}_y \\ & - \frac{\bar{D}^* r}{\bar{D}^*(1-v^2)} (\bar{w}_{,yy}\bar{M}_y - v\bar{w}_{,yy}\bar{M}_x - v^2\bar{w}_{,xx}\bar{M}_x + v\bar{w}_{,xx}\bar{M}_y) \\ & - \frac{r}{\bar{D}^*(1-v^2)} \bar{M}_y\bar{M}_y + \frac{vr}{\bar{D}^*(1-v^2)} \bar{M}_y\bar{M}_x - 2r\bar{w}_{,xy}\bar{M}_{xy} \\ & - \frac{2r}{\bar{D}^*(1-v)} \bar{M}_{xy}\bar{M}_{xy} + r\bar{T}\bar{w} - r\bar{M}(\bar{w}') + r(\bar{w}')\bar{M} - r\bar{w}\bar{T} \\ & - \hat{T}\bar{w} + \hat{M}(\bar{w}') - (\hat{w}')\bar{M} + \hat{w}\bar{T} \end{aligned} \right\} dr \quad (5.14)$$

With the application of some variational manipulations, the explicit form of the functional for viscoelastic Kirchhoff plates in Laplace-Carson domain is generated. For the functional, three different expressions can be obtained:

$$\begin{aligned} \mathbf{I}_1(\bar{\mathbf{u}}) = & - \left[\frac{\partial^2 \bar{w}}{\partial x^2}, \bar{M}_x \right] - \left[\frac{\partial^2 \bar{w}}{\partial y^2}, \bar{M}_y \right] - 2 \left[\frac{\partial^2 \bar{w}}{\partial x \partial y}, \bar{M}_{xy} \right] - [\bar{q}, \bar{w}] \\ & - \frac{1}{2\bar{D}^*(1-v^2)} [\bar{M}_x, \bar{M}_x] - \frac{1}{2\bar{D}^*(1-v^2)} [\bar{M}_y, \bar{M}_y] \\ & + \frac{v}{\bar{D}^*(1-v^2)} [\bar{M}_x, \bar{M}_y] - \frac{1}{\bar{D}^*(1-v)} [\bar{M}_{xy}, \bar{M}_{xy}] \\ & - \left[\hat{T}, \bar{w} \right]_\sigma - \left[\hat{M}, (\bar{w}') \right]_\sigma + \left[((\bar{w}') - (\hat{w}')), \bar{M} \right]_\epsilon - \left[(\bar{w} - \hat{w}), \bar{T} \right]_\epsilon \end{aligned} \quad (5.15)$$

$$\begin{aligned} \mathbf{I}_2(\bar{\mathbf{u}}) = & - \left[\frac{\partial^2 \bar{M}_x}{\partial x^2}, \bar{w} \right] - \left[\frac{\partial^2 \bar{M}_y}{\partial y^2}, \bar{w} \right] - 2 \left[\frac{\partial^2 \bar{M}_{xy}}{\partial x \partial y}, \bar{w} \right] - [\bar{q}, \bar{w}] \\ & - \frac{1}{2\bar{D}^*(1-v^2)} [\bar{M}_x, \bar{M}_x] - \frac{1}{2\bar{D}^*(1-v^2)} [\bar{M}_y, \bar{M}_y] \\ & + \frac{v}{\bar{D}^*(1-v^2)} [\bar{M}_x, \bar{M}_y] - \frac{1}{\bar{D}^*(1-v)} [\bar{M}_{xy}, \bar{M}_{xy}] \\ & + \left[(\bar{T} - \hat{T}), \bar{w} \right]_\sigma - \left[(\bar{M} - \hat{M}), (\bar{w}') \right]_\sigma - \left[(\hat{w}'), \bar{M} \right]_\epsilon + \left[\hat{w}, \bar{T} \right]_\epsilon \end{aligned} \quad (5.16)$$

$$\begin{aligned}
\mathbf{I}_3(\bar{\mathbf{u}}) = & \left[\frac{\partial \bar{w}}{\partial x}, \frac{\partial \bar{M}_x}{\partial x} \right] + \left[\frac{\partial \bar{w}}{\partial y}, \frac{\partial \bar{M}_y}{\partial y} \right] + \left[\frac{\partial \bar{w}}{\partial x}, \frac{\partial \bar{M}_{xy}}{\partial y} \right] + \left[\frac{\partial \bar{w}}{\partial y}, \frac{\partial \bar{M}_{xy}}{\partial x} \right] \\
& - [\bar{q}, \bar{w}] - \frac{1}{2\bar{D}^*(1-\nu^2)} [\bar{M}_x, \bar{M}_x] - \frac{1}{2\bar{D}^*(1-\nu^2)} [\bar{M}_y, \bar{M}_y] \\
& + \frac{\nu}{\bar{D}^*(1-\nu^2)} [\bar{M}_x, \bar{M}_y] - \frac{1}{\bar{D}^*(1-\nu)} [\bar{M}_{xy}, \bar{M}_{xy}] \\
& - [\hat{T}, \bar{w}]_\sigma - \left[(\bar{M} - \hat{M}), (\bar{w}') \right]_\sigma - [(\hat{w}'), \bar{M}]_\varepsilon - [(\bar{w} - \hat{w}), \bar{T}]_\varepsilon
\end{aligned} \tag{5.17}$$

where $[\cdot, \cdot]$ is the inner product which is defined as:

$$[f, g] = \int_{\Omega} f g \, d\Omega \tag{5.18}$$

In this thesis study, equation (5.17) is considered during the analysis. In equation (5.17), the parentheses with subscripts σ and ε indicate dynamic and geometric boundary conditions, respectively. Explicit expressions of boundary conditions are:

$$\begin{aligned}
[\bar{T}, \bar{w}] &= \left[\left(\frac{\partial \bar{M}_x}{\partial x} + \frac{\partial \bar{M}_{xy}}{\partial y} \right) n_x + \left(\frac{\partial \bar{M}_y}{\partial y} + \frac{\partial \bar{M}_{xy}}{\partial x} \right) n_y, \bar{w} \right] \\
[\bar{M}, (\bar{w}')] &= [\bar{M}_x, \bar{w}_{,x} n_x] + [\bar{M}_y, \bar{w}_{,y} n_y] + [\bar{M}_{xy}, (\bar{w}_{,x} n_y + \bar{w}_{,y} n_x)]
\end{aligned} \tag{5.19}$$

Equation (5.19) shows the work done by the shear force at the boundary and the work done by the moment force at the boundary, respectively. For dynamic analysis, the expression $[\bar{q}, \bar{w}]$ in equation (5.17) corresponds to:

$$[\bar{q}, \bar{w}] = \frac{1}{2} \rho h s^2 [\bar{w}, \bar{w}] \tag{5.20}$$

where ρ represents the mass density per unit volume of the plate.



6. FINITE ELEMENT FORMULATION

6.1 Finite Element Method

An exact solution of the governing *pdes* is often difficult for the general field problems. Among the approximate analytical methods available for the solution, the Rayleigh-Ritz and the Galerkin methods are the most commonly used ones and they are referred to as classical variational methods. The classical variational methods are limited to simple geometries because of the difficulty in constructing approximation functions for complicated geometries. The use of numerical methods provide alternative means of finding solutions for the problems with geometric and material complexities. The finite element method is a powerful numerical method of solving solid and structural mechanics problems that involve complicated physics, geometry, and/or boundary conditions. In the application of the finite element method, the domain of the problem is divided into a set of simple subdomains, called finite elements. Over each finite element, an approximate solution to the problem is developed. As outlined by Reddy (2006), the finite element method has three main features that give it superiority over the classical variational methods.

1. It allows accurate representation of geometrically complex domains by a collection of geometrically simple subdomains.
2. It enables derivation of approximation functions over each finite element. The solution is approximated by a linear combination of physical quantities at selective points, called nodes of the element, and approximation functions, almost always polynomials.
3. It allows assemblage of the element equations using continuity of physical quantities in order to obtain solution to the whole.

The finite element method consists of decomposing the domain of the problem Ω into a collection of N subdomains, Ω_e called finite elements, such that

$$\Omega = \sum_{e=1}^N \Omega_e \quad (6.1)$$

Since the solution is represented by approximation functions on each element $\bar{\Omega}_e$, an approximation of the solution of the whole $\bar{\Omega}$ can be obtained in the form:

$$\Omega \approx \bar{\Omega} = \sum_{e=1}^N \bar{\Omega}_e \quad (6.2)$$

The approximation of the solution within a typical finite element Ω_e is assumed to be of the form:

$$u_h^e = \sum_{j=1}^n u_j^e \psi_j^e(x) \quad (6.3)$$

where u_j^e are the values of the solution $u(x)$ at the nodes of the finite element Ω_e , and ψ_j^e are the approximation functions over the element. The approximate solution is sought in the form of algebraic polynomials, although this is not always the case. The reason for this choice is two-fold (Reddy, 2006):

- The interpolation theory of numerical analysis can be used to develop the approximation functions systematically over an element.
- Numerical evaluation of integrals of algebraic polynomials is easy.

In order to derive the approximate solution u_h^e that is convergent to the actual solution u as the number of elements is increased, the following conditions must be satisfied:

1. The approximate solution should be continuous over the element and differentiable.
2. The approximate solution should be a complete polynomial (all lower-order and highest-order terms are included).
3. The approximate solution should be an interpolant of the primary variables at the nodes of the finite element.

The first condition ensures a nonzero coefficient matrix. The second condition is necessary in order to capture all possible states of the actual solution and the third condition is necessary in order to enforce continuity of the primary variables at points common to the elements.

For one-dimensional domain, the finite element approximation u_h^e of $u(x)$ can be an interpolant, that is, must be equal to u_1^e at x_a and u_2^e at x_b (see Figure 6.1). A complete linear polynomial is of the form:

$$u_h^e(x) = c_1^e + c_2^e x \quad (6.4)$$

where c_1^e and c_2^e are constants. The expression in equation (6.4) satisfies the first and second conditions of an approximation. The third condition is fulfilled if c_1^e and c_2^e meet the conditions:

$$\begin{aligned} u_h^e(x_a) &= c_1^e + c_2^e x_a \equiv u_1^e \\ u_h^e(x_b) &= c_1^e + c_2^e x_b \equiv u_2^e \end{aligned} \quad (6.5)$$

where u_1^e and u_2^e are the nodal values of $u_h^e(x)$ at $x = x_a$ and $x = x_b$, respectively.

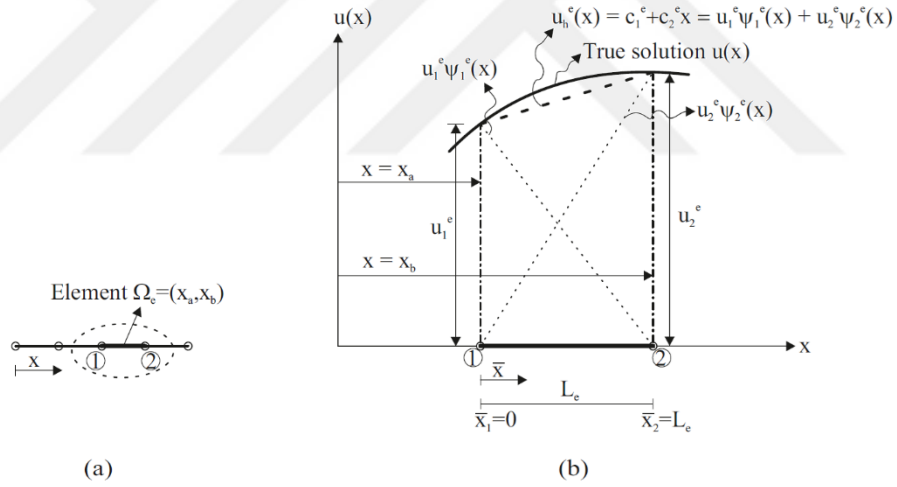


Figure 6.1 : (a) Finite element discretization of a one-dimensional domain (b) Linear finite element approximation over an element.

Equation (6.5) can be expressed in matrix form as:

$$\begin{bmatrix} 1 & x_a \\ 1 & x_b \end{bmatrix} \begin{Bmatrix} c_1^e \\ c_2^e \end{Bmatrix} = \begin{Bmatrix} u_1^e \\ u_2^e \end{Bmatrix} \rightarrow c_1^e = \frac{u_1^e x_b - u_2^e x_a}{x_b - x_a}, \quad c_2^e = \frac{u_2^e - u_1^e}{x_b - x_a} \quad (6.6)$$

where $x_b - x_a = L_e$. Substitution of equation (6.6) for c_i^e into equation (6.4) yields:

$$u_h^e(x) = u_1^e \psi_1^e(x) + u_2^e \psi_2^e(x) = \sum_{j=1}^2 u_j^e \psi_j^e(x) \quad (6.7)$$

where

$$\psi_1^e(x) = \frac{x_b - x}{L_e}, \quad \psi_2^e(x) = \frac{x - x_a}{L_e} \quad (6.8)$$

which are called the linear finite element approximation functions.

The approximation functions $\psi_i^e(x)$ have some interesting properties. First, note that:

$$u_1^e(x) \equiv u_h^e(x_a) = u_1^e \psi_1^e(x_a) + u_2^e \psi_2^e(x_a) \quad (6.9)$$

implies $\psi_1^e(x_a) = 1$ and $\psi_2^e(x_a) = 0$. Similarly,

$$u_2^e(x) \equiv u_h^e(x_b) = u_1^e \psi_1^e(x_b) + u_2^e \psi_2^e(x_b) \quad (6.10)$$

gives $\psi_1^e(x_b) = 0$ and $\psi_2^e(x_b) = 1$. In other words, ψ_i^e is unity at the i^{th} node and zero at the other node as:

$$\psi_i^e(x_j) = \begin{cases} 1, & \text{if } i = j \\ 0, & \text{if } i \neq j \end{cases} \quad (6.11)$$

This property is known as the interpolation property of $\psi_i^e(x)$ and they are also called interpolation functions. In finite element analysis, two basic types of interpolation functions are used. The Lagrange interpolation function and the Hermite interpolation function. The Lagrange interpolation functions are derived to interpolate function values only and not the derivatives of the function. The Hermite family of interpolation functions are derived to interpolate the function and its derivatives. The finite elements developed using the Lagrange type interpolation are called C^0 elements, and finite elements developed using the Hermite type interpolation are called C^m elements, where $m > 0$ is the order of the derivatives included in the interpolation. In addition, $\psi_i^e(x)$ satisfy the property, known as the "partition of unity", that their sum is unity.

$$\sum_{i=1}^n \psi_i^e(x) = 1 \quad (6.12)$$

In order to express the element interpolation functions, ψ_i^e which were derived in terms of the global coordinate x as in equation (6.8), in terms of the local (or element) coordinate $\bar{x} = x - x_a$ as follows:

$$\begin{aligned}\psi_1^e(\bar{x}) &= 1 - \frac{\bar{x}}{L_e} \\ \psi_2^e(\bar{x}) &= \frac{\bar{x}}{L_e}\end{aligned}\tag{6.13}$$

the origin is fixed at node 1 of the element Ω_e as shown in Figure 6.1 (b).

To improve the calculational accuracy without increasing the number of elements, the degree (or order) of the polynomial approximation can be increased (see Figure 6.2).

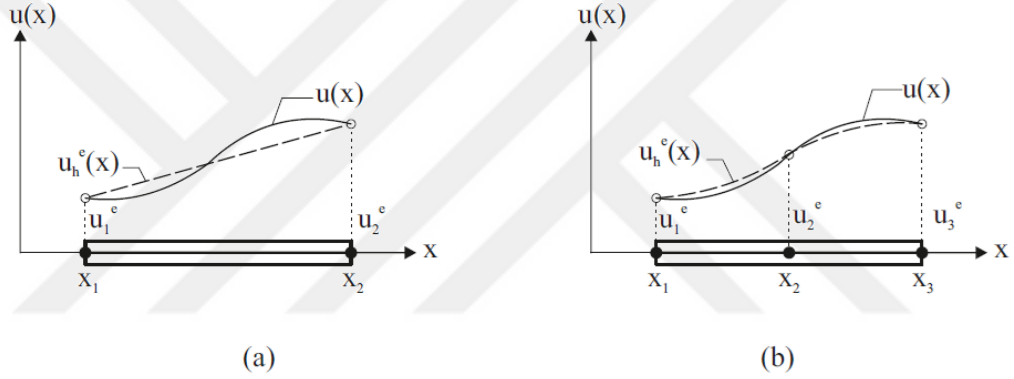


Figure 6.2 : (a) Linear approximation (b) Quadratic approximation.

Derivation of interpolation functions depends only on the geometry of the element and the number and location of the nodes. The number of nodes must be equal to the number of terms in the polynomial. For instance, second-order polynomial approximation (quadratic approximation) has the form:

$$u_h^e(x) = c_1^e + c_2^e x + c_3^e x^2\tag{6.14}$$

Since there are three parameters, c_i^e ($i = 1, 2, 3$) three nodes in the element must be identified as shown in Figure 6.2 (b).

In two dimensions, the domain is approximated by simple two-dimensional elements, such as triangles, rectangles and/or quadrilaterals. Let's consider the complete polynomial

$$u_h^e(x, y) = c_1^e + c_2^e x + c_3^e y + c_4^e xy \quad (6.15)$$

which contains four linearly independent terms and is linear in x and y , with a bilinear term in x and y . This polynomial requires an element with four nodes like a rectangular element with dimensions a and b along the x and y directions, respectively (see Figure 6.3 (a)).

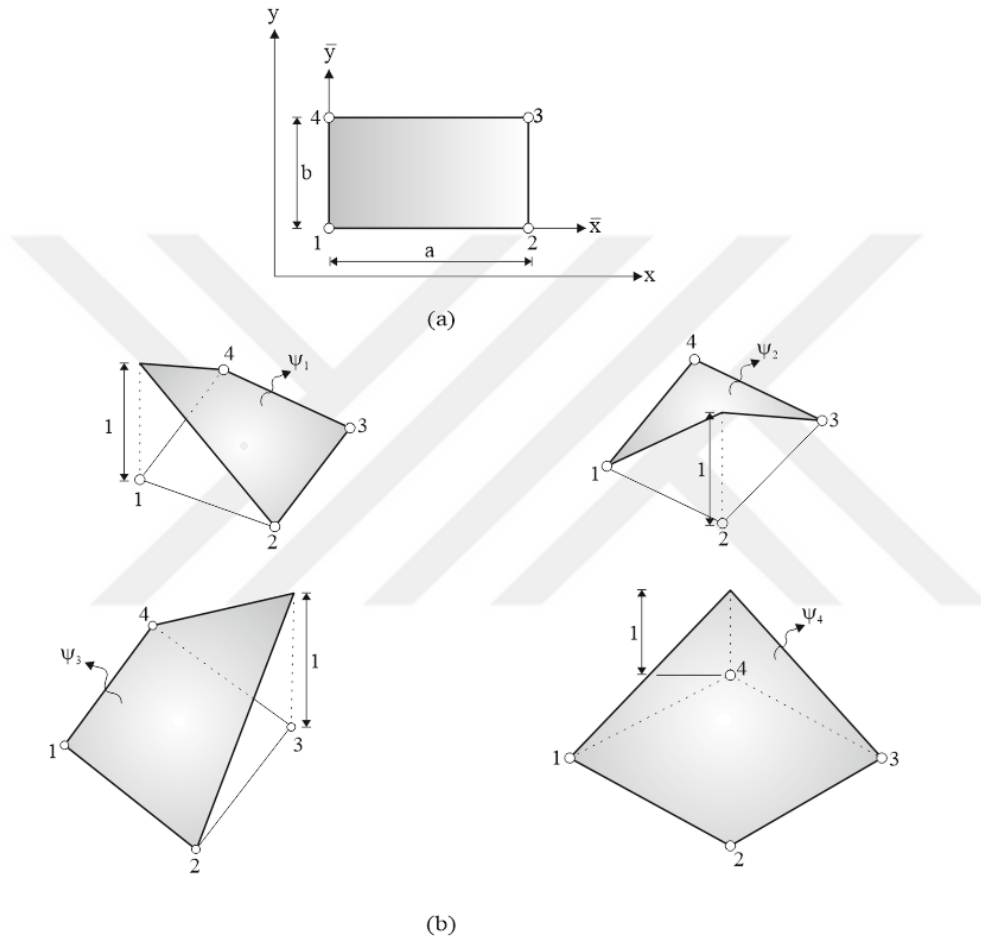


Figure 6.3 : (a) Linear rectangular element (b) its interpolation functions.

Following the same procedure as those described for one-dimensional element as eliminating c_i^e by rewriting $u_h^e(x, y)$ in terms of the four nodal values, $(u_1^e, u_2^e, u_3^e, u_4^e)$ and substituting the obtained c_i^e into equation (6.15), the linear interpolation functions can be derived for the four-node rectangle in terms of the local (or element) coordinate system (\bar{x}, \bar{y}) :

$$\begin{aligned}
\psi_1^e(\bar{x}, \bar{y}) &= \left(1 - \frac{\bar{x}}{a}\right) \left(1 - \frac{\bar{y}}{b}\right) \\
\psi_2^e(\bar{x}, \bar{y}) &= \frac{\bar{x}}{a} \left(1 - \frac{\bar{y}}{b}\right) \\
\psi_3^e(\bar{x}, \bar{y}) &= \frac{\bar{x}}{a} \frac{\bar{y}}{b} \\
\psi_4^e(\bar{x}, \bar{y}) &= \left(1 - \frac{\bar{x}}{a}\right) \frac{\bar{y}}{b}
\end{aligned} \tag{6.16}$$

Interpolation functions given in equation (6.16) also satisfy the properties illustrated by equations (6.11) and (6.12) (see Figure 6.3 (b)). For additional details about the derivation of the interpolation functions of two-dimensional basic elements (linear and/or higher-order rectangular and triangular elements), see Reddy (2006).

6.2 Coordinate Transformation

In general, the boundary of a two-dimensional domain is a curve. For an accurate representation of domains with curved boundaries, refined meshes and/or irregularly shaped curvilinear elements are used.

Since the interpolation functions are easily derivable for a rectangular element and it is easier to evaluate integrals over rectangular geometries, we transform the finite element integral statements defined over quadrilaterals to a rectangle. This transformation results in complicated expressions in terms of the coordinates used for the rectangular element. Therefore, numerical integration is used to evaluate such complicated expressions. The Gauss-Legendre quadrature requires the integral to be expressed over a square region $\hat{\Omega}$ of dimension 2×2 with respect to the coordinate system (ζ, η) to be such that $-1 \leq (\zeta, \eta) \leq 1$. For example, every quadrilateral element can be transformed to a square element that facilitates the use of Gauss-Legendre quadrature for the purpose of numerically evaluating the integrals defined over the quadrilateral element (see Figure 6.4).

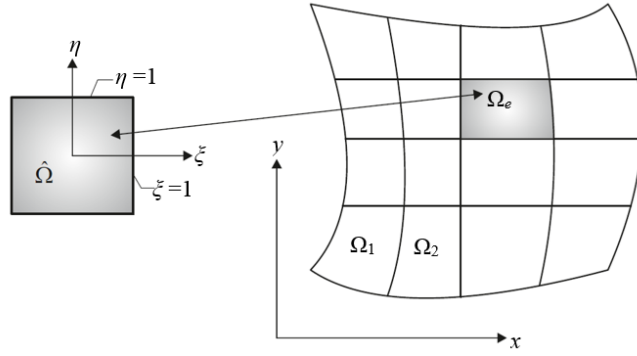


Figure 6.4 : Transformation of quadrilateral elements to the master element for numerical evaluation of integrals.

The element $\hat{\Omega}$ is called a master element. The transformation between a typical element Ω_e of the finite element mesh and the master element $\hat{\Omega}$ or equivalently between (x, y) and (ζ, η) is accomplished by a coordinate transformation of the form:

$$\begin{aligned} x &= \sum_{j=1}^m x_j^e \hat{\psi}_j^e(\zeta, \eta) \\ y &= \sum_{j=1}^m y_j^e \hat{\psi}_j^e(\zeta, \eta) \end{aligned} \quad (6.17)$$

where x_j^e and y_j^e represent the nodal coordinates of an element and $\hat{\psi}_j^e$ denote the finite element interpolation functions of the master element $\hat{\Omega}$. The transformation given in equation (6.17) maps a point (ζ, η) in the master element onto a point (x, y) in the element Ω_e and vice versa if the Jacobian of the transformation is positive-definite. Geometrically, the Jacobian J represents the ratio of an area element in the real element to the corresponding area element in the master element,

$$dA \equiv dx dy = J d\zeta d\eta \quad (6.18)$$

where $J \equiv \det [J] > 0$ everywhere in the element Ω_e . Here, $[J]$ is the Jacobian matrix. For one-dimensional element, the transformation of the problem coordinate x to a local coordinate ζ such that $-1 \leq \zeta \leq 1$, with its origin at the center of the element, the following interpolation functions are derived for an element with two nodes as shown in Figure 6.5,

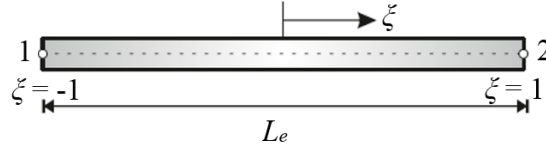


Figure 6.5 : Interpolation functions for one-dimensional element in terms of the local coordinate ζ .

$$\begin{aligned}\psi_1(\zeta) &= \frac{1}{2}(1 - \zeta) \\ \psi_2(\zeta) &= \frac{1}{2}(1 + \zeta)\end{aligned}\tag{6.19}$$

This choice of local coordinate is dictated by the Gauss-Legendre quadrature rule used in the numerical evaluation of integrals over the element.

For two-dimensional element, the transformation of the problem coordinate system (x, y) to a local coordinate system (ζ, η) such that $-1 \leq (\zeta, \eta) \leq 1$, with its origin at the center of the element, the following interpolation functions are derived for an element with four nodes as shown in Figure 6.6,

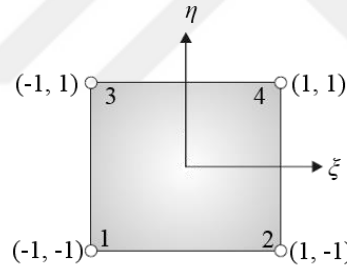


Figure 6.6 : Interpolation functions for two-dimensional element in terms of the local coordinate system (ζ, η) .

$$\begin{aligned}\psi_1(\zeta, \eta) &= \frac{1}{4}(1 - \zeta)(1 - \eta) \\ \psi_2(\zeta, \eta) &= \frac{1}{4}(1 + \zeta)(1 - \eta) \\ \psi_3(\zeta, \eta) &= \frac{1}{4}(1 - \zeta)(1 + \eta) \\ \psi_4(\zeta, \eta) &= \frac{1}{4}(1 + \zeta)(1 + \eta)\end{aligned}\tag{6.20}$$

This choice of local coordinate system is required in numerical integration using Gauss-Legendre quadrature.

6.3 Basic Steps to Obtain Element Matrix

The finite element approximation u_h^e satisfies the differential equation(s) and appropriate boundary condition(s). Since there are n unknown parameters, we need n relations to determine them. Substitution of the approximate solution into the functional $I(u)$ will give the necessary algebraic equations among the nodal values.

In order to obtain the element equations, the parameters u_i^e are determined by minimizing the functional $I(u)$. The necessary condition for the minimization of $I(u_1^e, u_2^e, \dots, u_n^e)$ is that its partial derivatives with respect to each of the parameters be zero:

$$\frac{\partial I}{\partial u_1^e} = 0, \quad \frac{\partial I}{\partial u_2^e} = 0, \quad \dots, \quad \frac{\partial I}{\partial u_n^e} = 0 \quad (6.21)$$

Thus, there are n linear algebraic equations in n unknowns, $u_i^e (i = 1, 2, \dots, n)$.

The algebraic equations can be expressed in matrix form as:

$$[K^e] \{u^e\} = \{F^e\} \quad (6.22)$$

Equation (6.22) is called the finite element model of the original equation.

Since the element is physically connected to its neighbors, it becomes necessary to put the elements together (i.e., assembly). After the assembly of element equations, the assembled system of equations can be expressed in the matrix form (Reddy, 1993) as:

$$[K] \{u\} = \{F\} \quad (6.23)$$

where $\{u\}$ denotes the global nodal unknowns vector, $[K]$ and $\{F\}$ denote the global coefficient matrix (or stiffness matrix) and the source vector (or force vector), respectively, in structural mechanics problems.

6.4 Element Matrix in Laplace-Carson Domain

In my thesis study, C^0 class finite element formulation is generated by introducing the coordinate transformation from (x, y) plane to (ζ, η) plane. A four node rectangular master element as illustrated in Figure 6.7

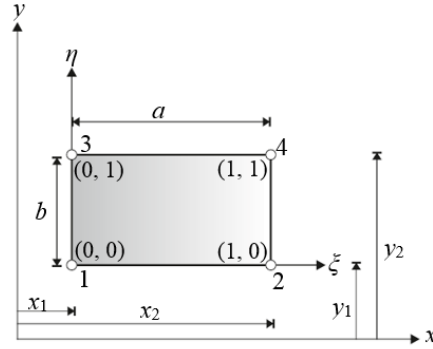


Figure 6.7 : Global and local coordinate system of rectangular master element.

with the following interpolation functions in terms of the global coordinate system (x, y) ,

$$\begin{aligned}
 \psi_1(x, y) &= \left(\frac{x_2 - x}{a} \right) \left(\frac{y_2 - y}{b} \right) \\
 \psi_2(x, y) &= \left(\frac{x - x_1}{a} \right) \left(\frac{y_2 - y}{b} \right) \\
 \psi_3(x, y) &= \left(\frac{x_2 - x}{a} \right) \left(\frac{y - y_1}{b} \right) \\
 \psi_4(x, y) &= \left(\frac{x - x_1}{a} \right) \left(\frac{y - y_1}{b} \right)
 \end{aligned} \tag{6.24}$$

and local coordinate system (ξ, η) ,

$$\begin{aligned}
 \psi_1(\xi, \eta) &= (1 - \xi)(1 - \eta) \\
 \psi_2(\xi, \eta) &= \xi(1 - \eta) \\
 \psi_3(\xi, \eta) &= (1 - \xi)\eta \\
 \psi_4(\xi, \eta) &= \xi\eta
 \end{aligned} \tag{6.25}$$

is used.

The rectangular viscoelastic plate element has four nodes with four degrees of freedom per node (VPLT16): one transverse displacement, two bending moments and one torsional moment. The four variables of the functional given in equation (5.17) in Section 5.3 are approximated by using the interpolation functions as follows:

$$\begin{aligned}
\bar{w} &= \sum_{i=1}^{N=4} (\bar{w})_i \psi_i(\zeta, \eta) \\
\bar{M}_x &= \sum_{i=1}^{N=4} (\bar{M}_x)_i \psi_i(\zeta, \eta) \\
\bar{M}_y &= \sum_{i=1}^{N=4} (\bar{M}_y)_i \psi_i(\zeta, \eta) \\
\bar{M}_{xy} &= \sum_{i=1}^{N=4} (\bar{M}_{xy})_i \psi_i(\zeta, \eta)
\end{aligned} \tag{6.26}$$

where N represents the nodes of the element.

All expressions of unknown quantities in terms of interpolation functions are inserted into the functional (equation (5.17) in Section 5.3) to obtain the necessary algebraic equations among the nodal values. After minimization of the functional by using the procedure explained in Section 6.3, the following element matrix for mixed finite element formulation of the viscoelastic Kirchhoff plates named VPLT16 and load vector can be derived:

$$[K] = \begin{bmatrix} [k_5] & [k_2] & [k_3] & [k_4] \\ [k_2] & -\frac{[k_1]}{\bar{D}^* (1-\nu^2)} & \frac{\nu[k_1]}{\bar{D}^* (1-\nu^2)} & 0 \\ [k_3] & \frac{\nu[k_1]}{\bar{D}^* (1-\nu^2)} & -\frac{[k_1]}{\bar{D}^* (1-\nu^2)} & 0 \\ [k_4] & 0 & 0 & -\frac{[k_1]}{2\bar{D}^* (1-\nu)} \end{bmatrix} \tag{6.27}$$

$$\{u\} = \begin{Bmatrix} \{\bar{w}\} \\ \{\bar{M}_x\} \\ \{\bar{M}_y\} \\ \{\bar{M}_{xy}\} \end{Bmatrix} \quad \{F\} = \begin{Bmatrix} [k_1] \{\bar{q}\} \\ 0 \\ 0 \\ 0 \end{Bmatrix}$$

The explicit form of the submatrices $[k_i]$ is defined (for $i = 1, 2, 3, 4$ and 5) by the expressions:

$$[k_1] = \int_A \psi_i \psi_j dA = \begin{bmatrix} ab/9 & ab/18 & ab/18 & ab/36 \\ ab/18 & ab/9 & ab/36 & ab/18 \\ ab/18 & ab/36 & ab/9 & ab/18 \\ ab/36 & ab/18 & ab/18 & ab/9 \end{bmatrix} \tag{6.28}$$

$$[k_2] = \int_A \frac{\partial \psi_i}{\partial x} \frac{\partial \psi_j}{\partial x} dA = \begin{bmatrix} b/3a & -b/3a & b/6a & -b/6a \\ -b/3a & b/3a & -b/6a & b/6a \\ b/6a & -b/6a & b/3a & -b/3a \\ -b/6a & b/6a & -b/3a & b/3a \end{bmatrix} \quad (6.29)$$

$$[k_3] = \int_A \frac{\partial \psi_i}{\partial y} \frac{\partial \psi_j}{\partial y} dA = \begin{bmatrix} a/3b & a/6b & -a/3b & -a/6b \\ a/6b & a/3b & -a/6b & -a/3b \\ -a/3b & -a/6b & a/3b & a/6b \\ -a/6b & -a/3b & a/6b & a/3b \end{bmatrix} \quad (6.30)$$

$$[k_4] = \int_A \frac{\partial \psi_i}{\partial x} \frac{\partial \psi_j}{\partial y} dA = \begin{bmatrix} 1/2 & 0 & 0 & -1/2 \\ 0 & -1/2 & 1/2 & 0 \\ 0 & 1/2 & -1/2 & 0 \\ -1/2 & 0 & 0 & 1/2 \end{bmatrix} \quad (6.31)$$

$$[k_5] = k_w [k_1] \quad (6.32)$$

where k_w is the modulus of the foundation. Here, the submatrix $[k_5]$ characterizes the interaction between the viscoelastic Kirchhoff plate and Winkler-type elastic foundation. In order to obtain a standard viscoelastic Kirchhoff plate bending element, one should simply let $[k_5] = 0$.

In Figure 6.8, a flowchart for a special mixed finite element program that is written in Fortran is presented. This program is capable of performing quasi-static and dynamic analysis of viscoelastic plates in transformed domain and converting the solutions in real time domain.

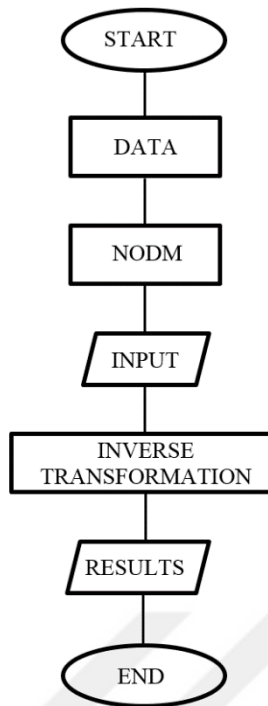


Figure 6.8 : Flowchart for Fortran program.

When the program is started, a series of statements as a subprogram (or subroutine) is called in order. Notice that there are three types of symbols in this flowchart: START and END symbols represented as rounded rectangles, processing steps represented as rectangles and INPUT/OUTPUT (RESULTS) represented as a parallelogram. A subroutine DATA contains structural parameters, load parameters and material parameters. A subroutine NODM creating a mesh of finite elements. An INPUT data file ask user to enter the type of analysis (such as quasi-static or dynamic), the type of loading, the type of inverse transform technique and values of the effective parameters of inverse transform techniques. Obtained results in the Laplace-Carson domain are transformed into real time domain in a subroutine called INVERSE TRANSFORMATION. The results are saved in an output file, the name of which is also required at the beginning of the program execution.

7. INVERSE TRANSFORM TECHNIQUES

The most important and difficult step to get the solution of viscoelasticity problem is inversion which is used to convert the obtained solution from the Laplace domain into the real time-domain. Instead of extensive tables are available for inversion, these tables by no means cover all cases arising in practice and they are useless. Thus, the need arises for numerical methods of inversion of the Laplace transform. According to the Krlyov and Skoblya (1969), inversion of the Laplace transform is one of a class of so-called improper problems of modern mathematics. These problems possess two properties which make their solution very difficult:

1. They are not solvable for all values of the numerical or functional parameters determining the problem.
2. Small perturbations of these parameters may induce large perturbations in the solution.

For the numerical inversion of Laplace transform using real or complex data, a great number of methods have been proposed. Piessens (1975) and Piessens and Dang (1976) compiled an almost complete bibliography on the numerical inversion of Laplace transform and its applications. There are numerous applications of the numerical Laplace transform in wave propagation, structural dynamics, viscoelasticity, heat conduction, fluid dynamics and other areas of applied mechanics. The study of Narayanan and Beskos (1982) discussed only the applications of the numerical Laplace transform in applied mechanics, reviewed various existing methods of numerical Laplace transform inversion and classified them into the following three groups:

- Interpolation-collocation methods
- Methods based on expansion in orthogonal functions
- Methods based on numerical Fourier transform

The Maximum Degree of Precision (Krlyov and Skoblya, 1969), Schapery's Collocation (Schapery, 1962) and the multidata method of Cost and Becker (1970) are

three algorithms of interpolation-collocation methods. Trigonometric (Papoulis, 1957), Legendre (Bellman et al, 1966 and Krlyov and Skoblya, 1969) and Laguerre functions (Weeks, 1966 and Wing, 1967) are three algorithms of methods based on orthogonal function expansion. Direct Fourier transform (Cooley et al, 1970), sine-cosine transform of Durbin (Dubner and Abate, 1968 and Durbin, 1974) are two algorithms of methods based on Fourier transform. Eight algorithms of numerical Laplace transform inversion of which are applied certainly for problems with the transformed solution being given in numerical form were compared with each other with respect to their accuracy and computational efficiency. As a result, the following general conclusions were drawn on the basis of this study.

- 1) Trigonometric, Legendre and Schapery's collocation algorithms achieve relatively low accuracy with less computer time when compared to Laguerre, direct Fourier transform and sine-cosine transform of Durbin algorithms which achieve high accuracy with more computer time.
- 2) For slowly varying or non-oscillatory functions of time which characterize heat conduction or viscoelasticity problems, collocation methods should be preferred. However, they furnish acceptable results for very early times only if the functions are oscillatory, as it happens in structural dynamics.
- 3) Durbin algorithm is the most accurate algorithm for short as well as long time solutions when compared to the other studied algorithms.

These conclusions serve as the basis for algorithms evaluated within the context of this thesis for numerical Laplace transform inversion. In this thesis, three algorithms of numerical Laplace transform inversion such as Maximum Degree of Precision (MDOP), Dubner & Abate and Durbin are systematically discussed with respect to their accuracy and applicability.

7.1 Method of Maximum Degree of Precision (MDOP)

In this method, the integral (4.11) in Section 4.3 can be approximated by the quadrature formula

$$f(t) \cong \frac{1}{t} \sum_{k=1}^n A_k \varphi(p_k) \cong \frac{1}{t} \sum_{k=1}^n A_k p_k^m F\left(\frac{p_k}{t}\right) \quad (7.1)$$

by substituting $s = \frac{P}{t}$ in equation (4.11).

This method suppose that the regular function $F(p)$ tends to zero to the order of some power of $\frac{1}{p}$ and can be written as:

$$F(p) = \left(\frac{1}{p^m} \right) \varphi(p) \quad (7.2)$$

where $m > 0$ and $\varphi(p)$ is regular.

The numerical values of the weights A_k and the tabular points p_k are given in Krlyov and Skoblya (1969). Their values are in complex form and tabulated for n (number of terms) = (1, 2, ..., 10) and for the power m of $\left(\frac{1}{p} \right)$ in equation (7.2) varying from 0,01 to 3 at steps of 0,01. This method is recommended especially if a value of a function at any time is required because this value can be found directly. Other methods are time-consuming because there is no way to find the ‘only’ value at the desired time. For instance, if the value of a function at time t is desired, $(0, t)$ interval is scanned with Δt steps to reach time t .

7.2 Method of Dubner and Abate

Dubner and Abate (1968) developed a method to determine the inverse Laplace transform numerically based on the finite Fourier Cosine transform. The freedom in assigning the parameter ‘a’ provides the basis for a powerful computational method in determining the inverse integral. The inversion method of Dubner and Abate assumes that $f(t)$ be a real function. By letting $s = a + i\omega$, the integrals (4.10) and (4.11) in Section 4.3 become:

$$\operatorname{Re}\{F(s)\} = \int_0^{\infty} e^{-at} f(t) \cos \omega t dt \quad (7.3)$$

$$f(t) = \frac{2e^{at}}{\pi} \int_0^{\infty} \operatorname{Re}\{F(s)\} \cos \omega t dt \quad (7.4)$$

Equations (7.3) and (7.4) give alternative formulas of the Laplace transform and its inverse transform for real functions, respectively. An essential feature of the proposed method is that the error in the computed inverse transform can be controlled by varying the parameter ‘a’ or by the size of the step used.

Specifically, Dubner and Abate (1968) developed a method of inversion which approximates $f(t)$ as:

$$f(t) \cong \frac{2e^{at}}{T} \left[\frac{1}{2} \operatorname{Re}\{F(a)\} + \sum_{k=1}^{\infty} \operatorname{Re}\left\{F\left(a + \frac{k\pi i}{T}\right)\right\} \cos\left(\frac{k\pi}{T}t\right) \right] \quad (7.5)$$

where $a = \frac{aT}{T}$, T is the time interval of the solution, $\frac{\pi}{T}$ represents the step size.

Numerically equation (7.5) is valid only for the interval $0 \leq t \leq \frac{T}{2}$ since the error becomes prohibitively large as t approaches T .

7.3 Method of Durbin

This method is a modification of the inversion method of Dubner and Abate (1968). Since Durbin’s method is compared to the Dubner and Abate’s method, the inversion method of Durbin combined both finite Fourier sine and cosine transforms.

According to the method described by Durbin (1974), the advantage of this modified procedure are twofold:

1. The error bound on the inverse $f(t)$ becomes independent of t , instead of being exponential in t .
2. The trigonometric series obtained for $f(t)$ in terms of $F(s)$ is valid on the whole period $2T$ of the series.

Durbin (1974) developed a method of inversion which approximates $f(t)$ as:

$$f(t_j) \cong \frac{2e^{aj\Delta t}}{T} \left\{ -\frac{1}{2} \operatorname{Re}\{F(a)\} + \operatorname{Re}\left[\sum_{k=0}^{N-1} L_k [A(k) + iB(k)] W^{jk} \right] \right\} \quad (7.6)$$

with $t_j = j\Delta t = j\frac{T}{N}$, $j = (0, 1, 2, \dots, N-1)$.

$$\begin{aligned}
A(k) &= \sum_{l=0}^L \operatorname{Re} \left\{ F \left(a + i(k + lN) \frac{2\pi}{T} \right) \right\} \\
B(k) &= \sum_{l=0}^L \operatorname{Im} \left\{ F \left(a + i(k + lN) \frac{2\pi}{T} \right) \right\} \\
W &= \cos \left(\frac{2\pi}{N} \right) + i \sin \left(\frac{2\pi}{N} \right) = \exp \left(i \frac{2\pi}{N} \right) \\
L_k &= \frac{\sin \left(\frac{k\pi}{N} \right)}{\left(\frac{k\pi}{N} \right)}
\end{aligned} \tag{7.7}$$

since $l = 1, 2, 3, \dots$. Here i is the complex number $i = \sqrt{-1}$, T is the time interval of the solution, N is the equidistant points for which $f(t)$ is required. For this method, we take $L=1$.

7.4 Comparison of the Methods of Numerical Laplace Transform Inversion

In this section, the three methods of numerical Laplace transform inversion described above are compared on the basis of the following three examples to illustrate the numerical accuracy and computational efficiency. The accuracy of the methods for the numerical inversion of Laplace transforms significantly depends on the values of some parameters. Therefore, these examples also serve to determine the optimum values of these parameters.

The following comparison studies are performed by using a computer program written in Fortran language. For comparison, three function of t (i.e., a function of time domain) and their Laplace transforms (i.e., a function of s where s is a variable denoting Laplace parameter) are considered. To test the numerical inversion techniques, the approximate function $f_a(t)$ obtained by numerical inversion is compared with the exact function $f(t)$. For different values of the independent variable t , the accuracy of the various numerical Laplace transform inversion algorithms are discussed on the basis of the values of characteristic parameters of each method.

7.4.1 Example 1

The first example is for a function:

$$f(t) = \frac{t}{2} \sin(t) \quad (7.8)$$

The Laplace transform of this function is:

$$F(s) = \frac{s}{(s^2 + 1)^2} \quad (7.9)$$

Let's prove that solution of equation (7.9) for a sequence of values of s has already been known and its numerical inversion finally furnishes the time domain response has been tried to find out.

The exact values of $f(t)$ and the approximate values obtained by the application of the MDOP method are illustrated in Figure 7.1. The most important parameter in MDOP method is m because without knowledge of its value, A_k and p_k cannot be determined. The other important parameter in this method is n whose increasing values lead to higher accuracy. To determine the most suitable values for the effective parameters of the MDOP inverse transform technique, different values of n has been considered. As illustrated in Figure 7.1, the results obtained using $n = 10$ overlap the exact results. In MDOP inverse Laplace transform technique, better numerical results are obtained for $m = 1$ and $n = 10$.

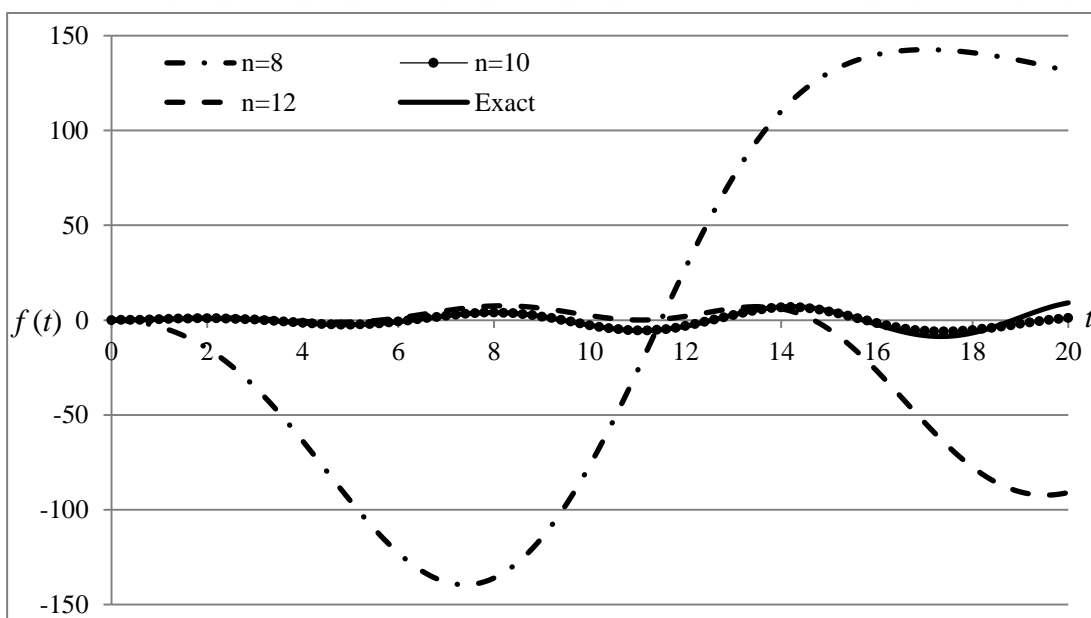


Figure 7.1 : Effect of the changes in the value of the n parameter.

This example continues for a function which is unbounded:

$$f(t) = \frac{t}{2} \cos(t) \quad (7.10)$$

The Laplace transform of this function is:

$$F(s) = \frac{s^2 - 1}{2(s^2 + 1)^2} \quad (7.11)$$

Let's assume that solution of equation (7.11) for a sequence of values of s has already been known and its numerical inversion finally furnishes the time domain response has been tried to find out. The exact values of $f(t)$ and the approximate values $f_a(t)$ obtained by the application of the MDOP method is tabulated in Table 7.1.

The format of this example is as follows: the 1st column gives values of the independent time variable t and the 2nd column gives approximate values of $f(t)$, so $f_a(t)$. The 3rd column gives exact values of $f(t)$. This representation is restricted to the interval $0 \leq t \leq 20$ s. In this example, the performance of the MDOP method is tested at different time intervals of $\Delta t = 0,2; 0,5$ and 2 s and the results are compared. It was found that the accuracy of this inversion method is independent from the sampling interval Δt . Therefore, in Table 7.1, the performance of the MDOP method is illustrated only for time intervals of $\Delta t = 0,5$ s.

Table 7.1 : Performance of the MDOP method.

Time (t)	Approximate $f_a(t)$	Exact $f(t)$	Time (t)	Approximate $f_a(t)$	Exact $f(t)$
0,5	0,219	0,219	10,5	-2,494	-2,497
1,0	0,270	0,270	11,0	0,026	0,024
1,5	0,053	0,053	11,5	2,776	2,779
2,0	-0,416	-0,416	12,0	5,046	5,063
2,5	-1,001	-1,001	12,5	6,189	6,236
3,0	-1,485	-1,485	13,0	5,816	5,898
3,5	-1,639	-1,639	13,5	3,921	4,016
4,0	-1,307	-1,307	14,0	0,932	0,957
4,5	-0,474	-0,474	14,5	-2,388	-2,573
5,0	0,709	0,709	15,0	-5,154	-5,698
5,5	1,949	1,949	15,5	-6,649	-7,583
6,0	2,880	2,881	16,0	-6,558	-7,661
6,5	3,174	3,174	16,5	-5,048	-5,795
7,0	2,639	2,639	17,0	-2,652	-2,339
7,5	1,300	1,300	17,5	-0,034	1,920
8,0	-0,582	-0,582	18,0	2,239	5,943
8,5	-2,559	-2,559	18,5	3,824	8,691
9,0	-4,100	-4,100	19,0	4,618	9,393
9,5	-4,736	-4,737	19,5	4,699	7,759
10,0	-4,194	-4,195	20,0	4,237	4,081

7.4.2 Example 2

The second example is for a function given by:

$$f(t) = e^{-\frac{t}{2}} \cos(2t) \quad (7.12)$$

The Laplace transform of this function is:

$$F(s) = \frac{(s + \frac{1}{2})}{(s + \frac{1}{2})^2 + 4} \quad (7.13)$$

Let's approve that solution of equation (7.13) for a sequence of values of s has already been known and its numerical inversion finally furnishes the time domain response has been tried to find out. The exact values of $f(t)$ and the approximate values $f_a(t)$ obtained by the application of the two algorithms of numerical Laplace transform inversion as Dubner & Abate and Durbin are illustrated in Figure 7.2 and Figure 7.3, respectively.

In these methods, the parameters which affect the inversion results are N and aT . For this example, the value of aT is increased in order to determine the optimum value of this parameter.

The time interval for which we require $f(t)$ is $0 \leq t \leq 25$ s, therefore we take $T = 50$ s. $f(t)$ is computed for $N = 100$ equidistant points. In other words, the desired sampling interval is $\Delta t = T / N = 0,5$ s. The values of aT were chosen as 5, 8 and 10 because these values have been used by Dubner and Abate (1968) to test the performance of the numerical Laplace inversion method. In addition, Durbin (1974) implied that if the value of aT is chosen from 5 to 10, good results are obtained.

The results illustrated in Figure 7.2 show that fluctuation scattering increases as aT in Dubner and Abate's inverse transform technique increases. For instance, in Dubner & Abate's inversion method, reasonably accurate results can be obtained up to $t = 35$ s if $aT = 8$ and departure from the exact solution is relatively small whereas the time is decreases up to $t = 25$ s if $aT = 10$. In addition, the approximate values $f_a(t)$ overlap with the exact values $f(t)$ for $aT = 5$.

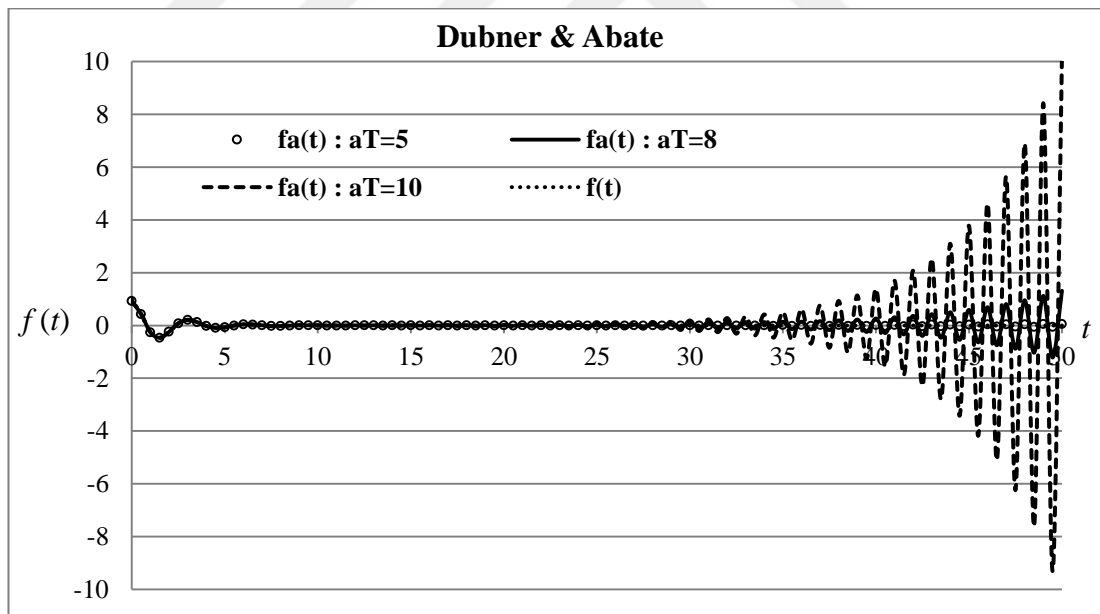


Figure 7.2 : Effect of the changes in the value of the aT parameter in Dubner & Abate.

The results illustrated in Figure 7.3 show that the approximate values $f_a(t)$ obtained through the application of the Durbin's inversion method tend to infinity as time increases. In addition, departure from the exact solution increases for increasing values

of aT . For instance, departure is observed for $t > 40$ s as $aT = 5$, for $t > 35$ s as $aT = 8$ and for $t > 25$ s as $aT = 10$.

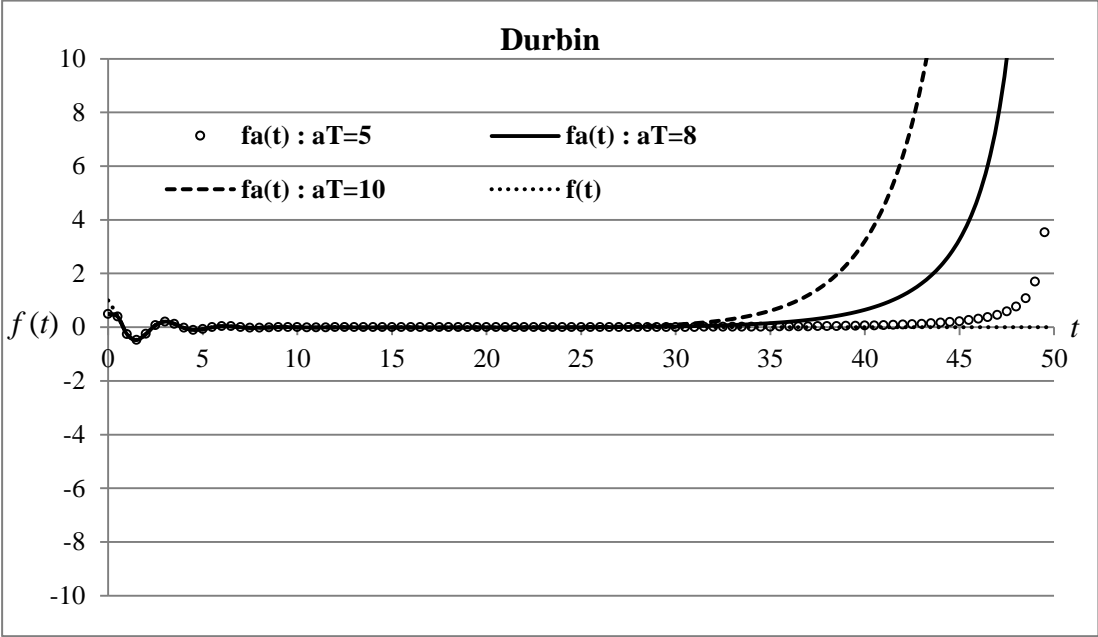


Figure 7.3 : Effect of the changes in the value of the aT parameter in Durbin.

7.4.3 Example 3

The last example is presented to illustrate the approximation of a function having a jump discontinuity:

$$f(t) = H(t - 5) - H(t - 15) \tag{7.14}$$

The Laplace transform of this function is:

$$F(s) = \frac{e^{-5s}(1 - e^{-10s})}{s} \tag{7.15}$$

Let's approve that solution of equation (7.15) for a sequence of values of s has already been known and its numerical inversion finally furnishes the time domain response has been tried to find out. The accuracy and efficiency of the Dubner & Abate's and Durbin's methods proposed for the numerical inversion of Laplace transforms are compared on the basis of the choice of parameter N which greatly affects their accuracy.

In general, the calculation time of each value of $f(t)$ depends entirely on how many terms one takes. N is the total number of terms of interest in the time interval. In this representation, the interval for which we require $f(t)$ is $0 \leq t \leq 25$ s. Therefore, we take

$T = 50$ s. The value of the parameter aT used in this example is $aT = 5$ due to the reasons already mentioned in the previous example.

In Figure 7.4 and Figure 7.5, the exact values of $f(t)$ and the approximate values $f_a(t)$ obtained by the Dubner & Abate's and Durbin's numerical inversion techniques, respectively are compared for different number of terms of interest. The results are discussed for the cases that number of terms (N) are taken as: 100, 250 and 500. As illustrated in Figure 7.4, the fluctuation scattering decreases as N in Dubner and Abate's inverse transform technique increases.

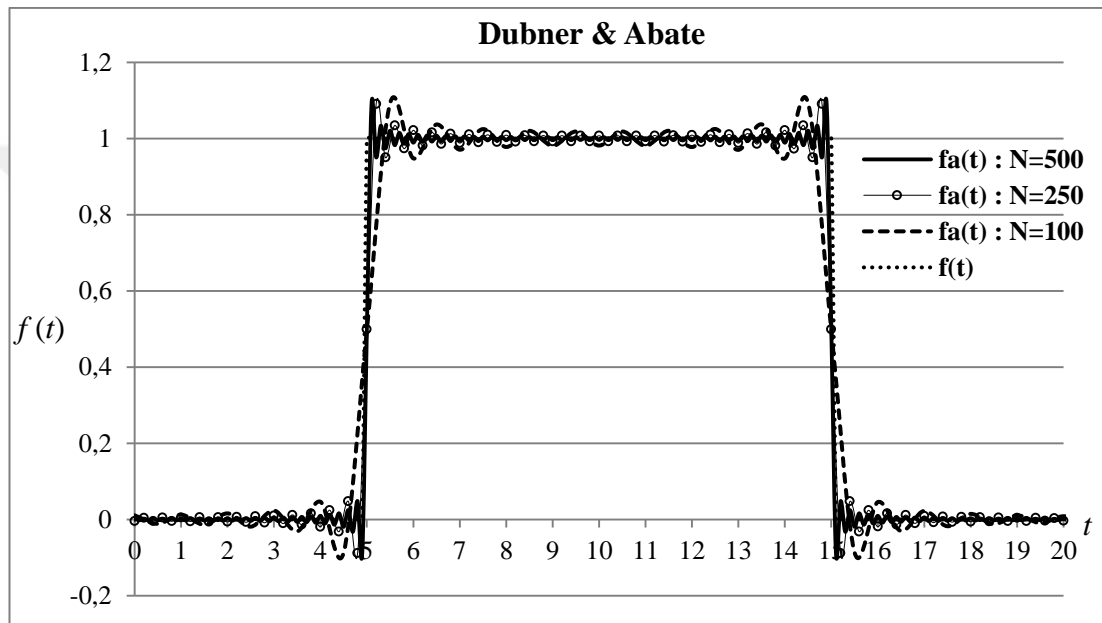


Figure 7.4 : Effect of the changes in the value of the N parameter in Dubner & Abate.

In addition, it was observed that if $f(t)$ is computed for $N = 100$ equidistant points, significant departures from the exact solution occur for $t > 35$ s in Durbin's inverse transform technique. On the other hand, for $N = 500$ terms, the time can be increased significantly up to $t > 45$ s as illustrated in Figure 7.5.

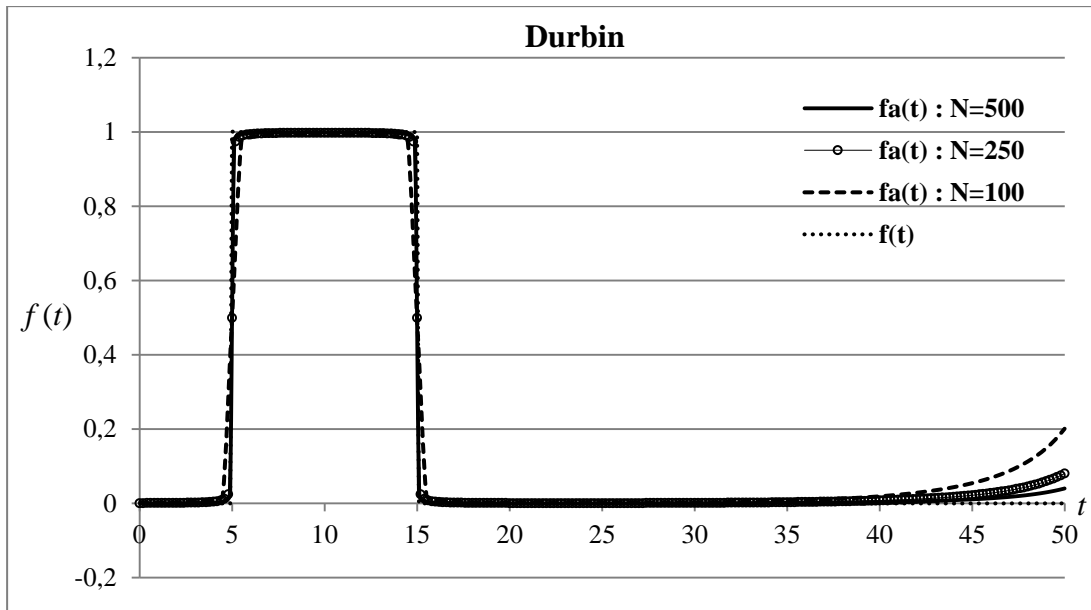


Figure 7.5 : Effect of the changes in the value of the N parameter in Durbin.

8. ILLUSTRATIVE EXAMPLES AND DISCUSSION

In this section, the application of the proposed mixed finite element formulation to a variety of quasi-static and dynamic problems is illustrated. In numerical computation, a plate with length $L_x = 4\text{m}$, width $L_y = 4\text{m}$ and thickness h , simply supported on all edges as shown in Figure 8.1 and subjected to time-dependent loads in the form of a step-function, sinusoidal impulsive, rectangular impulsive and wave-type as shown in Figure 8.2 has been analyzed.

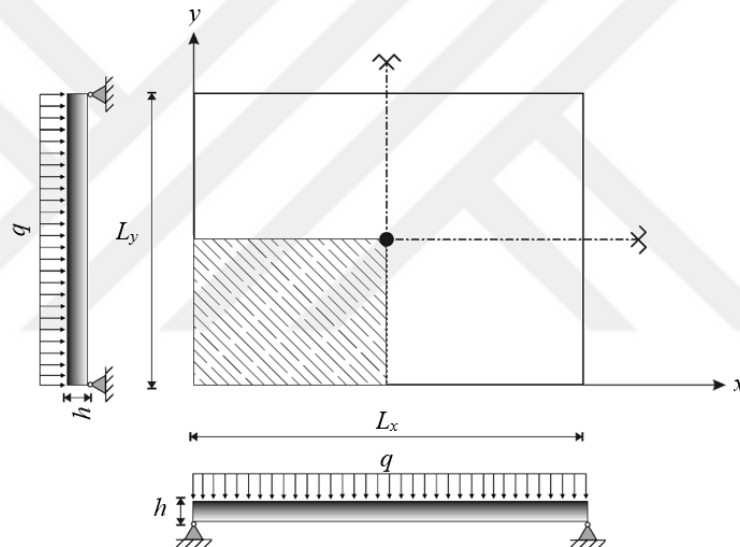


Figure 8.1 : Geometrical properties of the simply supported plate subjected to a uniform pressure load $q = q(x, y)$.

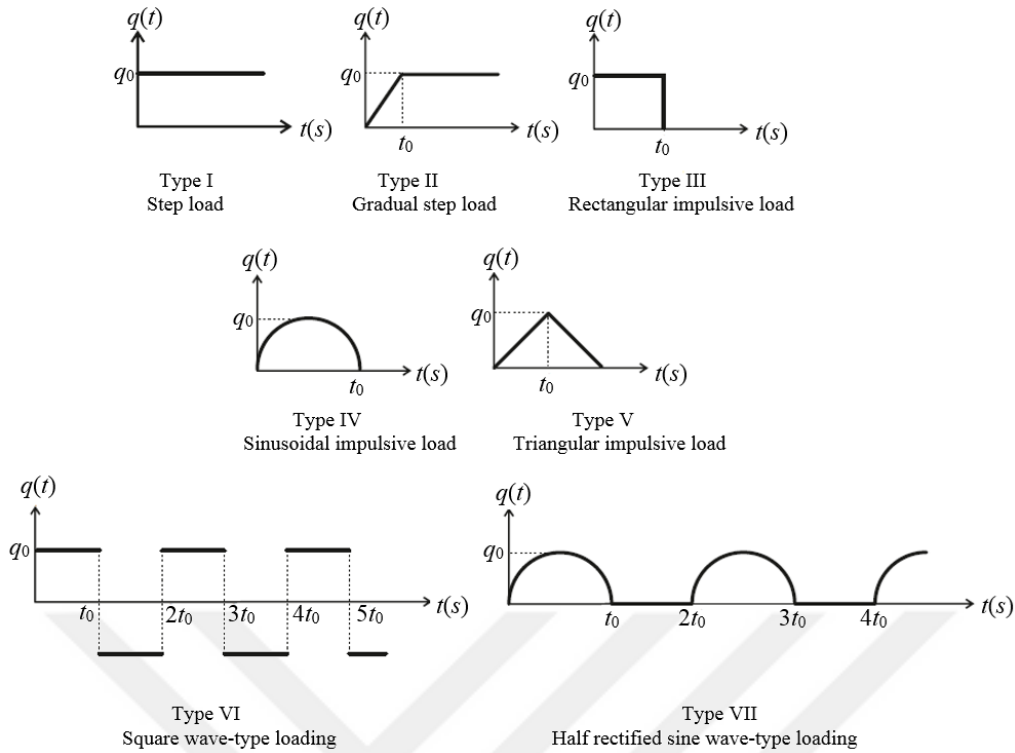


Figure 8.2 : Time histories of external loads.

Due to symmetry, the computations are carried out in one quarter of the plate as shown in Figure 8.1. In all numerical examples, the values of displacements and bending moments' amplitudes are given at the center point of the plate. The displacement and time are measured in meters (m) and seconds (s), respectively.

For modeling the behavior of viscoelastic plate material, five different rheological models as illustrated in Figure 8.3 are utilized. The Kelvin model seen in Figure 8.3 (a) is one of the simple spring-and-dashpot model. Here, three-element models and four-element models are also discussed to provide some insight into the creep and relaxation characteristics of viscoelastic responses. There are two three-element models, as shown in Figure 8.3 (b) and (c). In the first one, an extra linear spring element is added in series to the Kelvin model, and in the second one a spring element is added in parallel to the Maxwell element. There are two four-element models, as shown in Figure 8.3 (d) and (e). The first one degenerates into the Kelvin model when its components parts are made equal and the second one is obtained by connecting the Maxwell element in parallel with the Kelvin element.

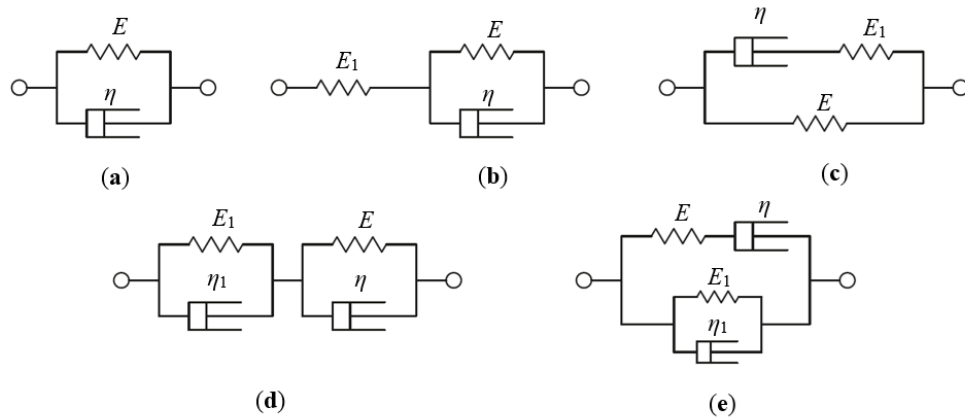


Figure 8.3 : Rheological models: mechanical analog for the Kelvin (a), Three-parameter-solid (b), Zener (c), Kelvin-chain (d) and Four-parameter-solid (e) model.

The Maxwell model has an initial elastic response to a suddenly applied stress, however the material described by the Maxwell model shows a typical property of a fluid: its capability of unlimited deformation under finite stress. The displacement of Kelvin, three-element, and four-element models approaches a finite value as $t \rightarrow \infty$. Note that Kelvin model and four-element models do not have an initial elastic response to a suddenly applied stress, however the three-element models have an elastic response to a suddenly applied stress. Therefore, three-element models also known as the standard linear solid.

The creep compliance function that describes, in a certain way, stress-strain behavior of the material is listed in Table 8.1 for each rheological model.

Table 8.1 : Creep compliance functions of viscoelastic material models.

Material Models	Creep Compliance Functions $J(t)$
Kelvin Model	$J(t) = \frac{1}{E} \left(1 - e^{-\left(\frac{E}{\eta}t\right)} \right)$
Three-parameter-solid Model	$J(t) = \frac{1}{E_1} + \frac{1}{E} \left(1 - e^{-\left(\frac{E}{\eta}t\right)} \right)$
Zener Model	$J(t) = \frac{1}{E} (1 - e^{-\alpha t}) + \frac{1}{E + E_1} e^{-\alpha t}$ $\alpha = \frac{EE_1}{\eta(E + E_1)}$
Kelvin-chain Model	$J(t) = \frac{1}{E} \left(1 - e^{-\left(\frac{E}{\eta}t\right)} \right) + \frac{1}{E_1} \left(1 - e^{-\left(\frac{E_1}{\eta_1}t\right)} \right)$
	$J(t) = \frac{E}{\eta_1} \left\{ \frac{1}{\eta} \left[\frac{1}{\beta\delta} - \frac{e^{-\beta t}}{\beta(\delta - \beta)} + \frac{e^{-\delta t}}{\delta(\delta - \beta)} \right] + \frac{1}{E} \left[\frac{e^{-\beta t}}{(\delta - \beta)} - \frac{e^{-\delta t}}{(\delta - \beta)} \right] \right\}$
Four-parameter-solid Model	$\beta = \frac{E}{2\eta_1} \left(\left(1 + \frac{E_1}{E} + \frac{\eta_1}{\eta} \right) - \sqrt{\left(1 + \frac{E_1}{E} + \frac{\eta_1}{\eta} \right)^2 - 4 \frac{E_1\eta_1}{\eta E}} \right)$ $\delta = \frac{E}{2\eta_1} \left(\left(1 + \frac{E_1}{E} + \frac{\eta_1}{\eta} \right) + \sqrt{\left(1 + \frac{E_1}{E} + \frac{\eta_1}{\eta} \right)^2 - 4 \frac{E_1\eta_1}{\eta E}} \right)$

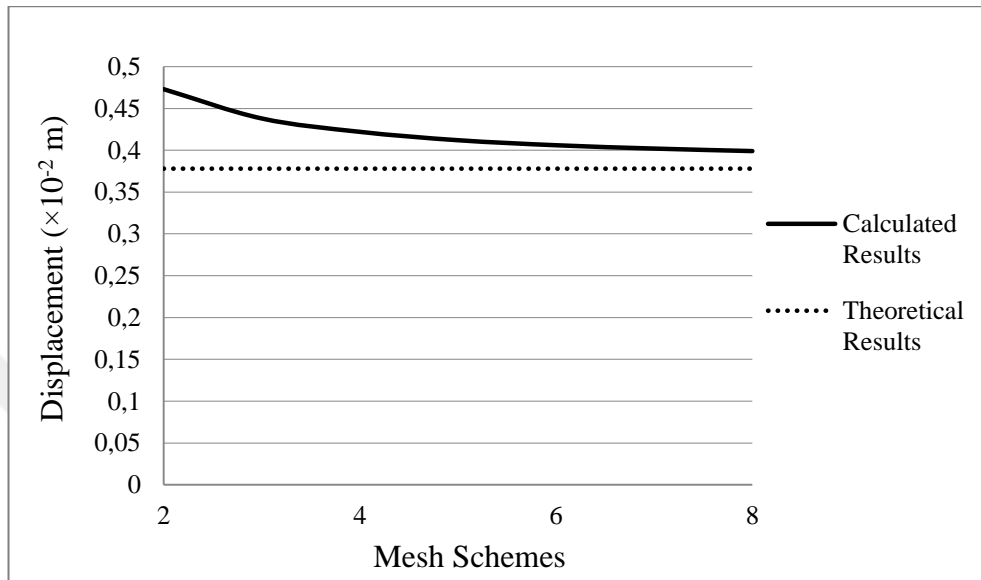
The analysis was performed with the aid of a coded computer program in Fortran language.

8.1 Example 1

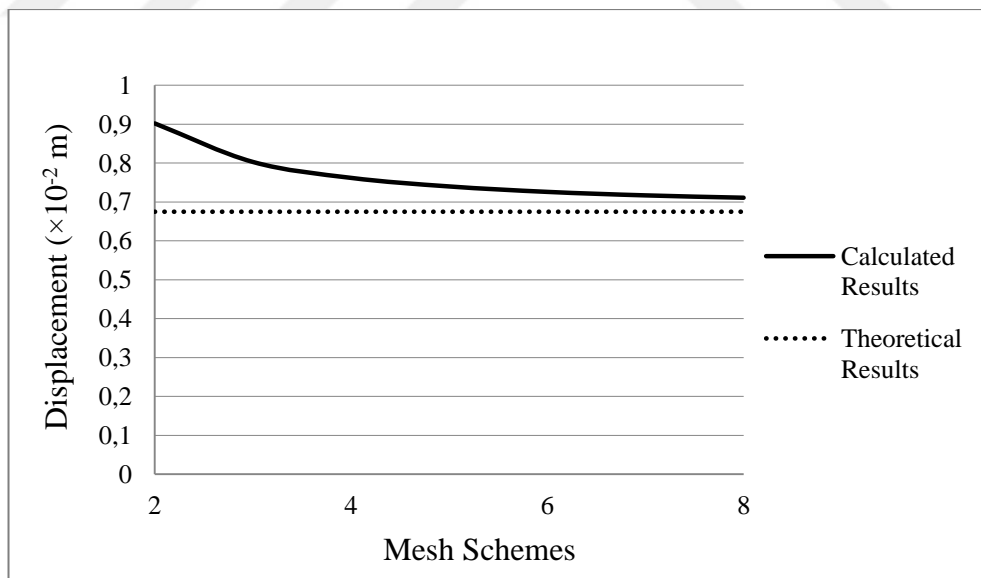
The performance of the developed computer program is tested through this example. This program consists of two parts, elastic and viscoelastic. As a first step, the elastic part is tested.

A plate is subjected to a Type I load of $q_0 = 10$ kPa and a Type I point load $P_0 = 100$ kN separately. The material properties are $E = 3 \times 10^7$ kPa and $\nu = 0,3$. The

displacement values at the center of the elastic plate are computed for different orders of mesh schemes, 2×2 , 4×4 , 6×6 and 8×8 , and the results are presented in Figure 8.4 (a) - (b). The results are compared with existing results in the literature in order to determine the most suitable mesh scheme. For the theoretical results of elastic plates, see Timoshenko and Woinowsky-Krieger (1959).



(a)



(b)

Figure 8.4 : Comparison of theoretical and calculated deflection results under Type I loading (a) distributed load, (b) point load.

Simulations show that if the mesh gets finer, the results of the developed mixed finite element solution show good agreement with the theoretical results. However, an increase in the number of mesh cells naturally increases the time of computer solution.

As illustrated in Figure 8.4 (a) - (b), the 4×4 mesh scheme results are very satisfactory and this scheme has the advantage of saving time. Therefore, through this study, the results of the 4×4 mesh scheme are considered in all numerical examples.

Once the results of elastic plates and the most suitable mesh scheme for the solution are obtained, the performance of the viscoelastic part of the developed program is tested for the elastic plates.

The viscosity coefficient, η , is set to zero in the developed viscoelastic computer program in order to obtain the results of the elastic plate. The results of the elastic plates obtained from the developed viscoelastic plate program are given in Figure 8.5 for the Type I load of $q_0 = 10$ kPa for $aT = 5$, $N = 100$ and $T = 20$ s. The numerical results show an excellent agreement with the theoretical results of elastic plates. Thus, it is proved that the performance of the developed viscoelastic computer program is efficient.

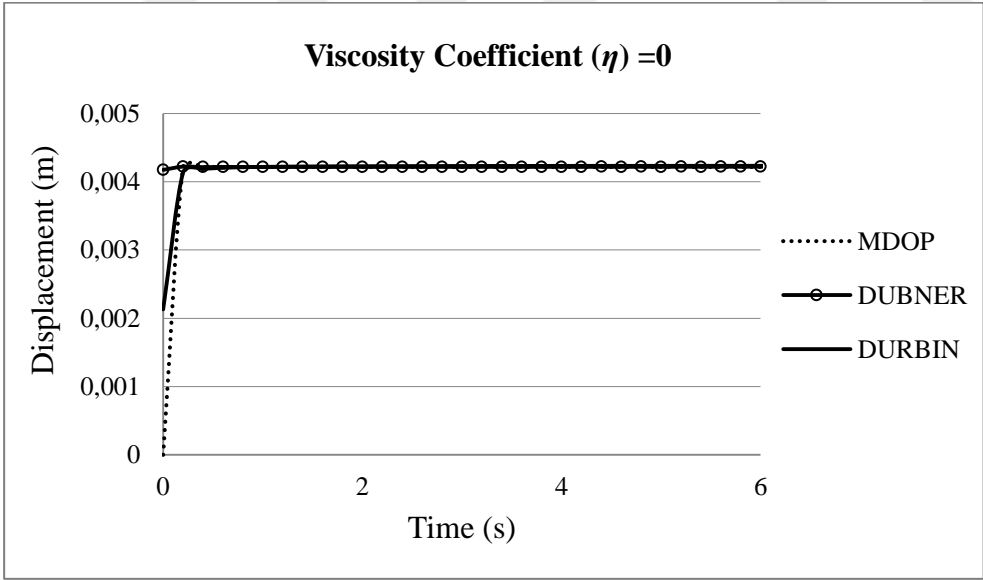


Figure 8.5 : The displacement-time variation of the center point of an elastic plate.

8.2 Example 2

The main objective of this example is to determine the most suitable values for the effective parameters of the inverse transform techniques. As the value of aT is

changed, fluctuation is observed in Dubner and Abate's and Durbin's inverse transform techniques. In addition to aT , the results depend also on parameter N . The error in the solution decreases as the value of N increases. This example is solved for a Kelvin solid employing MDOP, Dubner and Abate's and Durbin's inverse transform techniques for different values of aT ($aT = 5, 10$ and 20 , respectively). The time variation of the bending moment and displacement of the center point under the Type I load of $q_0 = 10$ kPa are computed for $N = 50$ and $T = 100$ s. The results are presented in Figure 8.6 for the following material properties: $E = 3 \times 10^7$ kPa; $\eta = 3 \times 10^7$ kPa s and $\nu = 0,3$.

It is observed that the results of the MDOP method are independent of aT . However, fluctuation is observed in the Dubner and Abate's and Durbin inverse transform methods when aT takes values bigger than 10. As observed from Figure 8.6, the fluctuation scattering increases as aT in Dubner and Abate's inverse transform technique increases. Fluctuation is observed for $t > 20$ s as $aT = 20$ and for $t > 30$ s as $aT = 10$ in Dubner and Abate's and Durbin's methods. If the time histories of the external loads in applications are considered, it is clearly seen that the behavior up to maximum 10 seconds is our interest. So throughout this study, all examples are solved for the values of aT less than or equal to 10. For the next examples, problems are solved for $aT = 5$ or 10 and $N = 100$ or 200 to decrease the fluctuation and the error in the solutions.

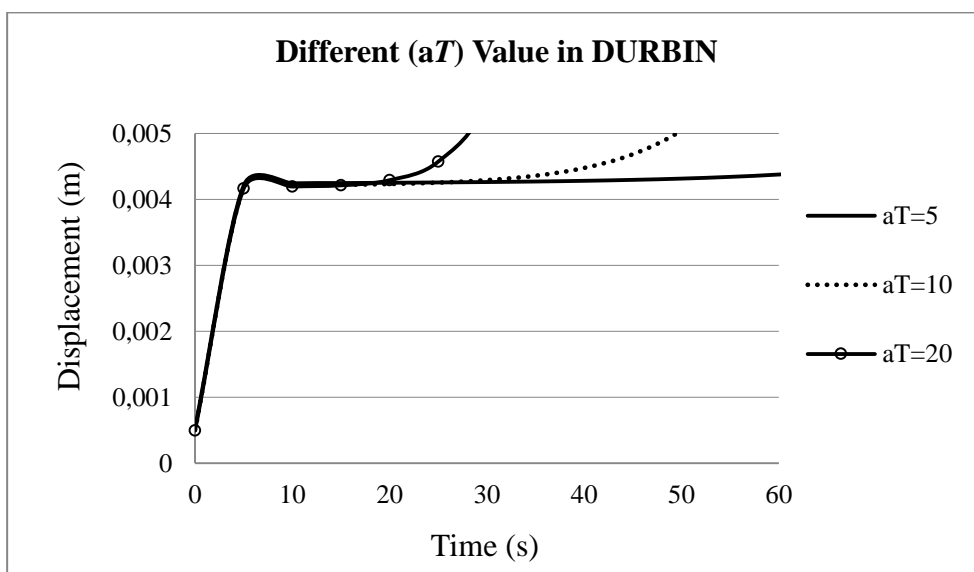
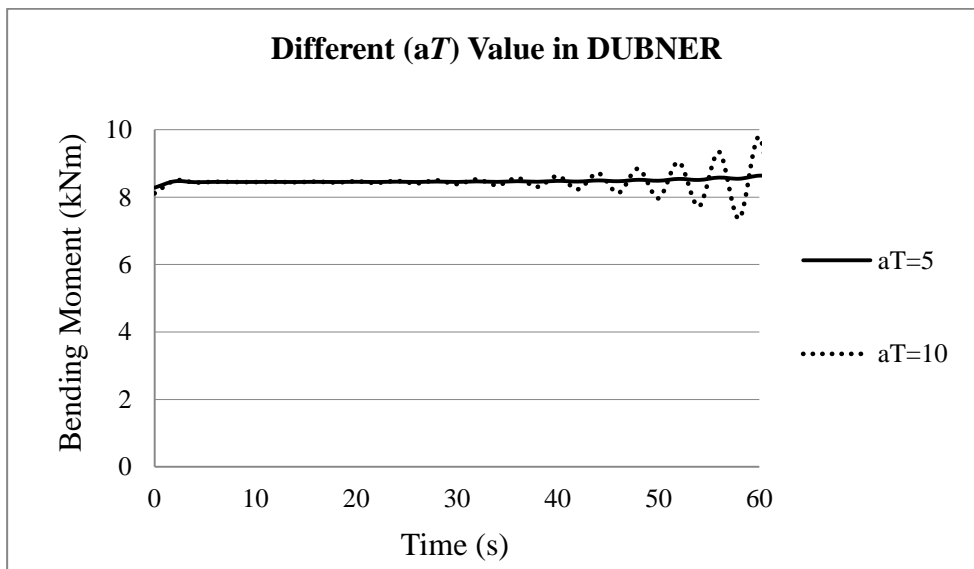
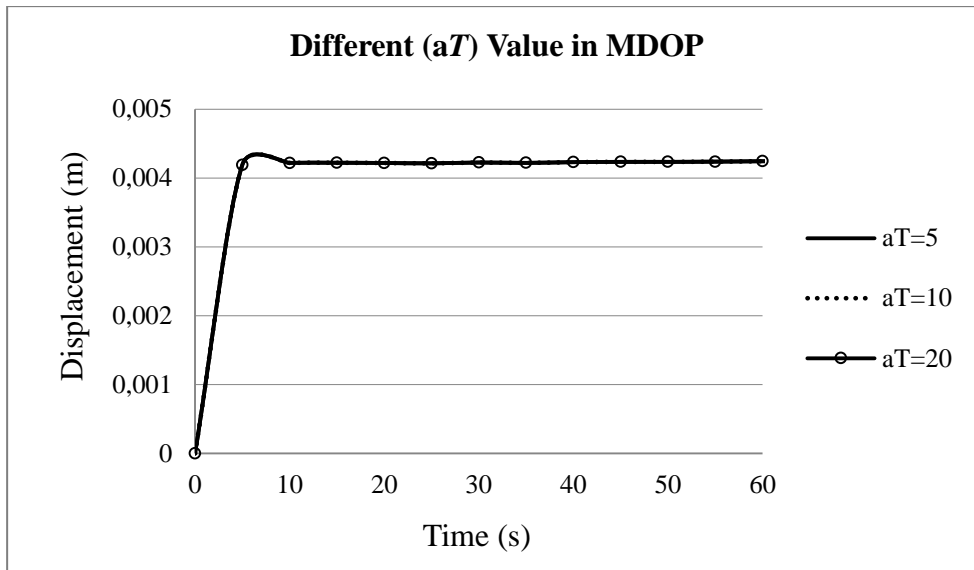


Figure 8.6 : Effect of the changes in the value of the aT parameter.

8.3 Example 3

A plate is subjected to different loads, and the time histories are illustrated in Figure 8.2. Kelvin solid model is employed. The material properties are assumed to be as follows: $E = 3 \times 10^7$ kPa; $\eta = 3 \times 10^7$ kPa s and $\nu = 0,3$. For the numerical inversion, the MDOP, Dubner and Abate's and Durbin's transform techniques are used. The time-dependent displacement and bending moment at the center of the plate are computed for $aT = 5$, $N = 100$ and $T = 20$ s and presented in Figure 8.7.

This example is solved for the η (viscosity coefficient of the material) / E (modulus of elasticity of the material) ratio being equal to one.

The success of the MDOP, Dubner and Abate's and Durbin's methods is tested for the Type I, Type II for $t_0 = 2$ s, Type III for $t_0 = 10$ s and Type IV for $t_0 = 10$ s loads. It is observed that the MDOP method gives good results for the displacement variation as compared to the bending moment variation. Fluctuation is observed in the time-dependent bending moment at the center of the plate as time increases in the MDOP inverse transform technique. Therefore, the time variation of the bending moment is presented only for the Dubner and Abate's and Durbin's inverse transform methods.

When the time variation of the bending moment at the center point is considered, it is observed that Durbin's method gives perfect results compared to Dubner and Abate's method for the Type III and IV loads. Since little fluctuation exists in the Dubner and Abate's method as time increases, the results are not shown in the next examples.

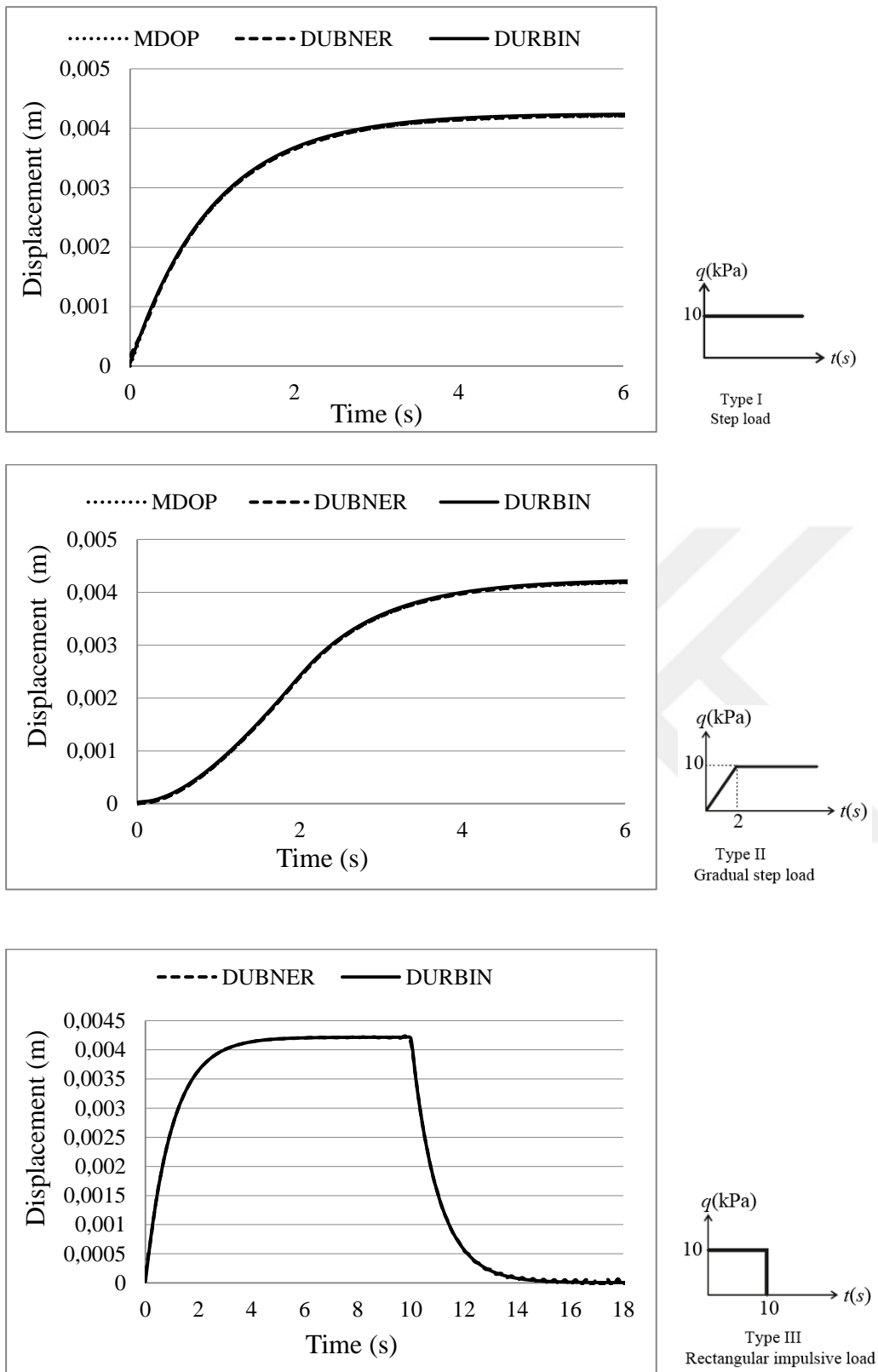


Figure 8.7 : The displacement and bending moment-time variation results for the damping ratio $\eta/E = 1$.

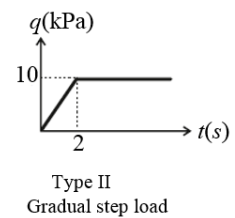
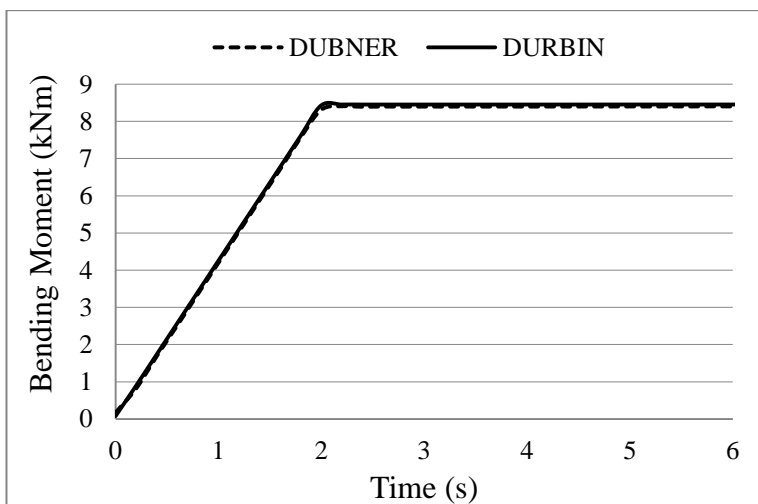
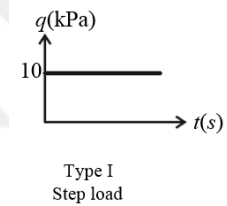
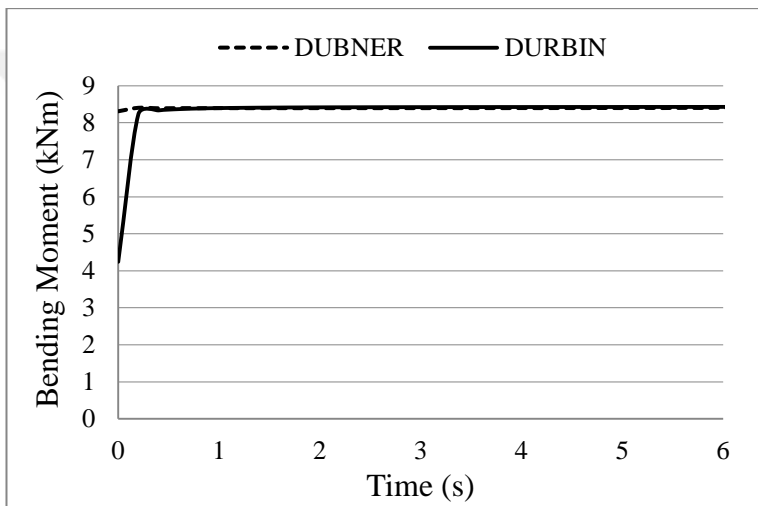
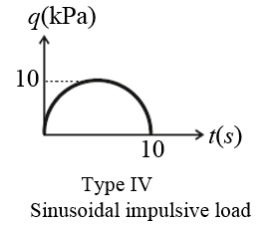
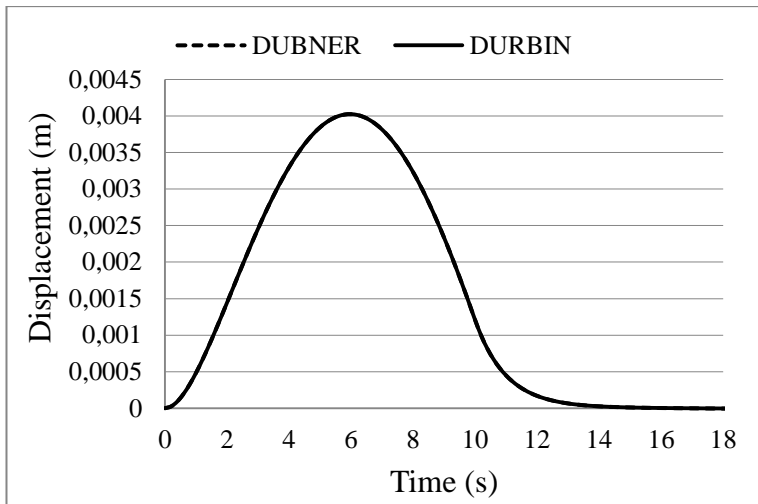


Figure 8.7 (continued): The displacement and bending moment-time variation results for the damping ratio $\eta/E = 1$.

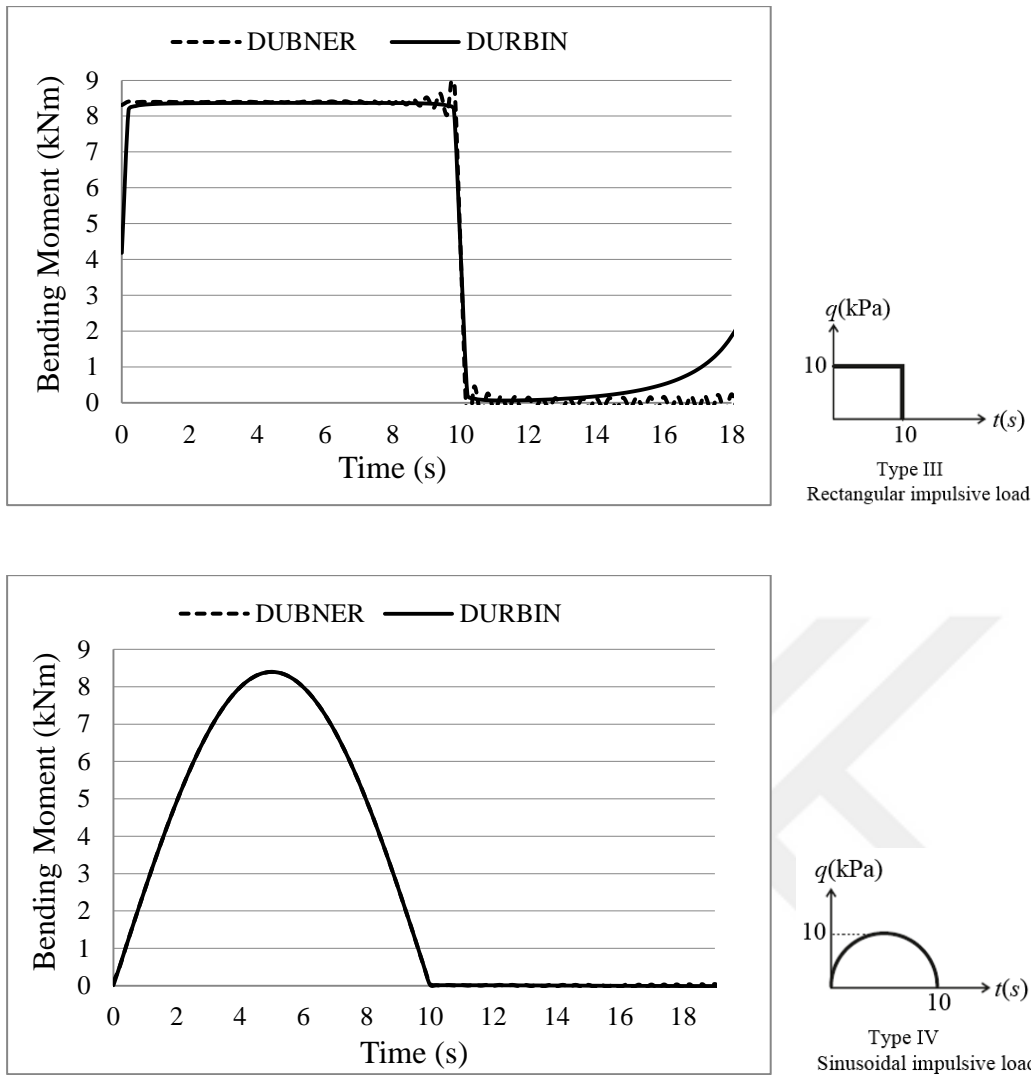


Figure 8.7 (continued): The displacement and bending moment-time variation results for the damping ratio $\eta/E = 1$.

8.4 Example 4

The problem is solved for a Kelvin solid employing different η/E ratios in order to show the damping effect in displacement variation of the center point. In the numerical process, the material properties of the plate are assumed to be $E = 3 \times 10^7$ kPa and $\nu = 0,3$. When the viscosity coefficient decreases, the time-dependent displacement behavior of the plate approaches the elastic behavior as expected. The results are given in Figure 8.8 only for the Type III load employing Durbin's inverse transform technique for $aT = 5$, $N = 100$ and $T = 20$ s.

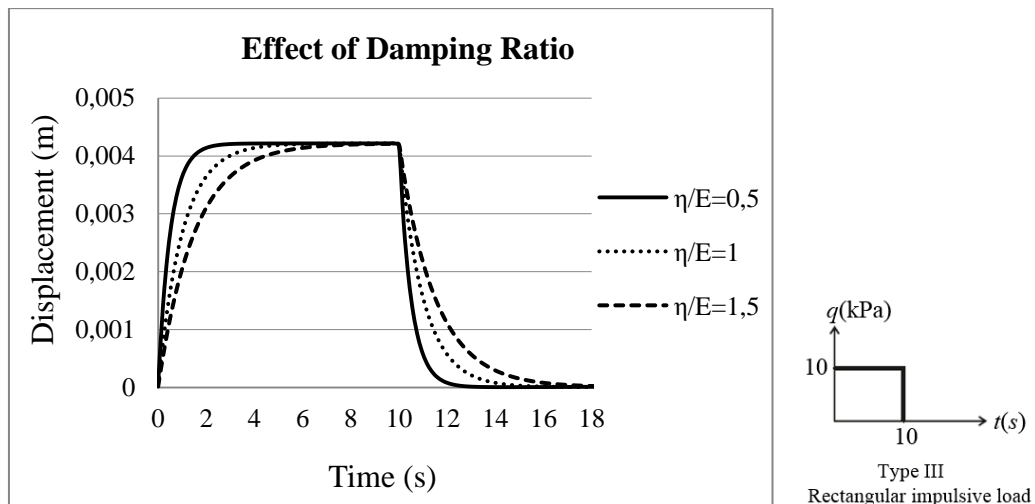


Figure 8.8 : Effect of different η/E ratios.

8.5 Example 5

In this example, the problem is solved for the Kelvin solid model employing Durbin's inverse transform technique for $aT = 5$, $N = 100$ and $T = 20$ s. A viscoelastic plate with the following properties $E = 3 \times 10^7$ kPa; $\eta = 3 \times 10^7$ kPa s and $\nu = 0,3$ is subjected to a Type I point load $P_0 = 100$ kN. The displacement values at the center of the viscoelastic plate are computed for the 4×4 mesh scheme. The results of the developed mixed finite element viscoelastic Kirchhoff plate program and the theoretical results of viscoelastic plates under point load are presented in Figure 8.9. The numerical results show an excellent agreement with the theoretical results of viscoelastic plates. Thus, it is proved that the performance of the developed viscoelastic computer program is efficient.

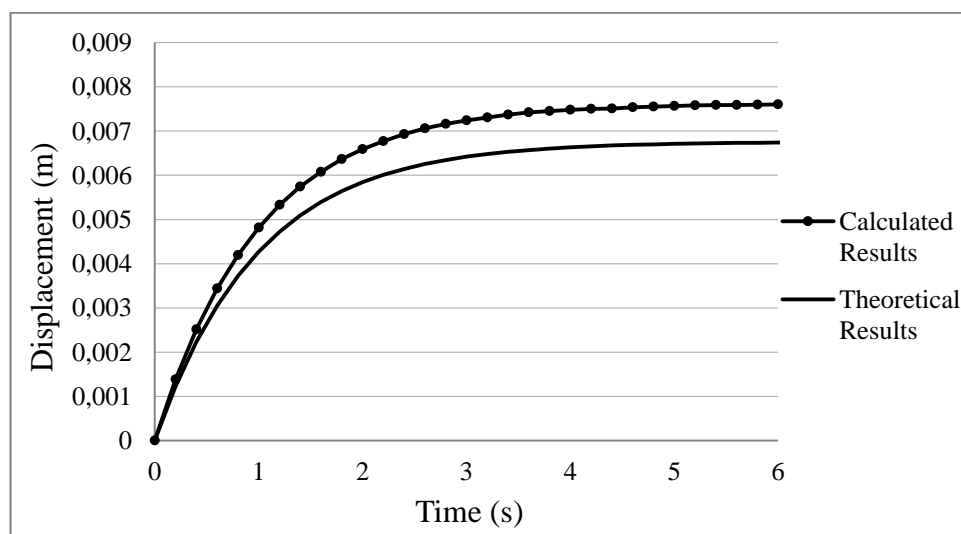


Figure 8.9 : Comparison of theoretical and calculated deflection results of viscoelastic plates under point load.

Moreover, in this example different η/E ratios are considered in order to show the damping effect in displacement variation of the center point of the viscoelastic plate under Type I point load $P_0 = 100$ kN. The results are given in Figure 8.10.

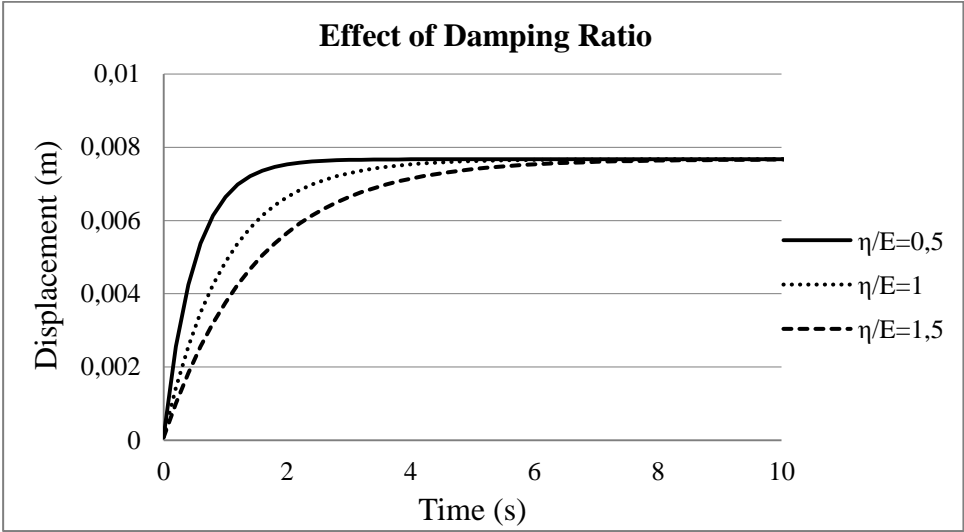


Figure 8.10 : Effect of the different η/E ratios under point load.

8.6 Example 6

This example is solved for a Three-parameter-solid model under the Type III load employing Durbin’s inverse Laplace transform technique for $aT = 5$, $N = 100$ and $T = 20$ s. In the numerical process, the material properties are assumed to be as follows: $E = 3 \times 10^7$ kPa and $\nu = 0,3$. The time-dependent displacement at the center of the plate is presented in Figure 8.11 for the damping ratio (η/E) equal to 1,5.

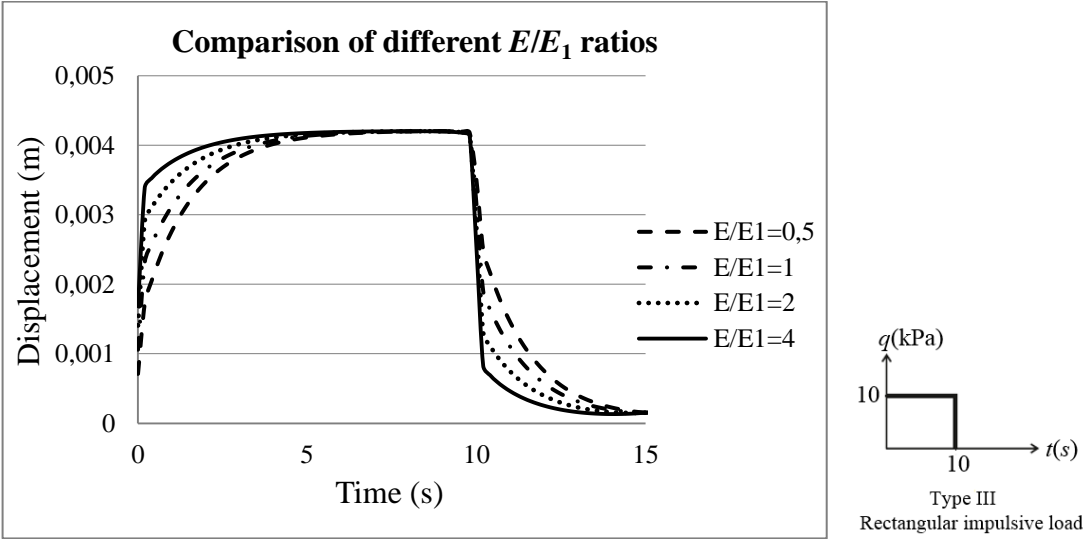


Figure 8.11 : Variation of different E/E_1 ratio curves when the damping ratio equals to 1,5.

The results are presented for different E/E_1 ratios, and the time-dependent displacements are compared with the previous example's results (the curve corresponds to the damping ratio equal to 1,5 in Example 4, Section 8.4). As expected, the E/E_1 ratio increases as the E_1 value of Three-parameter-solid model decreases, and the results of the Three-parameter-solid model coincide with those of the Kelvin solid model.

8.7 Example 7

The main objective of this example is to make comparison between different rheological models. One of the primary interests in rheology is to understand the advantages and disadvantages of the existing rheological models because rheological models can explain and predict various viscoelastic properties of materials. In this example, an analysis of three viscoelastic solid models are carried out: the Kelvin model, the three-parameter-solid model and the Zener model employing Durbin's inverse Laplace transform technique for $aT = 5$, $N = 100$ and $T = 20$ s. All three viscoelastic models studied in this example contain two common parameters, the Young's modulus of linear elastic springs (E and E_1) and the viscosity coefficient of linear viscous dashpot (η). Figure 8.12 shows the results of time-dependent displacement at the center of the plate, which is subjected to load Type III for $t_0 = 10$ s, constituted individually by the following material models with the following properties: Kelvin: $E = 3 \times 10^7$ kPa, $\eta = 3 \times 10^7$ kPa s, $\nu = 0,3$; Three-parameter-solid and Zener: $E = E_1 = 3 \times 10^7$ kPa, $\eta = 3 \times 10^7$ kPa s, $\nu = 0,3$.

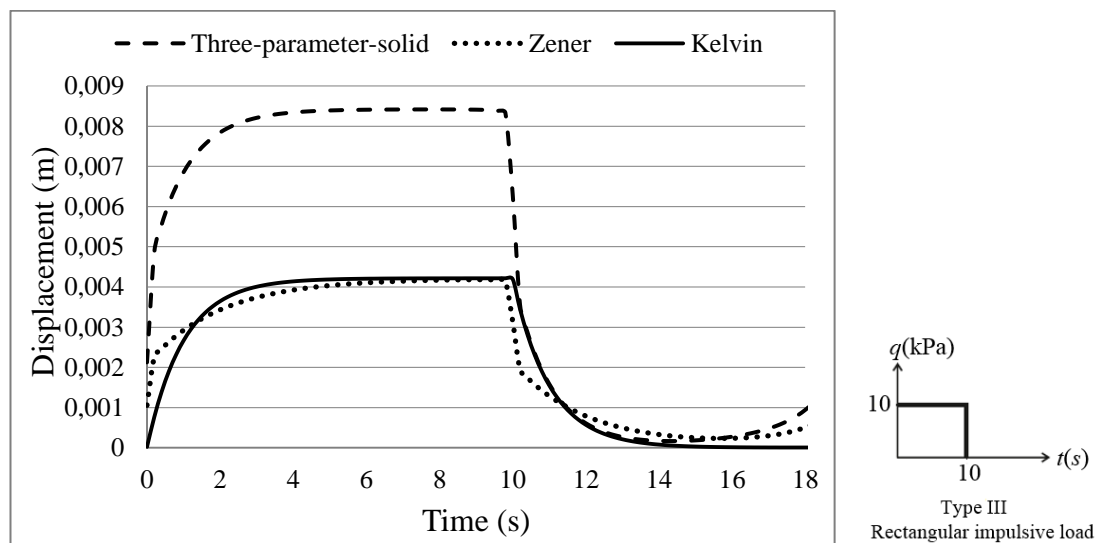


Figure 8.12 : Comparison between different rheological models.

A noticeable thing in Figure 8.12 is that the maximum displacement of the Three-parameter-solid model is two times bigger than those of the Kelvin and Zener models. It should be noted that the Kelvin model often prove insufficient, however; the Kelvin model does not describe the stress relaxation and does not exhibit the instantaneous elasticity, which is associated with a solid. Therefore, it is more convenient to use three-element models (Three-parameter-solid and Zener models) to provide good representations of viscoelastic solid behavior.

This apparent result leads to an important conclusion: comparing the Three-parameter-solid model and Zener model, it is seen that the plate structure constituted by the Zener model is stiffer than the plate structure constituted by Three-parameter-solid model.

It is also possible to reach the same displacement value by changing the material parameters of the Three-parameter-solid model. However, the deformation characterization of these materials will be different because of the arrangement of the elements and it should be evaluated by experiment.

8.8 Example 8

Plate-foundation interaction problems has been an important research topic in engineering fields. In many practical engineering applications, Winkler elastic foundation model (Winkler, 1867), which idealizes the soil as a series of isolated springs, provides satisfied results. In order to show the effect of elastic foundation on quasi-static behavior of a viscoelastic Kirchhoff plate, a plate constituted by the Zener model ($E = E_1 = 3 \times 10^7$ kPa, $\eta = 3 \times 10^7$ kPa s, $\nu = 0,3$) and subjected to load Type I and resting on a Winkler foundation with the stiffness $k_w = 1000$ kPa / m is considered. For numerical inversion, Durbin's inverse Laplace transform technique is employed for $aT = 5$, $N = 100$ and $T = 20$ s and time-dependent displacement values are depicted in Figure 8.13 for two different cases:

- Case 1: a viscoelastic plate with no foundation
- Case 2: a viscoelastic plate resting on elastic foundation

Results are quite reasonable. It can be seen that the time-dependent displacement values at the center of the plate decreases when it is supported by an elastic foundation.

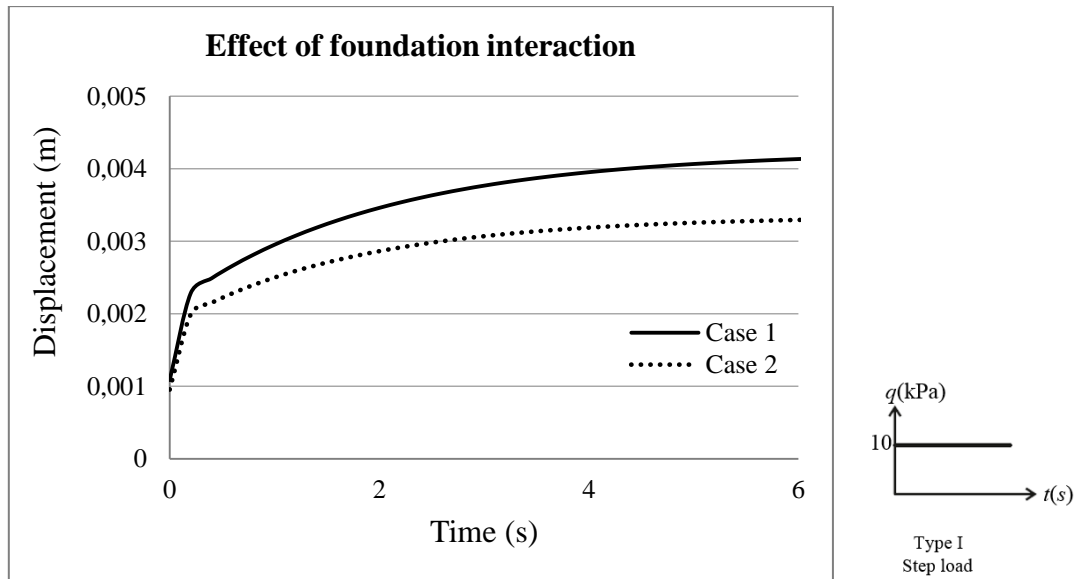


Figure 8.13 : Time-dependent displacement response of a viscoelastic Kirchhoff plate with or without elastic foundation interaction.

8.9 Example 9

The purpose of this example is investigation of the link between the Kelvin-chain model and the Kelvin model. Here the Kelvin-chain model which consists of two Kelvin units in series is analyzed. The problem is solved under the load Type I employing Durbin's inverse Laplace transform technique for $aT = 5$, $N = 100$ and $T = 20$ s. The material coefficients are chosen as follows:

- Kelvin-chain model: $E = E_1 = 3 \times 10^7$ kPa, $\eta = \eta_1 = 3 \times 10^7$ kPa s, $\nu = 0,3$
- Kelvin model: $E = 3 \times 10^7$ kPa, $\eta = 3 \times 10^7$ kPa s, $\nu = 0,3$

Figure 8.14 depicts the comparison between the Kelvin-chain model and the Kelvin model. Regarding the behavior in Figure 8.14, a plate modeled with the Kelvin-chain rheological model results in larger values of displacement than a plate modeled with the Kelvin rheological model due to the arrangement of the springs. As expected, if the springs are in series combination, the equivalent stiffness is equal to the reciprocal of sum of the reciprocal stiffness's of individual springs. One may extend this result to Kelvin chains of any length. In general, the longer the chain is, the greater the deformation there are.

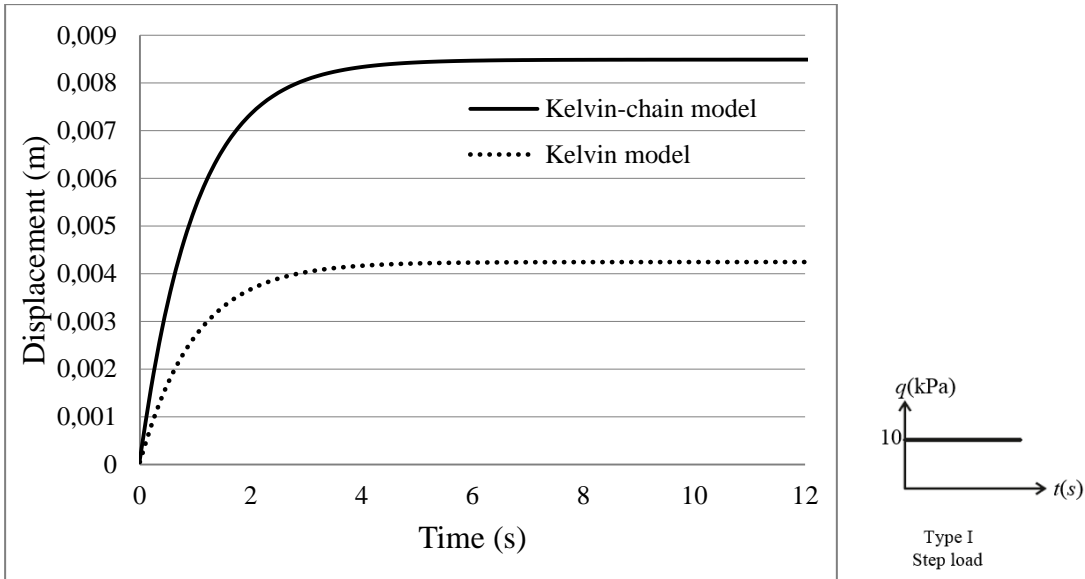


Figure 8.14 : Comparison between the two adopted viscoelasticity models.

8.10 Example 10

For evaluating the effect of variation of the height of the cross-section along sections **A-A** and **B-B** on the quasi-static response of viscoelastic plate, two uniformly varying thickness problems are solved. Thickness at the corner sides of the plate $h_c = 0,1$ m and at the center of the plate along section **A-A** $h_{my} = 0,1$ m is held constant, whereas the thickness at the center of the plate along section **B-B** is (b) $h_{mx} = 2h_c$, (c) $h_{mx} = 4h_c$ (as in Figure 8.15), respectively.

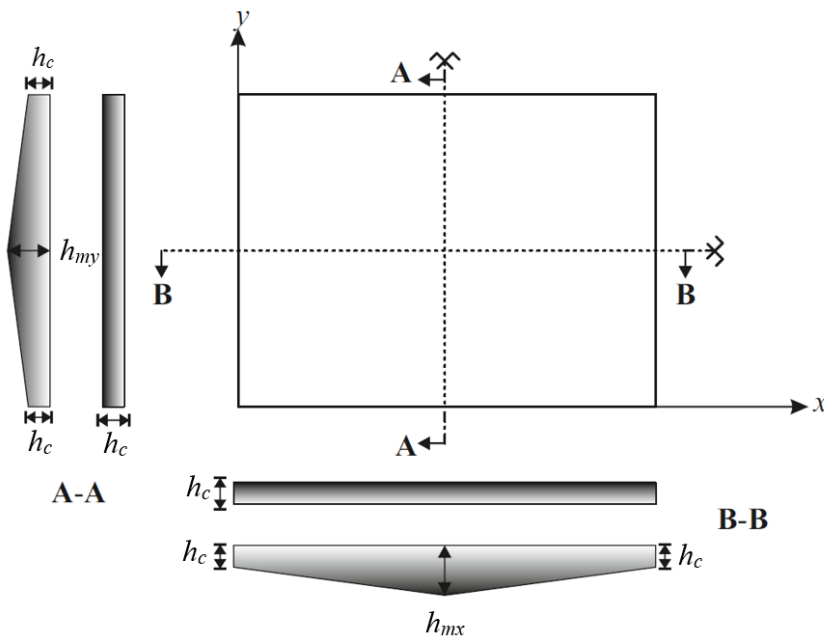


Figure 8.15 : Simply supported plate of variable thickness.

A viscoelastic plate with variable thickness constituted by the Kelvin-chain model and subjected to load Type V ($t_0 = 5$ s) with an amplitude $q_0 = 100$ kPa is considered. The parameters of the Kelvin-chain viscoelastic material are $E = E_1 = 6 \times 10^7$ kPa, $\eta = \eta_1 = 6 \times 10^7$ kPa s and $\nu = 0,3$. The problem is solved employing Durbin's inverse Laplace transform technique for $aT = 5$, $N = 200$ and $T = 40$ s.

Figure 8.16 displays the variation of displacement at the center of the plate: (a) Plate with constant thickness along sections **A-A** and **B-B**, (b) and (c) Plate with variable thickness: Thickness is constant along section **A-A** and uniformly increasing from supports to the center of the plate along section **B-B**. As expected, an increase in the value of plate thickness at the center of the plate along section **B-B** exerts the decrease in the central displacement response. Results are quite reasonable and show that the variable thickness formulation is reliable. The programming procedure is very simple for variable cross-sectional plates.

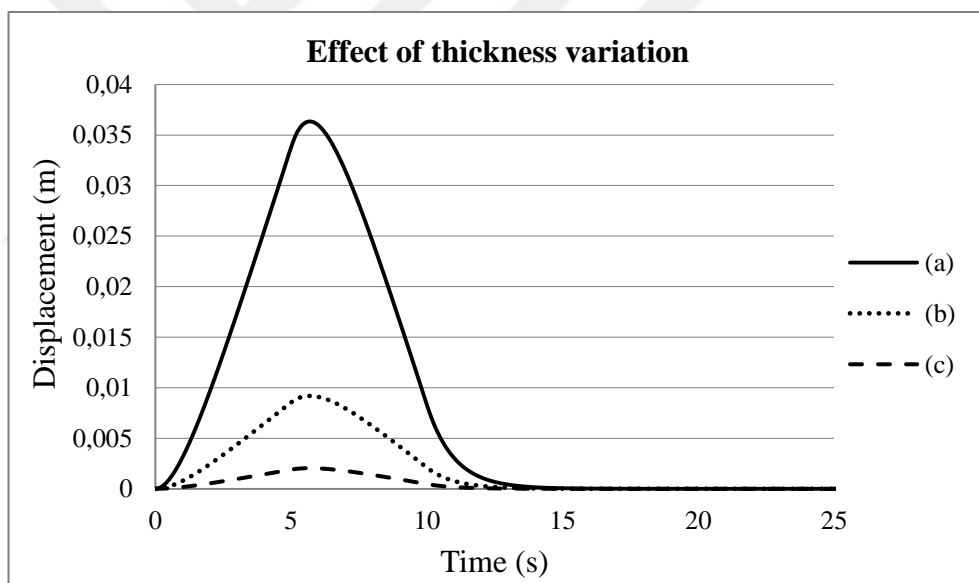


Figure 8.16 : Variation of time-dependent displacements at the center of the viscoelastic plate with constant thickness (a) and with variable thickness (b) and (c).

8.11 Example 11

In this example, viscoelastic Kirchhoff plate constituted by the Four-parameter-solid model is analyzed. The material properties are assumed to be as $E = E_1 = 3 \times 10^7$ kPa and $\nu = 0,3$.

In general, four-element models have found numerous applications, especially in geosciences, see e.g., the books by Klausner (1991) and Carcione (2007).

For evaluating the effect of material parameters on the quasi-static response of viscoelastic thin plates subjected to load Type II ($t_0 = 5$ s) with an amplitude $q_0 = 10$ kPa, each unit with different parameter values are considered. Dubner & Abate inverse Laplace transformation algorithm for $aT = 5$, $N = 150$ and $T = 30$ s is used for coming back to time domain solutions.

Figure 8.17 shows the variation of the central displacement values of the plate with respect to the time for different η/E and η_1/E_1 ratios.

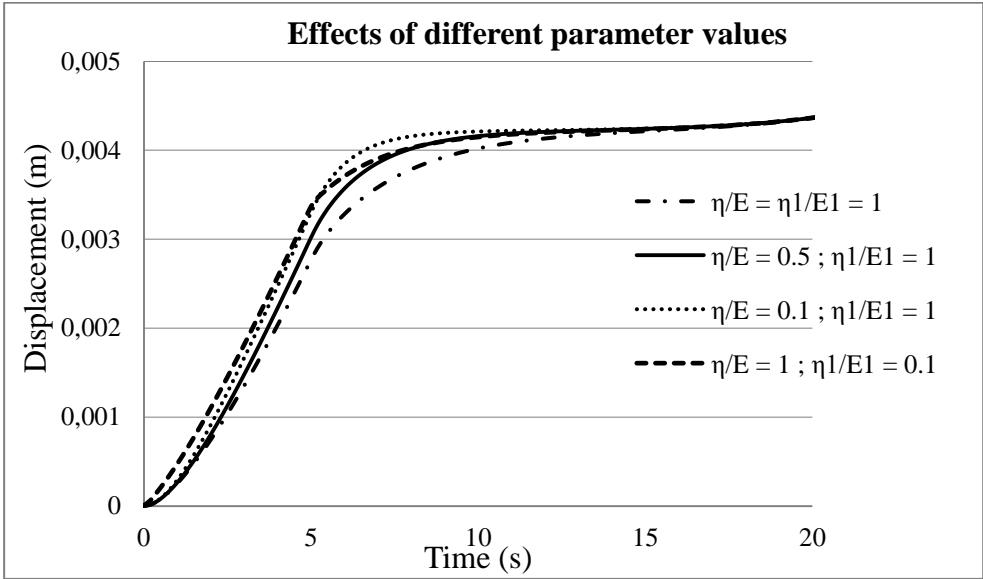


Figure 8.17 : Effect of different η/E and η_1/E_1 ratios.

The η/E and η_1/E_1 ratios decrease as the viscosity coefficient values of the Maxwell structure and the Kelvin structure decrease, respectively. It is well known that the dashpot or viscous element will cause a time delay in the mechanical response of the material. The time-dependent displacement response of a plate reaches 2,77 mm in 5 seconds if the η/E ratio equals to η_1/E_1 ratio. Whereas, at $t_0 = 5$ s, the amplitude of the displacement response of a plate is 3,3 mm with the minimization of the dashpot’s efficiency of the Maxwell structure and is 3,37 mm with the minimization of the dashpot’s efficiency of the Kelvin structure. As expected, decreasing the viscosity in the dashpot resulting in greater extensions. However, it is worth noting that even if the viscosity coefficient values of the Maxwell and Kelvin structures are decreased in the same ratio, remarkable changes in deformation behavior of material occurred.

8.12 Example 12

In this example, the quasi-static response of the viscoelastic plate under different wave-type loadings is considered. Figure 8.18 shows the time-dependent displacement at the center of the plate constituted by the Four-parameter-solid model for the load Type VI ($t_0 = 5$ s) with an amplitude $q_0 = 10$ kPa. The parameters of the viscoelastic material are $E = E_1 = 3 \times 10^7$ kPa and $\nu = 0,3$.

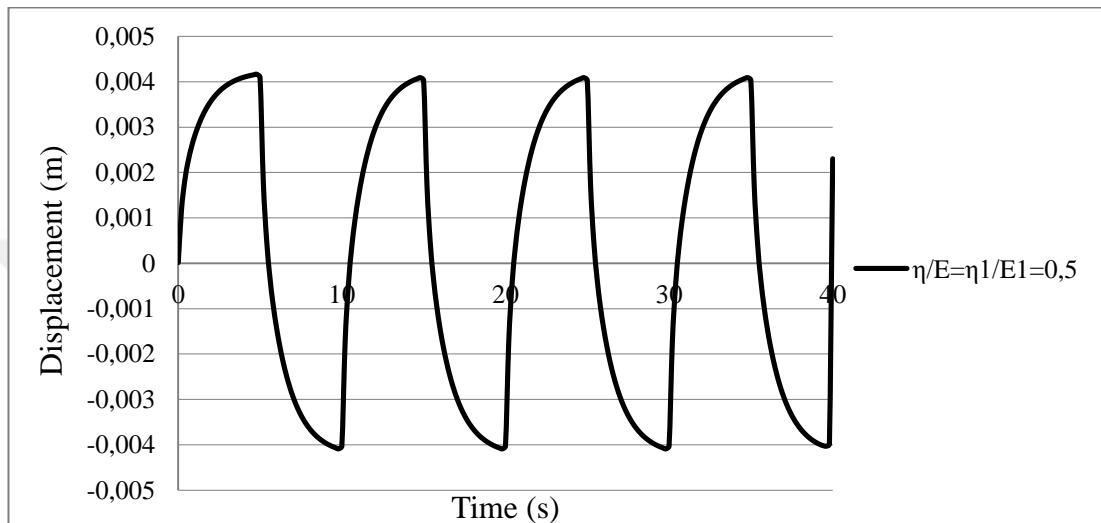


Figure 8.18 : The displacement-time variation results of viscoelastic plates under wave-type loading Type VI employing Durbin's method.

The results of the plate constituted by the three parameter-solid model under the load Type VII ($t_0 = 10$ s) with an amplitude $q_0 = 10$ kPa are presented in Figure 8.19 for the following material properties: $E = E_1 = 6 \times 10^7$ kPa, $\eta = 6 \times 10^7$ kPa s and $\nu = 0,3$.

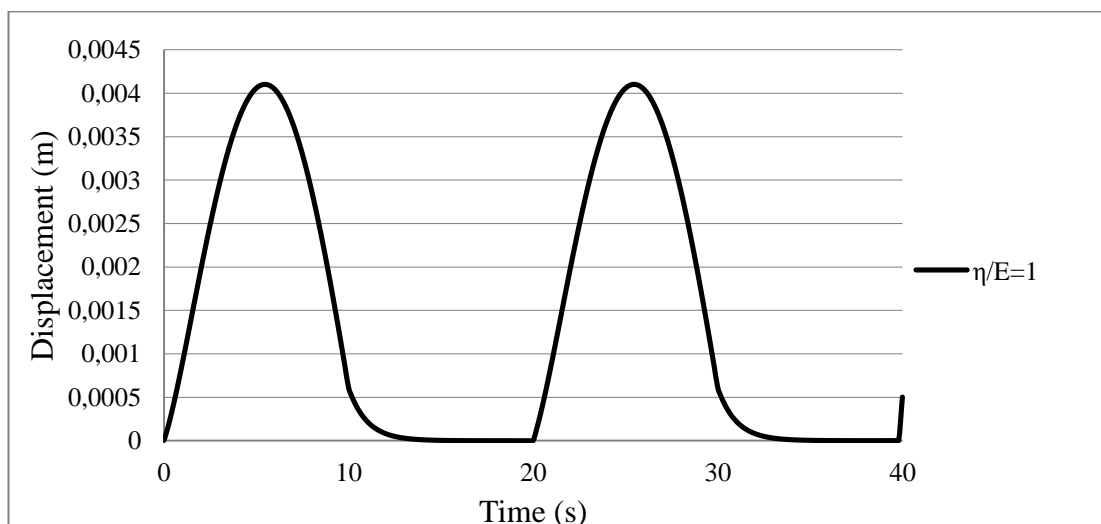


Figure 8.19 : The displacement-time variation results of viscoelastic plates under wave-type loading Type VII employing Durbin's method.

These problems are solved employing MDOP, Dubner & Abate's and Durbin's inverse transform techniques. Since little fluctuation exists in the MDOP and Dubner & Abate's inverse transform methods as time increases, the results are presented only for the Durbin's inverse transform method for $aT = 5$, $N = 200$ and $T = 40$ s. From the analysis results shown in Figure 8.18 and Figure 8.19, it would be reasonable to conclude that Durbin's inverse transform technique works well for periodic type loadings (i.e., wave-type loadings).

8.13 Example 13

In this example, the dynamic response of a simply supported viscoelastic plate ($L_x = L_y = 4$ m and $h = 0,1$ m) is considered. For the analysis, the Kelvin solid model is employed. The problem is solved for the Type I load of $q_0 = 10$ kPa, using the MDOP, Dubner and Abate's and Durbin's inverse transform techniques for $aT = 5$, $N = 200$ and $T = 0,2$ s. The material density ρ is defined as the mass density per unit volume of the plate, and it is assumed to be 2000 kg/m³; and we also take $E = 3 \times 10^7$ kPa and $\nu = 0,3$. In order to determine the frequency of vibration, free vibration analysis is carried out for ($m = 1$ and $n = 1$). The effect of the increasing viscosity coefficient η on the transient response and the frequency of vibration is shown in Figure 8.20.

When η is assumed to be 1500 kPa s, the vibration period, T , of the plate equals to $0,0435$ s. The vibration behavior of the viscoelastic plate resembles the vibration of an elastic plate for small values of the viscosity coefficient. This result is compared with the existing studies done by Leissa (1969), Craig and Kurdila (2006) and provides theoretical validation for the use of the vibration frequency of elastic plates (see Equation (8.1) for a review):

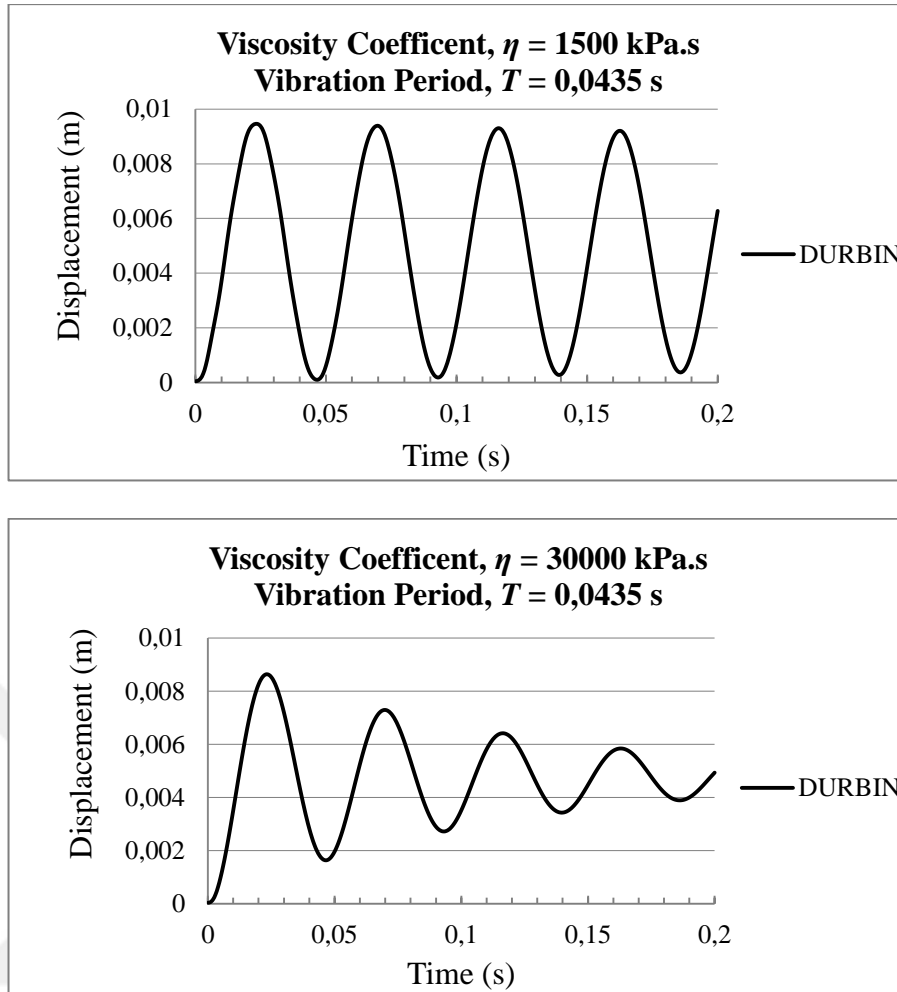


Figure 8.20 : Effect of viscosity coefficient on the vibration period and amplitude of displacement.

$$\omega = \sqrt{\frac{D}{\rho h}} \left[\left(\frac{m\pi}{L_x} \right)^2 + \left(\frac{n\pi}{L_y} \right)^2 \right] \quad (8.1)$$

where

$$D = \frac{Eh^3}{12(1-\nu^2)} \quad (8.2)$$

If D is substituted in Equation (8.1), then

$$\omega = \frac{2\pi}{T} = h \sqrt{\frac{E}{12(1-\nu^2)\rho}} \left[\left(\frac{m\pi}{L_x} \right)^2 + \left(\frac{n\pi}{L_y} \right)^2 \right] \quad (8.3)$$

is obtained.

When the viscosity coefficient is assumed to be 30000 kPa s, the viscoelastic plate shows vibration in the same period as the elastic plate, and the time behavior under the Type I load is illustrated in Figure 8.20. As it is known, the period of vibration depends on the viscosity coefficient, and a change in the value of free vibration period is expected when the viscosity coefficient is increased. However, it is observed that when the viscosity coefficient takes any value between 1500 and 30000, the viscoelastic plate will vibrate in the same period as the elastic plate.

Moreover, this example shows the effect of the thickness variation on the dynamic behavior of the viscoelastic plates. The material density ρ is taken as 2000 kg/m³, η is assumed to be 1500 kPa s, $\nu = 0,3$ and $E = 3 \times 10^7$ kPa. The thickness of the plate, h , is assumed as 0,01 m. The results are presented in Figure 8.21 for $aT = 5$, $N = 200$ and $T = 1$ s. It is observed that decreasing the thickness of the plate element does not cause shear locking.

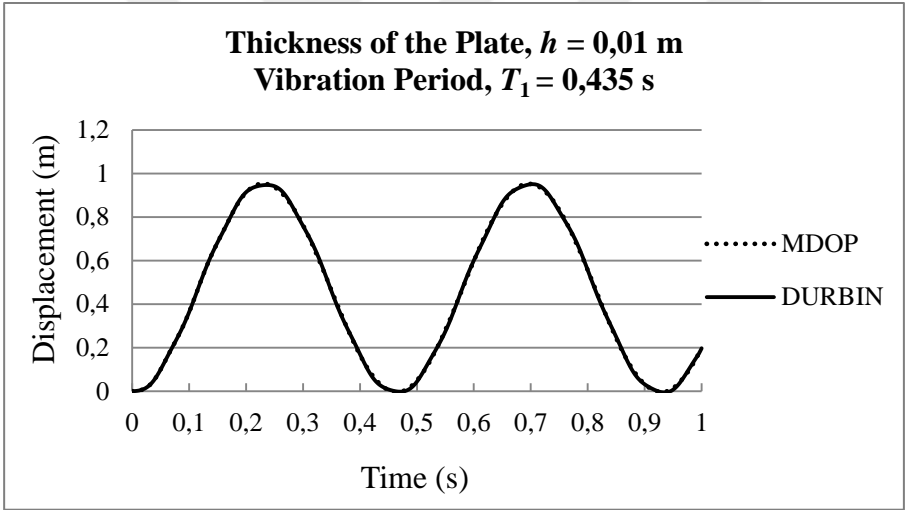


Figure 8.21 : Effect of plate thickness on the vibration period and amplitude of displacement.

In addition, the vibration period is inversely proportional to the thickness, as expected. If the thickness of the plate is changed from 0,1 m (the results are presented in Figure 8.20) to 0,01 m, according to Equation (8.3), the vibration period of the plate becomes $T_1 = 10 T$ and equals to 0,435 s as seen in Figure 8.21. This is a very important result to show that the new solution method is free from shear locking. It is impossible to obtain similar results using the well-known classical finite element method (see Bathe, 1982 and Reddy, 1993).

8.14 Example 14

In this example, the problem is solved for the Kelvin solid model employing Dubner and Abate's and Durbin's inverse transform techniques. The material density ρ is assumed as 2000 kg/m^3 , the viscosity coefficient η is assumed as 3000 kPa s , and $E = 3 \times 10^5 \text{ kPa}$. The dynamic behavior of the viscoelastic plate under the rectangular impulsive load is illustrated in Figure 8.22 for $aT = 5$, $N = 200$ and $T = 4 \text{ s}$. The time-dependent displacement amplitude at the center of the plate is continuous, whereas their derivatives show discontinuity at the time the load is removed ($t_0 = 1 \text{ s}$). When $t > 1 \text{ s}$, the plate starts to vibrate in the reverse direction.

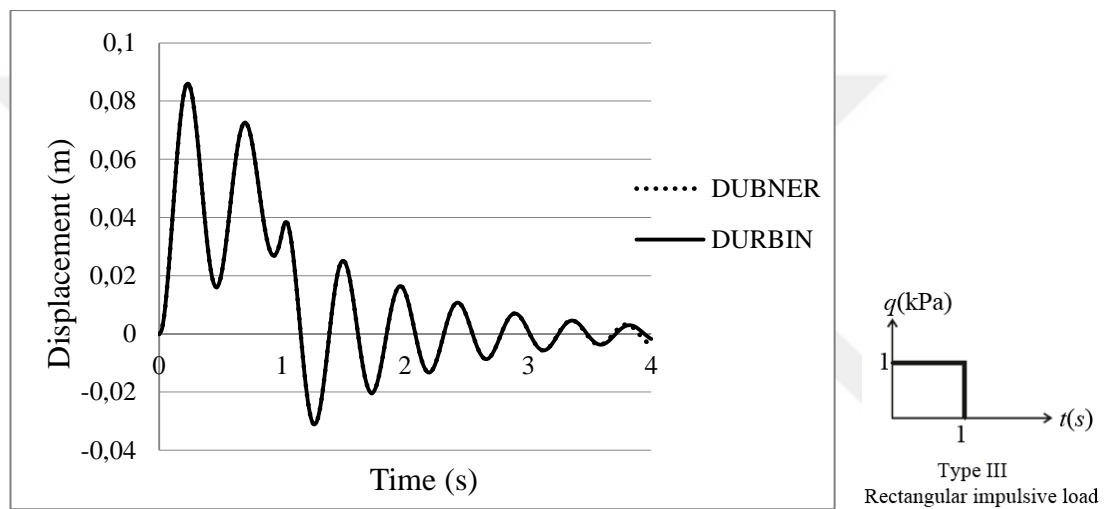


Figure 8.22 : Dynamic behavior of Kelvin solid model.

8.15 Example 15

In this example, the influence of elastic foundation stiffness parameter k_w on the displacement response and the natural frequency of vibration of simply supported viscoelastic plates has been investigated under Type I load of $q_0 = 10 \text{ kPa}$. For modelling the behavior of a viscoelastic plate material, three-parameter-solid model is employed for the following material properties: $E = E_1 = 6 \times 10^7 \text{ kPa}$, $\eta = 60000 \text{ kPa s}$ and $\nu = 0,3$. The material density of the plate ρ is assumed as 2000 kg/m^3 . The results for the viscoelastic plates without any elastic foundation and with Winkler-type elastic foundation are presented in Figure 8.23 employing Durbin's method for $aT = 5$, $N = 200$ and $T = 0,2 \text{ s}$ and it can be observed that the higher the value of k_w , the lesser the amplitude and time period of response. In the case of viscoelastic plate-Winkler elastic foundation interaction, results are sensitive to modulus of foundation reaction.

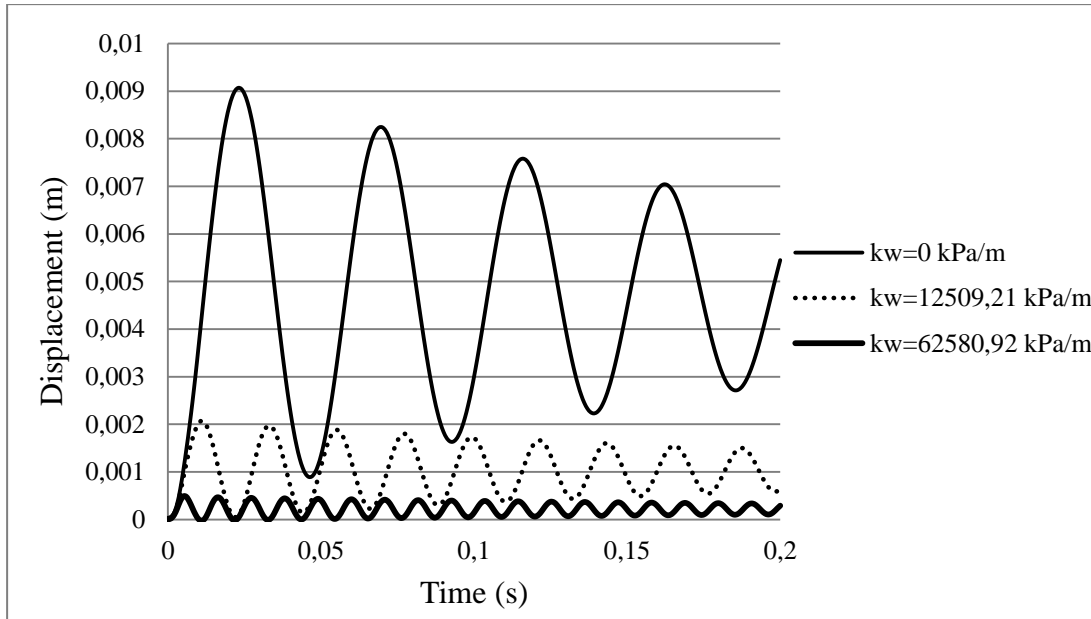


Figure 8.23 : Effect of foundation interaction on the vibration period and amplitude of displacement.

As in Example 13, vibration behavior of the viscoelastic plate resting on elastic foundation resembles the vibration of an elastic plate resting on elastic foundation for small values of the viscosity coefficient. This result provides theoretical validation for the use of the natural frequencies of vibration ω_{mn} of an elastic thin plate on elastic foundation, simply supported on all the edges, presented by Leissa (1969) and Rao (2007):

$$\omega_{mn} = \left[\frac{D\pi^4}{\rho h} \left[\left(\frac{m}{L_x} \right)^2 + \left(\frac{n}{L_y} \right)^2 \right]^2 + \frac{k_w}{\rho h} \right]^{1/2} \quad (8.4)$$

9. CONCLUSIONS AND RECOMMENDATIONS

In this thesis, it is focused on the quasi-static and dynamic analysis of linear viscoelastic plates considering the Kirchhoff hypothesis with the mixed finite element method in the Laplace-Carson domain. Using the hereditary integral form of the viscoelastic constitutive law and assuming that the Poisson ratio is constant:

- i. The field equations of Kirchhoff plates in the Laplace-Carson domain are obtained.
- ii. A new functional, which has geometric (essential) and dynamic (natural) boundary conditions in addition to displacement and stress variables in the Laplace-Carson domain, is constructed through a systematic procedure based on the Gâteaux differential method.
- iii. A special mixed finite element program is developed in Fortran programming language. Since the first derivatives of the variables exist in the functional, the conforming element formulation for the shape function ψ must satisfy only C^0 (r) continuity.
- iv. In order to transform the solutions obtained in the Laplace-Carson domain to the real time domain, various transform techniques are adopted. In particular, Maximum Degree of Precision (MDOP), Dubner & Abate and Durbin methods are employed. The performance of the methods are tested through various quasi-static and dynamic problems.
- v. Various viscoelastic material models are discussed for the plate structure to read from them possible patterns of viscoelastic behavior. In this respect, starting with the simplest and most common used mechanical (rheological) models such as the Maxwell and Kelvin models, more advanced mechanical models characterized by three or four parameters, that are referred to as Three-parameter-solid, Zener, Kelvin-chain and Four-parameter-solid models are considered.
- vi. The influences of the load, geometry and material parameters on the viscoelastic response of Kirchhoff plates are discussed by numerical example problems in detail.

The unique aspects of this thesis study and the possible contributions of the proposed method to the literature can be summarized as follows:

- By using this new functional, moment and shear force values that are important for engineers can be obtained directly without any mathematical operation.
- Geometric and dynamic boundary conditions can be obtained easily and a field variable can be included to the functional systematically.
- This presented formulation avoids shear locking.
- The results are quite in agreement with each other for a simply supported plate. The calculation is accomplished for different orders of mesh schemes, beginning with 2×2 and ending with 8×8 . The 4×4 mesh scheme results are very satisfactory and this scheme has the advantage of saving time.
- Two parameters control the flow of the numerical precision: aT and N , where a is the constant in numerical inverse Laplace transforms, T is the solution interval and N is the total number of terms of interest in the time interval and time increment is defined as $\Delta t = T / N$ in numerical precision. The results of the MDOP method are independent of aT and N . However, fluctuation scattering increases as aT in Dubner & Abate method increases and N in Dubner & Abate method decreases. Moreover, departure from exact solution increases for increasing values of aT and decreasing values of N in Durbin method. Satisfactory results can be obtained if the value of aT is chosen in the range 5-10 and N is chosen in the range 100-200.
- The MDOP method gives good results for the displacement variation as compared to the bending moment variation. Fluctuation is observed in the time-dependent bending moment as time increases in the MDOP inverse transform technique.
- When the time variation of the bending moment is considered, Durbin's method should be preferred over Dubner & Abate's method since it provides very good results not only for early times but also for later times.
- The quasi-static and dynamic responses of viscoelastic plates are investigated for various types of loading, such as a point load, a step load, a gradual step load, a rectangular impulsive load, a sinusoidal impulsive load, a triangular impulsive load, a square wave-type loading and a half rectified sine wave-type loading.

- Since the loading of the problem is not constant but varies in time, numerical inversion methods based on the sine-cosine transform are much more efficient.
- Special attention was devoted to the rheological models of linear viscoelasticity.
 - a) It is more convenient to use three-element models (Three-parameter-solid and Zener models) instead of Kelvin model to provide good representations of viscoelastic solid behavior.
 - b) The plate structure constituted by the Zener model is stiffer than the plate structure constituted by the Three-parameter-solid model.
 - c) The Kelvin-chain model consists of a chain of Kelvin units is considered. The longer the chain is, the greater the amount of deformation.
 - d) The Four-parameter-solid model is also considered. As expected, decreasing the viscosity in the dashpot resulting in greater extensions. However, it is worth noting that even if the viscosity coefficient values of the Maxwell and Kelvin structures are decreased in the same ratio, remarkable changes in deformation behavior of material occurred.
- The mixed finite element formulation introduced in this thesis is also applicable to the viscoelastic plate-elastic foundation interaction problems. The quasi-static and dynamic analysis of viscoelastic Kirchhoff plates resting on Winkler foundation is performed and reasonable results are obtained.
- Uniform variation of the thickness of the plate is also included into the mixed finite element formulation of the VPLT16.
- The free vibration period of a viscoelastic plate is obtained by the proposed mixed finite element model.
- A viscoelastic plate vibrates in the same period as does elastic plate for small values of viscosity coefficient, as expected.
- The free vibration period of a simply supported viscoelastic plate is inversely proportional to the thickness. Results are in good agreement with the periods of elastic plates in the literature for all thicknesses.
- Using different types of time-dependent loads and viscoelastic material models enhances the accuracy and applicability of the presented results for subsequent studies.

- It is expected that the results reported in this thesis may serve as a benchmark for future studies.
- The approach introduced can be applied for the higher order plate theories as well as shell theories. Following the described methodology, some of these problems are under study.



REFERENCES

- Aboudi, J., Cederbaum G., and Elishakoff, I.** (1990). Dynamic stability analysis of viscoelastic plates by Lyapunov exponents. *Journal of Sound and Vibration*, 139 (3), 459-467.
- Adey, R. A., and Brebbia, C. A.** (1973). Efficient method of solution of viscoelastic problems. *ASCE Journal of the Engineering Mechanics Division*, 99 (6), 1119-1127.
- Aköz, A. Y., and Kadioğlu, F.** (1999). The mixed finite element method for the quasi-static and dynamic analysis of viscoelastic Timoshenko beams. *International Journal for Numerical Methods in Engineering*, 44 (12), 1909-1932.
- Aköz, A. Y., Kadioğlu, F., and Tekin, G.** (2015). Quasi-static and dynamic analysis of viscoelastic plates. *Mechanics of Time-Dependent Materials*, 19 (4), 483-503.
- Aköz, A. Y., and Özçelikörs, Y.** (1985). A new functional for plates and a new finite element formulation, *The 9th National Applied Mechanics Meeting* (in Turkish), Bayramoğlu, Kocaeli, Turkey, September, 113-123.
- Aköz, A. Y., and Özütok, A.** (2000). A functional for shells of arbitrary geometry and a mixed finite element method for parabolic and circular cylindrical shells. *International Journal for Numerical Methods in Engineering*, 47, 1933-1981.
- Amoushahi, H., and Azhari, M.** (2013). Static analysis and buckling of viscoelastic plates by a fully discretized nonlinear finite strip method using bubble functions. *Composite Structures*, 100, 205-217.
- Amoushahi, H., and Azhari, M.** (2014). Static and instability analysis of moderately thick viscoelastic plates using a fully discretized nonlinear finite strip formulation. *Composites: Part B: Engineering*, 56, 222-231.
- Andrews, L. C., and Phillips, R. L.** (2003). *Mathematical Techniques for Engineers and Scientists*. USA: SPIE Press.
- Arani, A. G., and Haghparast, E.** (2017). Size-dependent vibration of axially moving viscoelastic micro-plates based on sinusoidal shear deformation theory. *International Journal of Applied Mechanics*, 9 (2), 1750026 (20pp.).
- Bathe, K. J.** (1982). *Finite Element Procedures in Engineering Analysis*. New Jersey: Prentice-Hall.
- Bellman, R. E., Kalaba, R. E., and Lockett, J. A.** (1966). *Numerical Inversion of the Laplace Transform*. New York: Elsevier.
- Boltzmann, L.** (1874). Zur Theorie der elastischen Nachwirkung. *Sitzber. Kaiserl. Akad. Wiss. Wien, Math.-Naturw. Kl.*, 70, 275-300.

- Carcione, J. M.** (2007). *Wave Fields in Real Media. Theory and Numerical Simulation of Wave Propagation in Anisotropic, Anelastic and Porous Media.* (2nd ed.). Amsterdam: Elsevier.
- Chen, T. M.** (1995). The hybrid Laplace transform / finite element method applied to the quasi-static and dynamic analysis of viscoelastic Timoshenko beams. *International Journal for Numerical Methods in Engineering*, 38 (1), 509-522.
- Chen, Q., and Chan, Y. W.** (2000). Integral finite element method for dynamical analysis of elastic-viscoelastic composite structures. *Computers and Structures*, 74 (1), 51-64.
- Chen, W. H., and Lin, T. C.** (1982). Dynamic analysis of viscoelastic structures using incremental finite element method. *Engineering Structures*, 4 (4), 271-276.
- Cheng, C-J., and Zhang, N-H.** (1998). Variational principles on static-dynamic analysis of viscoelastic thin plates with applications. *International Journal of Solids and Structures*, 35 (33), 4491-4505.
- Christensen, R. M.** (1982). *Theory of Viscoelasticity* (2nd ed.). New York: Academic Press.
- Cooley, J. W., Lewis, P. A. W., and Welch, P. D.** (1970). The fast Fourier transform algorithm: programming considerations in the calculation of sine, cosine and Laplace transforms. *Journal of Sound and Vibration*, 12 (3), 315-337.
- Cost, T. L., and Becker, E. B.** (1970). A multidata method of approximate Laplace transform inversion. *International Journal for Numerical Methods in Engineering*, 2 (2), 207-219.
- Craig Jr, R. R., and Kurdila, A. J.** (2006). *Fundamentals of Structural Dynamics.* (2nd ed.). New Jersey: John Wiley & Sons.
- Dirac, P. A. M.** (1958). *The Principles of Quantum Mechanics* (4th ed.). New York: Oxford University.
- Donnell, L. H., Drucker, D. C., and Goodier, J. N.** (1946). Discussion of the paper by Reissner: the effect of transverse shear deformation on the bending of elastic plates. *ASME Journal of Applied Mechanics*, 13 (1), 249-252.
- Dubner, H., and Abate, J.** (1968). Numerical inversion of Laplace transforms by relating them to the finite Fourier cosine transform. *Journal of the Association for Computing Machinery*, 15 (1), 115-123.
- Durbin, F.** (1974). Numerical inversion of Laplace transforms: an efficient improvement to Dubner and Abate's method. *The Computer Journal*, 17 (4), 371-376.
- Dyke, P.** (2014). *An Introduction to Laplace Transforms and Fourier Series.* (2nd ed.). London: Springer-Verlag.
- Findley, W. N., Lai, J. S., and Onaran, K.** (1976). *Creep and Relaxation of Nonlinear Viscoelastic Materials.* New York: North-Holland.
- Flügge, W.** (1975). *Viscoelasticity* (2nd ed.). New York: Springer-Verlag.

- Gurtin, M. E., and Sternberg, E.** (1962). On the linear theory of viscoelasticity. *Archive for Rational Mechanics and Analysis*, 11 (1), 291-356.
- Gutierrez-Lemini, D.** (2014) *Engineering Viscoelasticity*. New York: Springer.
- Han, J. W., Kim, J. S., Nguyen, S-N., and Cho, M.** (2016). Improved viscoelastic analysis of laminated composite and sandwich plates with an enhanced first-order shear deformation theory. *ASME Journal of Applied Mechanics*, 83 (3), 031004-1:10.
- Hatami, S., Ronagh, H. R., and Azhari, M.** (2008). Exact free vibration analysis of axially moving viscoelastic plates. *Computers and Structures*, 86 (17), 1738-1746.
- Hellinger, E.** (1914). Die allgemeinen ansatze der mechanik der kontinua. *Encyklopädie der Mathematischen Wissenschaften IV*, 4, 602-694.
- Hu, H-C.** (1955). On some variational principles in the theory of elasticity and the theory of plasticity. *Scientia Sinica*, 4 (1), 33-54.
- Ilyasov, M. H., and Aköz, A. Y.** (2000). The vibration and dynamic stability of viscoelastic plates. *International Journal of Engineering Sciences*, 38 (6), 695-714.
- Jaberzadeh, E., and Azhari, M.** (2015). Local buckling of moderately thick stepped skew viscoelastic composite plates using the element-free Galerkin method. *Acta Mechanica*, 226 (4), 101-1025.
- Jafari, N., Azhari, M., and Heidarpour, A.** (2011). Local buckling of thin and moderately thick variable thickness viscoelastic composite plates. *Structural Engineering and Mechanics*, 40 (6), 783-800.
- Jafari, N., Azhari, M., and Heidarpour, A.** (2014). Local buckling of rectangular viscoelastic composite plates using finite strip method. *Mechanics of Advanced Materials and Structures*, 21 (4), 263-272.
- Kadioğlu, F.** (1999). *Quasi-static and dynamic analysis of viscoelastic beams* (Doctoral dissertation), (in Turkish). Istanbul Technical University, Graduate School of Science Engineering and Technology, ISTANBUL.
- Kadioğlu, F., and Aköz, A. Y.** (1999). The mixed finite element method for the dynamic analysis of visco-elastic circular beams, *The 4th International Conference on Vibration Problems*, Jadavpur University, India, November 27-30, 40-52.
- Kadioğlu, F., and Aköz, A. Y.** (2000). The quasi-static and dynamic responses of viscoelastic parabolic beams, *The 11th National Applied Mechanics Meeting* (in Turkish), Bolu, Turkey, September 6-10, 397-407.
- Kadioğlu, F., and Aköz, A. Y.** (2003). The mixed finite element for the quasi-static and dynamic analysis of viscoelastic circular beams. *An International Journal of Structural Engineering and Mechanics*, 15 (6), 735-752.
- Kadioğlu, F., and Tekin, G.** (2015). Viscoelastic Kirchhoff plate analysis via mixed finite element formulation, *The 3rd International Conference on Advances in Civil, Structural and Mechanical Engineering*, ACSM 2015, Bangkok, Thailand, December 28-29.

- Kadioğlu, F., and Tekin, G.** (2016a). Viscoelastic plate analysis based on Gâteaux differential, *The 3rd International Conference on Mechanical, Electronics and Computer Engineering*, CMECE 2016, New York, USA, January 7-9.
- Kadioğlu, F., and Tekin, G.** (2016b). Dynamic response of visco-elastic plates, *The 12th International Conference of Computational Methods in Science and Engineering*, ICCMSE 2016, Athens, Greece, March 17-20.
- Kadioğlu, F., and Tekin, G.** (2017a). Analysis of four-element rheological model, *The 25th International Conference on Composites / Nano-Engineering*, ICCE-25, Rome, Italy, July 16-22.
- Kadioğlu, F., and Tekin, G.** (2017b). Mixed finite element formulation for the free vibration analysis of viscoelastic plates with uniformly varying cross-section, *The 4th International Conference on Mechanical, Electronics and Computer Engineering*, CMECE 2017, Phnom Penh, Cambodia, September 14-16.
- Kadioğlu, F., and Tekin, G.** (2017c). Analysis of plates under point load using Zener material model, *The 4th International Conference on Mechanical, Electronics and Computer Engineering*, CMECE 2017, Phnom Penh, Cambodia, September 14-16.
- Kirchhoff, G. R.** (1850). Über das gleichgewichi und die bewegung einer elastissem scheibe. *J Fuer die Reine und Angewandte Mathematik*, 40, 51-88.
- Klausner, Y.** (1991). *Fundamentals of Continuum Mechanics of Soils*. New York: Springer-Verlag.
- Kocatürk, T., and Şimşek, M.** (2006). Dynamic analysis of eccentrically prestressed viscoelastic Timoshenko beams under a moving harmonic load. *Computers and Structures*, 84 (31-32), 2113-2127.
- Krylov, V. I., and Skoblya, N. S.** (1969). *Handbook of Numerical Inversion of Laplace Transforms* (Translated from Russian by D. Louvish). Jerusalem: Israel Program for Scientific Translations.
- Kusama, T., and Mitsui, Y.** (1982). Boundary element method applied to linear viscoelastic analysis. *Applied Mathematical Modelling*, 6 (4), 285-290.
- Lakes, R. S.** (2009). *Viscoelastic Materials*. New York: Cambridge University Press.
- Lee, E. H.** (1955). Stress analysis in viscoelastic bodies. *Quarterly of Applied Mathematics*, 13 (2), 183-190.
- Leissa, A. W.** (1969). *Vibration of Plates*. NASA SP-160., Washington, DC: US Government Printing Office.
- Marynowski, K.** (2010). Free vibration analysis of the axially moving Levy-type viscoelastic plate. *European Journal of Mechanics A / Solids*, 29 (5), 879-886.
- Mesquita, A. D., and Coda, H. B.** (2002). Alternative Kelvin viscoelastic procedure for finite elements. *Applied Mathematical Modelling*, 26 (4), 501-516.
- Mindlin, R. D.** (1951). Influence of rotary inertia and shear on flexural motions of isotropic, elastic plates. *ASME Journal of Applied Mechanics*, 18 (1), 31-38.

- Narayanan, G. V., and Beskos, D. E.** (1982). Numerical operational methods for time-dependent linear problems. *International Journal of Numerical Methods in Engineering*, 18 (12), 1829-1854.
- Nguyen, S-N., Lee, J., and Cho, M.** (2015). Efficient higher-order zig-zag theory for viscoelastic laminated composite plates. *International Journal of Solids and Structures*, 62, 174-178.
- Nguyen, S-N., Lee, J. and Cho, M.** (2016). A triangular finite element using Laplace transform for viscoelastic laminated composite plates based on efficient higher-order zigzag theory. *Composite Structures*, 155, 223-244.
- Oden, J. T., and Reddy, J. N.** (1976). *Variational Methods in Theoretical Mechanics*. New York: Springer-Verlag.
- Omurtag, M. H., and Kadioğlu, F.** (1998). Free vibration analysis of orthotropic plates resting on Pasternak foundation by mixed finite element formulation. *Computers and Structures*, 67 (4), 253-265.
- Omurtag, M. H., Özütok, A., Aköz, A. Y., and Özçelikörs, Y.** (1997). Free vibration analysis of Kirchhoff plates resting on elastic foundation by mixed finite element formulation based on Gâteaux differential. *International Journal of Numerical Methods in Engineering*, 40 (2), 295-317.
- Papoulis, A.** (1957). A new method of inversion of the Laplace transform. *Quarterly of Applied Mathematics*, 14, 405-414.
- Piovan, M. T., and Cortínez, V. H.** (2008). Linear viscoelastic analysis of straight and curved thin-walled laminated composite beams. *International Journal of Solids and Structures*, 45 (11-12), 3466-3493.
- Pipkin, A. C.** (1972). *Lectures on Viscoelasticity Theory* (Applied Mathematical Sciences, 7). New York: Springer-Verlag.
- Pissens, R.** (1975). A bibliography on numerical inversion of the Laplace transform and applications. *Journal of Computational and Applied Mathematics*, 1 (2), 115-128.
- Pissens, R., and Dang, N. D. P.** (1976). A bibliography on numerical inversion of the Laplace transform and applications: A Supplement. *Journal of Computational and Applied Mathematics*, 2 (3), 225-228.
- Purushothaman, N., Moore, I. D., and Heaton, B. S.** (1988). Finite element analysis of viscoelastic solids responding to periodic disturbances. *International Journal for Numerical Methods in Engineering*, 26 (7), 1471-1483.
- Rao, S. S.** (2007). *Vibration of Continuous Systems*: USA: John Wiley & Sons.
- Reddy, J. N.** (1993). *An Introduction to the Finite Element Method*. (2nd ed.). New York: McGraw-Hill.
- Reddy, J. N.** (2006). *An Introduction to the Finite Element Method*. (3rd ed.). New York: McGraw-Hill.
- Reddy, J. N.** (2008). *An Introduction to Continuum Mechanics with Applications*. New York: Cambridge University Press.
- Reissner, E.** (1944). On the theory of bending of elastic plates. *Journal of Mathematical Physics*, 23, 184-191.

- Reissner, E.** (1945). The effect of transverse shear deformation on the bending of elastic plates. *ASME Journal of Applied Mechanics*, 12, A69-A77.
- Reissner, E.** (1948). Note on the method of complementary energy. *Journal of Mathematics and Physics*, 27, 159-160.
- Reissner, E.** (1953). On a variational theorem for finite deformation. *Journal of Mathematics and Physics*, 32, 129-135.
- Rencis, J. J., Saigal, S., and Jong, K-Y.** (1990). A Dynamic viscoelastic beam model for finite element method. *ASCE Journal of Aerospace Engineering*, 3 (1), 19-29.
- Rizzo, F. J., and Shippy, D. J.** (1971). An application of the correspondence principle of linear viscoelasticity theory. *SIAM Journal on Applied Mathematics*, 21 (2), 321-330.
- Roylance, D.** (2001). *Lecture Notes on Engineering Viscoelasticity*, Department of Materials Science and Engineering, Massachusetts Institute of Technology MIT, Cambridge, MA 02139.
- Saleeb, A. F., and Chang, T. Y.** (1987). An efficient quadrilateral element for bending analysis. *International Journal for Numerical Methods in Engineering*, 24 (6), 1123-1155.
- Salerno, V. L., and Goldberg, M. A.** (1960). Effect of shear deformation on the bending of rectangular plates. *ASME Journal of Applied Mechanics*, 27 (1), 54-58.
- Santos, H. A. F. A., Pimenta, P. M., and Almeida, J. P. Moitinho de** (2010). Hybrid and multi-field variational principles for geometrically exact three-dimensional beams. *International Journal of Non-Linear Mechanics*, 45 (8), 809-820.
- Schapery, R. A.** (1962). Approximate methods of transform inversion for viscoelastic stress analysis, *The 4th US National Congress on Applied Mechanics*, Berkeley, USA, 2, 1075-1085.
- Schwartz, L.** (1950). *Théorie des Distributions. 1*, Paris: Hermann.
- Schwartz, L.** (1951). *Théorie des Distributions. 2*, Paris: Hermann.
- Shariyat, M.** (2011). A double-superposition global-local theory for vibration and dynamic buckling analyses of viscoelastic composite / sandwich plates: A complex modulus approach. *Archive of Applied Mechanics*, 81 (9), 1253-1268.
- Signals and Systems/Engineering Functions.** (2017, October 15). Wikibooks, The Free Textbook Project. Retrieved 09:19, October 27, 2017 from https://en.wikibooks.org/w/index.php?title=Signals_and_Systems/Engineering_Functions&oldid=3314118.
- Sorvari, J., and Hämäläinen, J.** (2010). Time integration in linear viscoelasticity-a comparative study. *Mechanics of Time-Dependent Materials*, 14 (3), 307-328.
- Szilar, R.** (2004). *Theories and Applications of Plate Analysis*. New Jersey: JohnWiley & Sons.

- Tekin, G., and Kadioğlu, F.** (2016a). Dynamic analysis of viscoelastic plates with variable thickness, *The 18th International Conference on Construction and Civil Engineering*, ICCCE 2016, London, United Kingdom, February 25-26.
- Tekin, G., and Kadioğlu, F.** (2016b). Mixed finite element method for analysis of viscoelastic plates, *The 12th International Congress on Advances in Civil Engineering*, ACE 2016, Istanbul, Turkey, September 21-23.
- Tekin, G., and Kadioğlu, F.** (2016c). Developing three-element model for quasi-static analysis of viscoelastic plates, *The 12th International Congress on Advances in Civil Engineering*, ACE 2016, Istanbul, Turkey, September 21-23.
- Tekin, G., and Kadioğlu, F.** (2017a). Viscoelastic behavior of shear-deformable plates. *International Journal of Applied Mechanics*, 9 (6), 1750085 (23 pages).
- Tekin, G., and Kadioğlu, F.** (2017b). Four-parameter viscoelastic model for the plates of uniformly varying cross-section, *The 6th International Conference on Engineering and Innovative Materials*, ICEIM 2017, Tokyo, Japan, September 3-5.
- Tekin, G., and Kadioğlu, F.** (2017c). Analysis of viscoelastic plates under point loads, *The 20th National Mechanics Conference* (in Turkish), Uludağ University, Bursa, Turkey, September 5-9.
- Tekin, G., Kadioğlu, F., and Aköz, A. Y.** (2015). The mixed finite element method for the quasi-static analysis of viscoelastic plates of varying thickness, *The Civil & Construction Engineering and Technologies Conference*, CONSTENG'15, Istanbul, Turkey, December 4-5.
- Temel, B., Çalm, F. F., and Tütüncü, N.** (2004). Quasi-static and dynamic response of viscoelastic helical rods. *Journal of Sound and Vibration*, 271 (3-5), 921-935.
- Temel, B., and Şahan, M. F.** (2013). Transient analysis of orthotropic, viscoelastic thick plates in the Laplace domain. *European Journal of Mechanics A/Solids*, 37, 96-105.
- Timoshenko, S. P.** (1953). *History of Strength of Materials*. New York: McGraw-Hill.
- Timoshenko, S. P., and Woinowsky-Krieger, S.** (1959). *Theory of Plates and Shells*. New York: McGraw-Hill.
- Truesdell, C.** (1968). *Essays in the History of Mechanics*. New York: Springer-Verlag.
- Tschoegl, N. W.** (1989). *The Phenomenological Theory of Linear Viscoelastic Behavior: An Introduction*. New York: Springer-Verlag.
- Vallala, V., Ruimi, A., and Reddy, J. N.** (2012). Nonlinear viscoelastic analysis of orthotropic beams using a general third-order theory. *Composite Structures*, 94, 3759-3768.
- Ventsel, E., and Krauthammer, T.** (2001). *Thin Plates and Shells: Theory, Analysis, and Applications*. New York: Marcel Dekker.

- Voyiadjis, G. Z., Baluch, M. H., and Chi, W. K.** (1985). Effects of shear and normal strain on plate bending. *ASCE Journal of Engineering Mechanics*, 111 (9), 1130-1143.
- Wang, Y. Z., and Tsai, T. J.** (1988). Static and dynamic analysis of a viscoelastic plate by the finite element method. *Applied Acoustics*, 25 (2), 77-94.
- Wang, C. M., Yang, T. Q., and Lam, K. Y.** (1997). Viscoelastic Timoshenko beam solutions from Euler-Bernoulli solutions. *Journal of Engineering Mechanics*, 123 (7), 746-748.
- Washizu, K.** (1955). *On the Variational Principles of Elasticity and Plasticity*, (Technical Report No: 25-18). Cambridge: MIT Aeroelastic and Structures Research Laboratory.
- Weeks, W. T.** (1966). Numerical inversion of Laplace transforms using Laguerre functions. *Journal of the Association for Computing Machinery*, 13 (3), 419-426.
- White, J. L.** (1986). Finite elements in linear viscoelastic analysis, *The 2nd Conference On Matrix Method in Structural Mechanics*, Wright Patterson Air Force Base, Ohio, AFFDL-TR-68-150, October, 489-516.
- Wing, O.** (1967). An efficient method of numerical inversion of Laplace transforms. *Computing*, 2 (2), 153-166.
- Winkler, E.** (1867). *Die Lehre von der Elasticität und Festigkeit*. Prag: Verlag H. Dominicus.
- Yang, C. M., Jin, G. Y., Xu, W. J., and Liu, Z. G.** (2016). A modified Fourier solution for free damped vibration analysis of sandwich viscoelastic-core conical shells and annular plates with arbitrary restraints. *International Journal of Applied Mechanics*, 8 (8), 1650094 (30pp.).
- Yi, S., and Hilton, H. H.** (1994). Dynamic finite element analysis of viscoelastic composite plates in the time domain. *International Journal for Numerical Methods in Engineering*, 37 (23), 4081-4096.
- Yi, S., Pollock, G. D., Ahmad, M. F., and Hilton, H. H.** (1992). Time-dependent analysis of anisotropic viscoelastic composite shell structures. *Computing Systems in Engineering*, 3 (1-4), 457-467.
- Zhou, Y-F., and Wang, Z-M.** (2007). Transverse vibration characteristics of axially moving viscoelastic plate. *Applied Mathematics and Mechanics*, 28 (2), 209-218.
- Zhu, X. Y., Chen, W. Q., Huang, Z. Y., and Liu, Y. J.** (2011). A fast multipole boundary element method for 2D viscoelastic problems. *Engineering Analysis with Boundary Elements*, 35 (2), 170-178.

CURRICULUM VITAE



Name Surname : Gülçin Tekin Özkan

Place and Date of Birth : Konya, 09.02.1984

E-Mail : gulcintekin@itu.edu.tr

EDUCATION :

- **B.Sc.** : 2006, Yıldız Technical University, Faculty of Civil Engineering, Department of Civil Engineering
- **M.Sc.** : 2010, Boğaziçi University, Faculty of Engineering, Department of Civil Engineering

PROFESSIONAL EXPERIENCE AND REWARDS:

- 2006 Yıldız Technical University Honour Student

PUBLICATIONS, PRESENTATIONS AND PATENTS ON THE THESIS:

- Aköz, A. Y., Kadioğlu, F., and **Tekin, G.** (2015). Quasi-static and dynamic analysis of viscoelastic plates. *Mechanics of Time-Dependent Materials*, 19 (4), 483-503.
- Kadioğlu, F., and **Tekin, G.** (2015). Viscoelastic Kirchhoff plate analysis via mixed finite element formulation, *The 3rd International Conference on Advances in Civil, Structural and Mechanical Engineering*, ACSM 2015, Bangkok, Thailand, December 28-29.
- Kadioğlu, F., and **Tekin, G.** (2016). Viscoelastic plate analysis based on Gâteaux differential, *The 3rd International Conference on Mechanical, Electronics and Computer Engineering*, CMECE 2016, New York, USA, January 7-9.

- Kadioğlu, F., and **Tekin, G.** (2016). Dynamic response of visco-elastic plates, *The 12th International Conference of Computational Methods in Science and Engineering*, ICCMSE 2016, Athens, Greece, March 17-20.
- Kadioğlu, F., and **Tekin, G.** (2017). Analysis of four-element rheological model, *The 25th International Conference on Composites / Nano-Engineering*, ICCE-25, Rome, Italy, July 16-22.
- Kadioğlu, F., and **Tekin, G.** (2017). Mixed finite element formulation for the free vibration analysis of viscoelastic plates with uniformly varying cross-section, *The 4th International Conference on Mechanical, Electronics and Computer Engineering*, CMECE 2017, Phnom Penh, Cambodia, September 14-16.
- Kadioğlu, F., and **Tekin, G.** (2017). Analysis of plates under point load using Zener material model, *The 4th International Conference on Mechanical, Electronics and Computer Engineering*, CMECE 2017, Phnom Penh, Cambodia, September 14-16.
- **Tekin, G.**, and Kadioğlu, F. (2016). Dynamic analysis of viscoelastic plates with variable thickness, *The 18th International Conference on Construction and Civil Engineering*, ICCCE 2016, London, United Kingdom, February 25-26.
- **Tekin, G.**, and Kadioğlu, F. (2016). Mixed finite element method for analysis of viscoelastic plates, *The 12th International Congress on Advances in Civil Engineering*, ACE 2016, Istanbul, Turkey, September 21-23.
- **Tekin, G.**, and Kadioğlu, F. (2016). Developing three-element model for quasi-static analysis of viscoelastic plates, *The 12th International Congress on Advances in Civil Engineering*, ACE 2016, Istanbul, Turkey, September 21-23.
- **Tekin, G.**, and Kadioğlu, F. (2017). Four-parameter viscoelastic model for the plates of uniformly varying cross-section, *The 6th International Conference on Engineering and Innovative Materials*, ICEIM 2017, Tokyo, Japan, September 3-5.
- **Tekin, G.**, and Kadioğlu, F. (2017). Analysis of viscoelastic plates under point loads, *The 20th National Mechanics Conference* (in Turkish), Uludağ University, Bursa, Turkey, September 5-9.
- **Tekin, G.**, Kadioğlu, F., and Aköz, A. Y. (2015). The mixed finite element method for the quasi-static analysis of viscoelastic plates of varying thickness, *The Civil&Construction Engineering and Technologies Conference*, CONSTENG'15, Istanbul, Turkey, December 4-5.

OTHER PUBLICATIONS, PRESENTATIONS AND PATENTS:

- Ateş, N., **Tekin, G.**, and Kadioğlu, F. (2016). Alternative solution for cross-ply laminated composite thick plates. *Građevinar*, 68 (6), 451-460.
- Kadioğlu, F., and **Tekin, G.** (2016). Natural longitudinal frequencies of a uniform rod with a tip mass or a spring (Discussion for Vol 77, pp: 147, 1981). *Journal of Sound and Vibration*, 371, 446-447.

- Kadioğlu, F., and **Tekin, G.** (2015). Free vibration analysis of cross-ply laminated composite thick plates, *The 2nd International Conference On Advances in Civil, Structural and Mechanical Engineering*, ACSM 2015, Bangkok, Thailand, August 28-29.
- Kadioğlu, F., **Tekin, G.**, and Satır, N. (2016). Free vibration analysis of cross-Ply laminated composite thick plates resting on elastic foundation. *Süleyman Demirel University Journal of Natural and Applied Sciences*, 20 (2), 303-309.
- Najafov, A. M., Kadioğlu, F., Mammadov, Z., Zerim, Z., Sofiyev, A. H., and **Tekin, G.** (2015). Nonlinear behavior of composite truncated conical shells subjected to the dynamic loading. *Acta Physica Polonica A*, 127 (4), 904-906.
- Özkan, G., **Tekin, G.**, and Kadioğlu, F. (2017). An alternative method for analysing buckling of laminated composite beams. *Grđevinar*, 69 (9), 841-850.
- **Tekin, G.**, and Kadioğlu, F. (2017). Viscoelastic behavior of shear-deformable plates. *International Journal of Applied Mechanics*, 9 (6), 1750085 (23 pages).
- **Tekin, G.**, and Kadioğlu, F. (2015). Buckling Analysis of Composite Timoshenko Beams with Gâteaux Differential, *The 2nd International Conference on Advances in Civil, Structural and Mechanical Engineering*, ACSM 2015, Bangkok, Thailand, August 28-29.
- **Tekin, G.**, and Kadioğlu, F. (2015). Static Analysis of Cross-ply Laminated Composite Thick Plates on Winkler's Elastic Foundation, *The 19th National Mechanics Conference*, Karadeniz Technical University, Trabzon, Turkey, August 24-28.
- **Tekin G.**, Özkan, G., Kadioğlu, F., and Özütok, A. (2013). Buckling Analysis of Composite Straight Beams, *The 21st Annual International Conference on Composites / Nano Engineering*, ICCE-21, Tenerife, Spain, July 21-27.
- **Tekin, G.**, and Tanırcan, B. G. (2015). An Empirical Study for Calculation of Peak Elastic Displacements of Single Degree of Freedom Structures, *The 8th National Conference on Earthquake Engineering*, Istanbul, Turkey, May 11-15.
- **Tekin, G.**, Tanırcan, B. G., and Şafak, E. (2010). Probabilistic Earthquake Response Analyses of Single Degree of Freedom Structures, *The 14th European Conference of Earthquake Engineering*, 14 ECEE, Ohrid, Macedonia, August 30-September 3.
- **Tekin, G.**, Tanırcan, B. G., and Şafak, E. (2011). Probabilistic Earthquake Response Analysis of Single Degree of Freedom Structures, *The 7th National Conference on Earthquake Engineering*, Istanbul, Turkey, May 30-June 3.

